Exploration of acetate as a feedstock for propionate production in engineered *Escherichia coli*

by

Shane Kilpatrick

A thesis

presented to the University of Waterloo

in fulfillment of the

thesis requirement for the degree of

Master of Applied Science

in

Chemical Engineering

Waterloo, Ontario, Canada, 2017

Author's declaration

I hereby declare that I am the sole author of this thesis. This is a true copy of the thesis, including any required final revisions, as accepted by my examiners.

I understand that my thesis may be made electronically available to the public.

Abstract

With a relatively low reductance, acetate is considered as a poor and uncommon carbon source for microbial production and, therefore, the production strains will require major strain engineering for effective utilization of it. In this study, using our previously derived propionogenic (propionate-producing) bacterium *Escherichia coli*, we successfully demonstrated the production of propionate with acetate as the sole carbon source. A selection of genes involved in the relevant biotransformation pathways were manipulated, either knocked out or overexpressed, and these genetic effects on culture performance, specifically cell growth and propionate yield, were investigated. Our results show that acetate metabolism is sensitive to perturbation of the central metabolic pathways and the majority of engineered strains had lower rates of acetate utilization and cell growth relative to the control strain. For effective conversion of acetate to propionate, potential metabolic strategies should be developed towards manipulation of the genes enhancing the oxidative tricarboxylic acid (TCA) cycle and glyoxylate bypass so that more dissimilated carbon flux can be driven into the methylmalonyl-CoA (MM-CoA) pathway. Potential applications of acetate as a feedstock for biomanufacturing are described.

Acknowledgements

I would like to begin by thanking my supervisor Dr. C. P. Chou. You challenged me to be the very best student I could be. Along with your invaluable expertise, it was your honesty that pushed me to elevate my performance and challenge my way of thinking.

Next, I would like to thank Dr. Yim and Dr. Simakov for serving on my committee. Your time in evaluating my thesis and valuable feedback is much appreciated.

I would also like to thank Bradley Mozel, Dragon Miscavic, Adam Westbrooke and my other colleagues from Dr. C. P. Chou's Lab for their support, insights, expertise, and friendship throughout my time in the lab. A special thanks to Dr. Kajan.Srirangan of the CNRC for providing me with technical training at the beginning of my time here and for his continued support throughout.

In closing, I cannot thank enough the people closest to me who have made this all possible. The love and guidance my friends, family, and girlfriend have given me are the reason I could accomplish this life milestone. I'd like to thank my mother Donna Jaques for her relentless love and support and my grandfather Dr. R. P. Jaques for inspiring me to enter research.

Table of contents

List of figures

List of tables

List of abbreviations

1,3-PDO	1,3-Propandiol
2-MM	2-Methylmalate
3-HB	3-Hydroxybutyrate
3-HP	3-Hydroxypropionate
3-HV	3-Hydroxyvalerate
AceA	Isocitrate lyase
AceB	Malate synthase A
AceEF	Pyruvate dehydrogenase complex
AceK	Isocitrate dehydrogenase kinase
AckA	Acetate kinase
AcnAB	Citrate hydro-lyase/D-*thero*-isocitrate hydro-lyase
ActP	Acetate permease
ADP	Adenosine diphosphate
AldH	Aldehyde dehydrogenase
AMP	Adenosine monophosphate
ArcAB	Anoxic respiratory control system
ATP	Adenosine monophosphate
Bcd	Butyryl-CoA dehydrogenase
BktB	β-Ketothiolase
CoA	Coenzyme A
Crt	Crotonase
DhaB1	Glycerol dehydratase
DhaB2	Activating enzyme for DhaB1
DNA	Deoxyribonucleic acid
EtfAB	Electron-transfer flavoprotein complexes for Bcd
Flp	Flippase
Fnr	DNA-binding transcription dual regulator protein Fnr
FrdABCD	Fumarate reductase complex
FRT	Flippase recognition target
FumABC	Fumarases A,B, and C
GlcB	Malate synthase G
GldA	Glycerol dehydrogenase
GlpK	Glycerol kinase
GltA	Citrate synthase
Hbd	3-Hydroxybutryl-CoA dehydrogenase
IcdA	Isocitrate dehydrogenase
IclR	Transcriptional repressor protein IclR
ICT	Isocitrate
IPTG	β-D-1-thiogalactopyranoside

LB	Lysogeny Broth
MA	Malate
MaeB	Malate dehydrogenase
Mdh	Malate dehydrogenase
MMCL	Malyl-CoA/Methylmalonyl-CoA lysis
MM-CoA	Methylmalonyl-CoA
$NAD(P)^+$	Nicotinamide adenine dinucleotide (phosphate)
NAD(P)H	Reduced form of $NAD(P)^+$
OAA	Oxaloacetate
OD_{600}	Optical density measured at 600
PckA	Phosphoenolpyruvate carboxykinase
PCR	Polymerase chain reaction
PEP	Phosphoenolpyruvate
PhaA	β-Ketothiolase
PhaB	3-Hydroxybutryl-CoA dehydrogenase
PhaC	Polyhydroxyalkanoate polymerase/synthase
Ppc	Phosphoenolpyruvate carboxylase
PpsA	Phosphoenolpyruvate synthase
PrpE	Propionyl-CoA synthase complex
Pta	Phosphate acetyltransferase
PykAF	Pyruvate kinases I and II
RID	Refractive index detector
s.d.	Standard deviation
SatP	Acetate/succinate symporter
Sbm	Methylmalonyl-CoA mutase
SdhCDAB	Succinate:quinone oxidoreductase complex
SfcA	Malate dehydrogenase
SucAB	2-oxoglutarate dehydrogenase
SucCD	Succinyl-CoA synthetase
TCA	Tricarboxylic acid
TesB	Acyl-CoA thioesterase II
YgfG	Methylmalonyl-CoA decarboxylase
YqhD	1,3-PDO oxidoreductase
α-KG	α-Ketoglutarate

List of symbols

Cm^R	Chloramphenicol resistance
g	Grams
h	Hour
K_M	Michaelis-Menten constant
Km^R	Kanamycin resistance
L	Liter
mM	Millimolar
P_i	Phosphate
pH	Potential of hydrogen
PP_i	Diphosphate
Q	Quinone

Chapter 1 – Introduction

To date, the majority of commodity chemicals and products are still derived petrochemically and this is considered unstainable due to finite reserves and environmental impacts associated with the production and use of the petrochemical feedstocks [2, 3]. As we shift towards a green economy, there has been considerable interest in developing sustainable production platforms, and biomanufacturing, which uses biomasses as feedstocks, is one of them [4, 5]. However, biomanufacturing also has drawbacks. The use of first-generation edible feedstocks can lead to increases in food/grain prices and limited land for their production [6, 7]. Furthermore, biorefineries are not as economical as their counterpart petrorefineries due to high costs associated with biological feedstock processing and transportation [8]. Fortunately, these issues can be mitigated by identification of alternate feedstocks, such as biomass-derived syngas, lignocelluloses, and waste streams (e.g. crude glycerol) [9, 10].

Among various alternate feedstocks, the potential of acetate has been recently identified for the following reasons. First, acetate is a waste byproduct associated with various bioprocesses, such as syngas fermentation and lignocellulosic biomass processing [11, 12]. On the other hand, acetate can be economically synthesized via methanol carbonylation or oxidative condensation of methane [13, 14]. However, the feasibility of acetate as a feedstock has not been well investigated, evident by the shortage of publications. While bacterium *Escherichia coli* represents an ideal host for biomanufacturing, utilizing acetate as a feedstock has been uncommon for this workhorse. In fact, *E. coli* produces acetate during growth on most carbon sources, and acetate accumulation has been noted as a key technological issue to *E. coli*-based bioprocesses [15] by affecting biomass production and cell growth [16, 17], carbon dissimilation and oxygen consumption [16], recombinant protein production [18], and value-added metabolite production [19]. Biological conversion of cheap acetate to value-added products can not only enhance the economic feasibility of bioprocesses but also mitigate the unwanted acetate accumulation. *E. coli* normally exhibits diauxic growth on acetate following exhaustion of preferred carbon sources [20, 21], suggesting its biological capacity of using this carbon. However, unlike most common carbon sources such as glucose and glycerol, acetate has a low reductance and energy content, and, therefore, its utilization will require a significantly different metabolism with minimal metabolite production. The substantial metabolic changes are evident by comparing gene expression profiles of *E. coli* grown on glucose and acetate, respectively [1, 22].

For *E. coli* growing on acetate, acetate transport into the cytosol is facilitated by a permease (ActP) and an acetate/succinate symporter (SatP) [23, 24]. Intracellular acetate is then converted via two pathways, i.e. AckA-Pta and Acs, to acetyl-CoA, which is involved in various central metabolic pathways including tricarboxylic acid (TCA) cycle, glyoxylate bypass, and fatty acid and amino acid synthetic pathways [21]. Specific selection of the acetyl-CoA formation pathway will depend on the extracellular concentration of acetate, with the AckA-Pta pathway being preferred over the Acs pathway for acetate concentrations greater than 25-30 mM (i.e. 1.5-1.8 g/L) [25, 26]. Importantly, during growth on acetate, the glyoxylate bypass is activated to avoid the energy-generating decarboxylation steps within the TCA cycle [15]. This allows *E. coli* to replenish the carbon for use in other key pathways and establishes a tradeoff between carbon conservation and energy generation [15, 21]. Splitting the flux between the glyoxylate bypass and decarboxylating steps in the TCA cycle is regulated via expression of the glyoxylate-bypass-encoding operon (i.e. *aceABK*) and the binding affinity of isocitrate (ICT) to isocitrate dehydrogenase (IcdA) [15].

As acetate is still considered as an uncommon and poor feedstock for *E. coli* cultivation and is predominately used as a secondary carbon source to sustain cell growth [20], major work in strain engineering is required for effective utilization of it. Herein, we explored strain engineering strategies for exclusive propionate production from acetate in *E. coli* and characterized various genetic and metabolic factors relevant to propionate production. Propionate, a key industrial chemical used in the production of animal feed, antibiotics, herbicides, food preservatives, and plastics [27], was selected as the target product for the following reasons. First, the Sbm operon being genomically activated for driving propionate production is endogenous to *E. coli*, simplifying the overall genetic background of the parental propionogenic (i.e. propionate-producing) strain, which is plasmid-free, as well as facilitating subsequent strain engineering. Second, it was shown that activation of the Sbm operon can lead to high-level propionate production [28]. Third, as propionate became the major fermentative product, metabolite profiling was facilitated.

Conversion of acetate to propionate involves three major metabolic stages, i.e. acetyl-CoA formation, the TCA cycle (via reductive and/or oxidative pathways), and the methylmalonyl-CoA (MM-CoA pathway), with three hypothesized routes in the TCA cycle for metabolism of acetyl-CoA (**Figure 1**). Briefly, Route A begins with acetyl-CoA entering the TCA cycle through fusion with glyoxylate or oxaloacetate (OAA) and proceeds through the oxidative TCA cycle to succinyl-CoA. Route B utilizes the glyoxylate bypass to generate succinate followed by reduction to succinyl-CoA. Route C is the full reductive branch of the TCA cycle from OAA or malate to succinyl-CoA. The three routes merge at the node of succinyl-CoA, which enters the MM-CoA pathway. For cell growth with acetate as the sole carbon, a balance between carbon conservation and energy generation should also be achieved. Note that carbon can be conserved based on a combination of the oxidative TCA cycle and glyoxylate bypass, whereas energy can be generated using decarboxylation reactions coupled with NAD(P)H synthesis (**Figure 1**). Based on this metabolic network, key genes/proteins involved in driving or regulating a selection of conversion steps were manipulated to investigate their effects on acetate utilization and propionate production. The study not only demonstrated the potential of acetate as a feedstock but also offered alternate bioprocessing strategies for more effective and economical biomanufacturing.

Figure 1. Overview of acetate metabolism, identified routes to propionate, and genetic manipulations. A red 'X' indicates inactivation of a corresponding gene or enzyme complex component and a green '↑' indicates overexpression of the corresponding genes. A superscript "c" or "e" indicate involvement in carbon conservation or an energy generating reaction, respectively. Arrow colors represent routes to propionate: blue - Route A; yellow-Route B; orange-Route C, and dashed arrows represent catabolic pathway reactions. Acetyl-CoA formation enzymes: AckA, acetate kinase; Pta, phosphate acetyltransferase; Acs, acetyl-CoA synthetase. TCA cycle enzymes: Mdh, malate dehydrogenase; GltA, citrate synthase; and AcnAB citrate hydro-lyase/D-*thero*-isocitrate hydro-lyase.; IcdA, isocitrate dehydrogenase; and SucAB, 2-oxoglutarate dehydrogenase; SucCD, succinyl-CoA synthetase; SdhCDAB, succinate:quinone oxidoreductase complex; FumABC, fumarases. Glyoxylate bypass enzymes: AceA; isocitrate lyase; AceB, malate synthase A; and GlcB, malate synthase G. MM-CoA pathway enzymes: Sbm, methylmalonyl-CoA mutase; ygfG, methylmalonyl-CoA decarboxylase. PEP-pyruvate pathway enzymes: AceEF, pyruvate dehydrogenase; MaeB/SfcA, malate dehydrogenase; PykAF, pyruvate kinase; PpsA, phosphoenolpyruvate synthase; Ppc, phosphoenolpyruvate carboxylase; and PckA, phosphoenolpyruvate carboxykinase. Abbreviations: phosphoenolpyruvate (PEP), oxaloacetate (OAA), isocitrate (ICT), α-ketoglutarate (α-KG), methylmalonyl-CoA (MM-CoA).

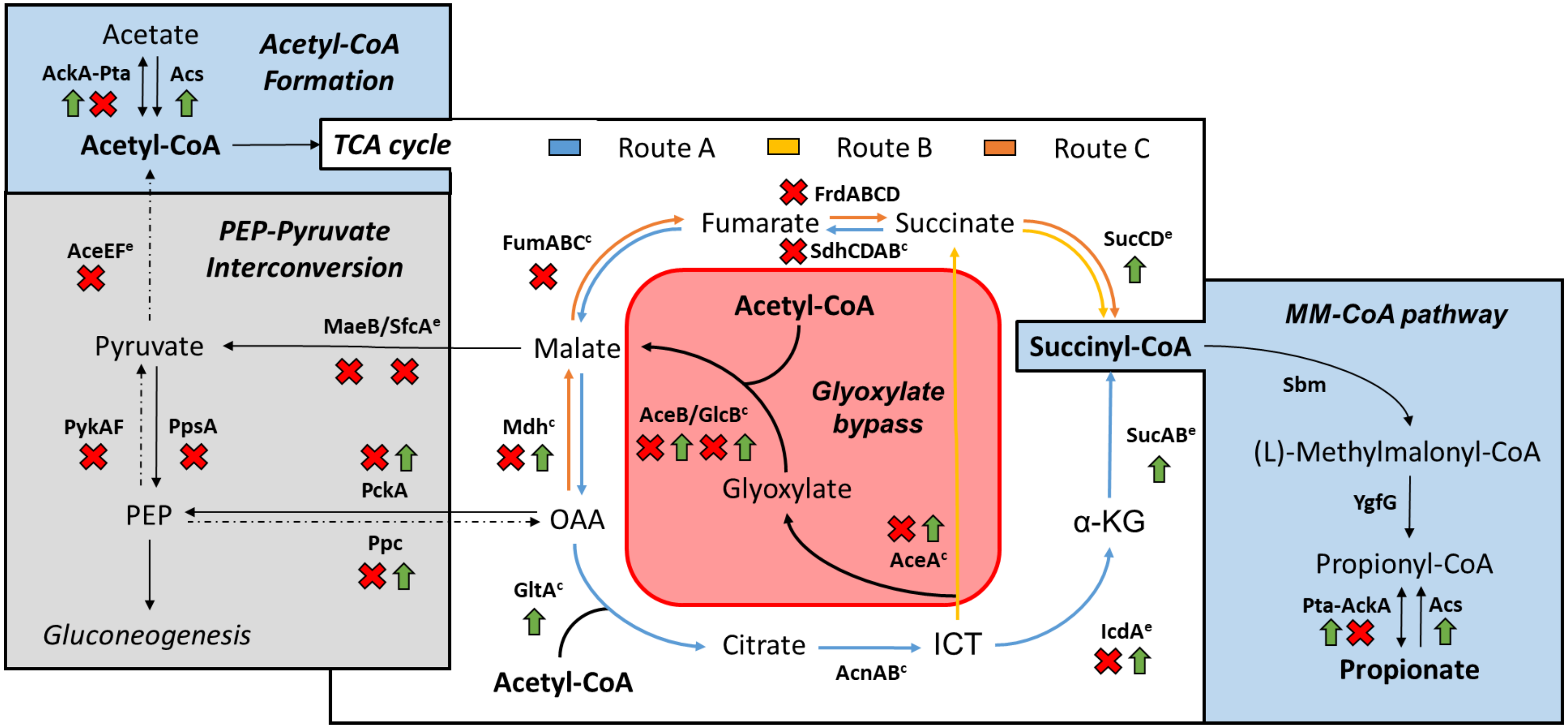

Acetate
AckA-Pta
Acs
Acetyl-CoA Formation
Acetyl-CoA
TCA cycle
Route A
Route B
Route C
AceEF[e]
PEP-Pyruvate Interconversion
Pyruvate
MaeB/SfcA[e]
PykAF
PpsA
PckA
PEP
Ppc
Gluconeogenesis
FrdABCD
Fumarate
Succinate
SdhCDAB[c]
FumABC[c]
SucCD[e]
Acetyl-CoA
Malate
Glyoxylate bypass
Succinyl-CoA
MM-CoA pathway
Sbm
Mdh[c]
AceB/GlcB[c]
SucAB[e]
(L)-Methylmalonyl-CoA
Glyoxylate
YgfG
OAA
α-KG
AceA[c]
Propionyl-CoA
GltA[c]
Pta-AckA
Acs
IcdA[e]
Citrate
ICT
Propionate
AcnAB[c]
Acetyl-CoA

Chapter 2 – Materials and methods

2.1 – Bacterial strains and plasmids

E. coli strains, plasmids and DNA primers used in this study are listed in **Table 1.** Standard recombinant DNA technologies for molecular cloning were applied [29]. *Phusion* and *Taq* DNA polymerases were obtained from New England Biolabs (Ipswich, MA, USA). All synthesized oligonucleotides were obtained from Integrated DNA Technologies (Coralville, IA, USA). DNA sequencing was conducted by the Centre for Applied Genomics at the Hospital for Sick Children (Toronto, Canada). *E. coli* BW25141 was the parental strain for derivation of all mutant strains in this study and *E. coli* DH5α was used for molecular cloning.

Activation of the genomic Sbm operon to form propionogenic *E. coli* (CPC-Sbm) was described previously [30]. Gene mutations were introduced into CPC-Sbm by P1 phage transduction [29] using the appropriate Keio Collection strains (The Coli Genetic Stock Center, Yale University, New Haven, CT, USA) as donors [31]. Elimination of the co-transduced flippase recognition site (FRT)-Km^R-FRT cassette was conducted according to a previous protocol using pCP20, a temperature sensitive plasmid expressing a flippase (Flp) recombinase [32]. The genotypes of derived mutant strains were confirmed by whole-cell colony polymerase chain reaction (PCR) using the appropriate "verification" primer sets listed in **Table 1**.

Table 1. List of E. coli strains and plasmids used in this study.

Name	Description, relevant genotype or primer sequence (5'→3')	Reference
***E. coli* host strains**		
DH5α	F−, *endA1, glnV44, thi-1, recA1, relA1, gyrA96, deoR, nupG φ80d lacZΔ M15, Δ(lacZYA – argF) U169, hsdR17(rK-mK +), λ-*	Lab stock
MC4100	F-, [*araD139*]B/r, Del(*argF-lac*)169, λ—, e14-, *flhD5301*, Δ(*fruK-yeiR*)*725*(*fruA25*), *relA1*, *rpsL150*(strR), *rbsR22*, Del(*fimB-fimE*)632(::IS1), *deoC1*	Casadaban [33]
BW25141	F⁻, Δ(*araD-araB*)567, Δ*lacZ4787*(::*rrnB-3*), Δ(*phoB-phoR*)*580*, λ-, *galU95*, Δ*uidA3*::pir+, *recA1*, *endA9*(del-ins)::FRT, *rph-1*, Δ(*rhaD-rhaB*)*568*, *hsdR514*	Datsenko and Wanner [34]
BW25113	F⁻, Δ(*araD-araB*)*567*, Δ*lacZ4787*(::*rrnB-3*), λ⁻, *rph-1*, Δ(*rhaD-rhaB*)*568*, *hsdR514*	Datsenko and Wanner [34]
BW-ΔldhA	BW25113Δ*ldhA* null mutant	Srirangan et al. [35]
CPC-Sbm	BW-Δ*ldhA*, P_{trc}::*sbm* (i.e. with the FRT -P_{trc} cassette replacing the 204-bp upstream of the Sbm operon)	Srirangan et al. [36]
CPC-SbmΔ*pta*	BW-Δ*ldhA*, Δ*pta,* P_{trc}::*sbm*	Srirangan et al. [36]
CPC-SbmΔ*aceF*	BW-Δ*ldhA*, Δ*aceF,* P_{trc}::*sbm*	This study
CPC-SbmΔ*pykF*	BW-Δ*ldhA*, Δ*pykF,* P_{trc}::*sbm*	This study
CPC-SbmΔ*ppsA*	BW-Δ*ldhA*, Δ*ppsA,* P_{trc}::*sbm*	This study
CPC-SbmΔ*maeB*	BW-Δ*ldhA*, Δ*maeB,* P_{trc}::*sbm*	This study

CPC-SbmΔ*sfcA*	BW-Δ*ldhA*, Δ*sfcA*, P_{trc}::*sbm*	This study
CPC-SbmΔ*pckA*	BW-Δ*ldhA*, Δ*pckA*, P_{trc}::*sbm*	This study
CPC-SbmΔ*ppc*	BW-Δ*ldhA*, Δ*ppc*, P_{trc}::*sbm*	This study
CPC-SbmΔ*mdh*	BW-Δ*ldhA*, Δ*mdh*, P_{trc}::*sbm*	This study
CPC-SbmΔ*icdA*	BW-Δ*ldhA*, Δ*icdA*, P_{trc}::*sbm*	This study
CPC-SbmΔ*frdB*	BW-Δ*ldhA*, Δ*frdB*, P_{trc}::*sbm*	This study
CPC-SbmΔ*sdhA*	BW-Δ*ldhA*, Δ*sdhA*, P_{trc}::*sbm*	This study
CPC-SbmΔ*fumA*	BW-Δ*ldhA*, Δ*fumA*, P_{trc}::*sbm*	This study
CPC-SbmΔ*fumC*	BW-Δ*ldhA*, Δ*fumC*, P_{trc}::*sbm*	This study
CPC-SbmΔ*aceA*	BW-Δ*ldhA*, Δ*aceA*, P_{trc}::*sbm*	This study
CPC-SbmΔ*aceB*	BW-Δ*ldhA*, Δ*aceB*, P_{trc}::*sbm*	This study
CPC-SbmΔ*glcB*	BW-Δ*ldhA*, Δ*glcB*, P_{trc}::*sbm*	This study
CPC-SbmΔ*arcA*	BW-Δ*ldhA*, Δ*arcA*, P_{trc}::*sbm*	This study
CPC-SbmΔ*fnr*	BW-Δ*ldhA*, Δ*fnr*, P_{trc}::*sbm*	This study
CPC-SbmΔ*aceK*	BW-Δ*ldhA*, Δ*aceK*, P_{trc}::*sbm*	This study

CPC-SbmΔ*iclR*	BW-Δ*ldhA*, Δ*iclR,* P_{trc}::*sbm*	This study
CPC-SbmΔ*aceB*Δ*glcB*	BW-Δ*ldhA*, Δ*aceB,* Δ*glcB,* P_{trc}::*sbm*	This study
CPC-Sbm-UE1	CPC-Sbm/pK-Acs(EC)	This study
CPC-Sbm-UE2	CPC-Sbm/pK-AckAPta	This Study
CPC-Sbm-UE3	CPC-Sbm/pK-Acs(BS)	This study
CPC-Sbm-TCA1	CPC-Sbm/pK-MdhGltA	This study
CPC-Sbm-TCA2	CPC-Sbm/pK-IcdASucAB	This study
CPC-Sbm-TCA3	CPC-Sbm/pB-SucCD	This study
CPC-Sbm-GLX1	CPC-Sbm/pK-AceABK	This study
CPC-Sbm-PEP1	CPC-Sbm/pT-Ppc	This study
CPC-Sbm-PEP2	CPC-Sbm/pT-PckA	This study
Plasmids		
pCP20	FLP^{+}, λ $cI857^{+}$, λ p_R Rep(pSC101 $ori)^{ts}$, Ap^R,Cm^R	Cherepanov and Wackernagel [32]
pKD46	$RepA101^{ts}$ ori, Ap^R, *araC*-P_{araB}::*gam-bet-exo*	Datsenko and Wanner [34]
pTrc100cat	ColE1 ori, Cm^R, P_{trc}	Sukhija et al. [37]

pKD3	R6K-γ ori, Ap^R, FRT-Cm^R-FRT	Datsenko and Wanner [34]
pK184	p15A ori, Km^R, P_{lac}::*lacZ'*	Jobling and Holmes [38]
pBBR1MC-3	broad host range ori, Tc^R, P_{lac}::*lacZ'*	Kovach et al. [39]
pK-Acs(EC)	Derived from pK184, P_{lac}:: *acs*(EC)	This study
pK-Acs(BS)	Derived from pK184, P_{lac}:: *acs*(BS)	This study
pK-AckAPta	Derived from pK184, P_{lac}:: *ackApta*	This study
pK-MdhGltA	Derived from pK184, P_{lac}:: *mdh*:: *gltA*	This study
pK-IcdASucAB	Derived from pK184, P_{lac}:: *icdA*:: *sucAB*	This study
pB-SucCD	Derived from pBBR1MCS-3, *araC*-P_{araB} ::*sucCD*	Srirangan et al. [35]
pK-AceABK	Derived from pK184, P_{lac}:: *aceABK*	This study
pT-PckA	Derived from pTrc100cat, P_{trc}:: *pckA*	This study
pT-Ppc	Derived from pTrc100cat, P_{trc}:: *ppc*	This study
Primers		
v-ldhA	GATAACGGAGATCGGGAATGATTAA; GGTTTAAAAGCGTCGATGTCCAGTA	Srirangan et al. [35]
v-pta	GGCATGAGCGTTGACGCAATCA; CAGCTGTACGCGGTGATACTCAGG	Srirangan et al. [40]

v-aceF	TGCGTCACCACTTCGAAGTT; GGATTTCTGGGTGCAGCAAG	This study
v-pykF	GGACTGTAGAACTCAACGAC; GCGTTCGATGCTTCTTTGAG	This study
v-ppsA	CGCGAACTACCTCAGGTA AA; CGAAGAGAGCAGATTTGCGC	This study
v-maeB	TGGAGAGATATTCGCTGTGG; GACAGGCATGGTATTGCTGG	This study
v-sfcA	TCAGTGAGCGCAGTGTTTTA; AACCCAACCGGCAGAAAACG	This study
v-pckA	CCGTTTCGTGACAGGAATCA; AACGGGATGCTGGAGCTTGG	This study
v-ppc	CGCCGAATGTAACGACAATTCC; TGCTGAAGCGATTTCGCAGC	This study
v-mdh	ATCTCTGCTCTGGAGACGAT; GCGCTAATGCATAAGCGACTGT	This study
v-icdA	AACGCGCATCTTTCATGACG; AGAACTACCACCTGACCGGC	This study
v-frdB	TCAATGCTGAACCACACAGC; TGGACGAAGGTTGCACCGAG	This study
v-sdhA	CTCTGCGTTCACCAAAGTGT; ACACACCTTCACGGCAGGAG	This study
v-fumA	TATCTGCCGGGACATCAATC; CGGGAAGTAACCTGGAGCCG	This study
v-fumC	AA ACAAGTCCAACACGCCTG; CAATGCACCCGCTGTGTGAA	This study
v-aceA	ATGCTGGGCGAAGAGATGAA; GCCCTCATCAGGAGCAGAGA	This study
v-aceB	TTTCCGAAACGTACCTCAGC; CATTTTCGCTGCGCCCAGTT	This study

v-glcB	GCAGACGCAGAGTATCGTTA; ACAACGGACGTACCGCGTTC	This study
v-arcA	TTGGGAACCAGTGTGCTGGT; ACTGTCGGGTCCTGAGGGAA	This study
v-fnr	GTGCCAGCTTGTTCACACTT; TGGGAACGCCAGCATTGAGA	This study
v-aceK	ACAACAACCGTTGCTGACTG; TTGGCAACACAAAGCCCCAC	This study
v-iclR	GGTGGAATGAGATCTTGCGA; CCGACACGCTCAACCCAGAT	This study
c-pK184	ATGACCATGATTACGAATTCG; AGCTGTTTCCTGTGTGAAATTGTTATCCG	This study
c-pTrc100cat	GGTCTGTTTCCTGTGTGAAATTG; ATGGAATTCGAGCTCGGTAC	This study
g-acsEC	cacacaggaaacagctATGAGCCAAATTCACAAACAC; attcgtaatcatggtcatTTACGATGGCATCGCGATAG	This study
g-aceBS	cacacaggaaacagctATGAACTTGAAAGCGTTACC; attcgtaatcatggtcatTTAATCCTCCATTGTTGACAG	This study
g-ackApta	cacacaggaaacagctATGTCGAGTAAGTTAGTACTGGTTC; attcgtaatcatggtcatTTACTGCTGCTGTGCAGAC	This study
g-mdh	cacacaggaaacagctATGAAAGTCGCAGTCCTC; gtctccttTTACTTATTAACGAACTCTTCGC	This study
g-gltA	ttaataagtaaAAGGAGACCTTAAATGGC; attcgtaatcatggtcatTACAACTTAGCAATCAACCATTAAC	This study
g-icdA	cacacaggaaacagctATGGAAAGTAAAGTAGTTGTTCC; ccttaagcaTTACATGTTTTCGATGATCG	This study
g-sucAB	aaacatgtaaTGCTTAAGGGATCACGATG; attcgtaatcatggtcatCTACACGTCCAGCAGCAG	This study
c-sucCD	ATGAACTTACATGAATATCAGGCAAAACAA; CCCCCCTCGAGTTATTTCAGAACAGTTTTCAGTGCTTCACC	Srirangan et al. [35]

g-aceABK	cacacaggaaacagctATGACTGAACAGGCAACAAC; attcgtaatcatggtcatTCAAAAAAGCATCTCCCC	This study
g-pckA	acacaggaaacagaccATGCGCGTTAACAATGGTTTG; cgagctcgaattccatTTACAGTTTCGGACCAGCC	This study
g-ppc	acacaggaaacagaccATGAACGAACAATATTCCG; cgagctcgaattccatTTAGCCGGTATTACGCATAC	This study

Notation for primers: **v**- verification primer, **c**- cloning primer, and **g**-Gibson DNA assembly primer. Homology arms are in lower case

For episomal overexpression, single genes (i.e. *pckA, ppc, acs, mdh, gltA, icdA*) or operon genes (i.e. *sucAB,* and *aceABK*) were PCR-amplified from the genomic DNA of *E. coli* BW25141 using appropriate Gibson assembly primer sets listed in **Table** 1. To generate plasmid pK-Acs(EC) harboring the *acs* gene under the control of the P_{lac} promoter, the *acs* amplicon was fused with the PCR-linearized pK184 (linearized using primer set c-pK184) using the Gibson enzymatic assembly [41]. A clone with the correct transcriptional orientation of the *acs* fragment with respect to the P_{lac} promoter was selected and verified by DNA sequencing. The same approach was used to generate pK-Acs(BS), pK-AckAPta, pK-MdhGltA, pK-IcdASucAB, pK-AceABK, pT-PckA, and pT-Ppc. Note that the PCR-linearized pTrc100cat replaced pK184 in plasmids pT-PckA, pT-Ppc, and the *acs* gene in pK-Acs(BS) was PCR-amplified from the genomic DNA of *Bacillus subtilis* 1A751. Derivation of plasmid pB-SucCD from pBBR1MC-3 was previously described [42].

2.2 – Media and cultivation conditions

All medium components were obtained from Sigma-Aldrich Co. (St Louis, MO, USA) except yeast extract and tryptone which were obtained from BD Diagnostic Systems (Franklin Lakes, NJ, USA). Media were supplemented with antibiotics as required (50 μg/mL kanamycin, 36 μg/mL chloramphenicol, or 10 μg/mL tetracycline). All propionate producing *E. coli* strains (stored as glycerol stocks at -80°C) were streaked on lysogeny broth (LB) agar plates with appropriate antibiotics and incubated at 37°C for 16 h. Single colonies were picked from LB plates to inoculate 25-mL LB medium (10 g/L tryptone, 5 g/L yeast extract, and 5 g/L NaCl) with appropriate antibiotics in 125-mL conical flasks. Overnight cultures were shaken at 37°C and 275 rpm in a rotary shaker (New Brunswick Scientific, NJ, USA) and used as seed cultures to inoculate 200 mL LB media at 1% (v/v) with appropriate antibiotics in 1-L conical flasks. This second seed culture was shaken at 37°C and 275 rpm until an optical density at 600 (OD_{600}) of 0.8 was achieved. Cells were then harvested by centrifugation at 8,000×g and 20 °C for 8 min and resuspended in 10-mL modified M9 production media. The suspended culture was transferred into a 125-mL screw cap plastic production flasks and sealed. Unless otherwise specified the modified M9 production medium contained 20 g/L acetate, 5 g/L yeast extract, 10 mM $NaHCO_3$, 1 mM $MgCl_2$, 0.2 µM cyanocobalamin (vitamin B12), 5th dilution of M9 salts mix (33.9 g/L Na_2HPO_4, 15 g/L KH_2PO_4, 5 g/L NH_4Cl, 2.5 g/L NaCl) and 1,000th dilution of Trace Metal Mix A5 (2.86 g/L H3BO3, 1.81 g/L MnCl2•4H2O, 0.222 g/L ZnSO4•7H2O, 0.39 g/L Na2MoO4•2H2O, 79 µg/L CuSO4•5H2O, 49.4 µg/L Co(NO3)2•6H2O), and supplemented with 0.1 mM isopropyl β-D-1-thiogalactopyranoside (IPTG). All cultivation experiments were performed in triplicate.

2.3 – Offline analysis

Culture samples were appropriately diluted with saline for measuring the cell density in OD_{600} using a spectrophotometer (DU520, Beckman Coulter, Fullerton, CA). Cell-free supernatant was collected and filter-sterilized for titer analysis of acetate and propionate using an HPLC (LC-10AT, Shimadzu, Kyoto, Japan) with a refractive index detector (RID-10A, Shimadzu, Kyoto, Japan) and a chromatographic column (Aminex HPX-87H, Bio-Rad Laboratories, CA, USA). The column temperature was maintained at 35 °C and the mobile phase was 5 mM H_2SO_4 (pH 2.0) running at 0.6 mL/min. The RID signal was acquired and processed by a data processing unit (Clarity Lite, DataApex, Prague, The Czech Republic).

Time-dependent data (provided in supplementary information) was converted to time-independent data using acetate concentration as the independent variable. For each strain, time samples were grouped based on similar acetate concentrations in a way which facilitated representation from each replicate. Acetate concentration and theoretical maximum propionate yield (referred to as "yield") values from the data points within each grouping were averaged and plotted against one another. The resulting plots allowed the use of a common axis (i.e. acetate concentration) to compare between strains, even with vastly different cultivation times. For each grouping, the horizontal error bars represent the standard deviation of the acetate concentration values, and the vertical error bars represent the standard deviation of the propionate yield values. Note that the number of data points within each grouping was not consistent within or between strains, leading to variable degrees of freedom when calculating the standard deviation. Groups with overlapping horizontal error bars are treated as direct comparisons between the respective strains. In situations involving no or multiple overlapping points, the groups having the smallest difference in their acetate concentrations were used for comparison between those strains.

Chapter 3 – Results

3.1 – Cultivation conditions and strain engineering

CPC-Sbm, in which the genomic Sbm operon was activated and the *ldhA* gene encoding lactate dehydrogenase was inactivated [28], was used as the control strain. Note that blocking lactate production can potentially increase the pool of pyruvate, which is a key intermediate for energy regeneration and gluconeogenesis during acetate metabolism. To assess the feasibility for propionate production from acetate, strains CPC-Sbm and BW-ΔldhA were cultured using acetate as the sole carbon source. Propionate production was observed exclusively in the CPC-Sbm culture, but not BW-ΔldhA (**Figure 2A**). Other common metabolites such as ethanol and succinate were not detected as their production would be unfavorable given the low reductance of acetate and the involvement of acetyl-CoA (i.e. the procurer of ethanol) and succinate within the TCA cycle and glyoxylate bypass during acetate metabolism.

CPC-Sbm was further characterized under various cultivation conditions, particularly the effects of temperature (**Figure 2B**) and initial acetate concentration (**Figure 2C**) on culture performance. While propionate production occurred under both 30°C and 37°C, the 30°C-culture had higher propionate titers. Propionate utilization was also observed as the propionate titer decreased following acetate exhaustion between 6 and 12 hours at 37°C. However, with minimal acetate remaining, the propionate titer doubled between 6 and 12 hours at 30°C, suggesting propionate utilization mainly occurs following acetate exhaustion. To minimize propionate utilization, we increased the initial acetate concentration (**Figure 2C**). Increasing the initial acetate concentration from 10 g/L to 20 g/L did not adversely affect cell growth or propionate production. Further increase to 30 g/L negatively affected cell growth and propionate titer and yield, possibly due to the inhibitory effects of acetate. Therefore, all subsequent cultivations were performed at 30°C with an initial acetate concentration of 20 g/L.

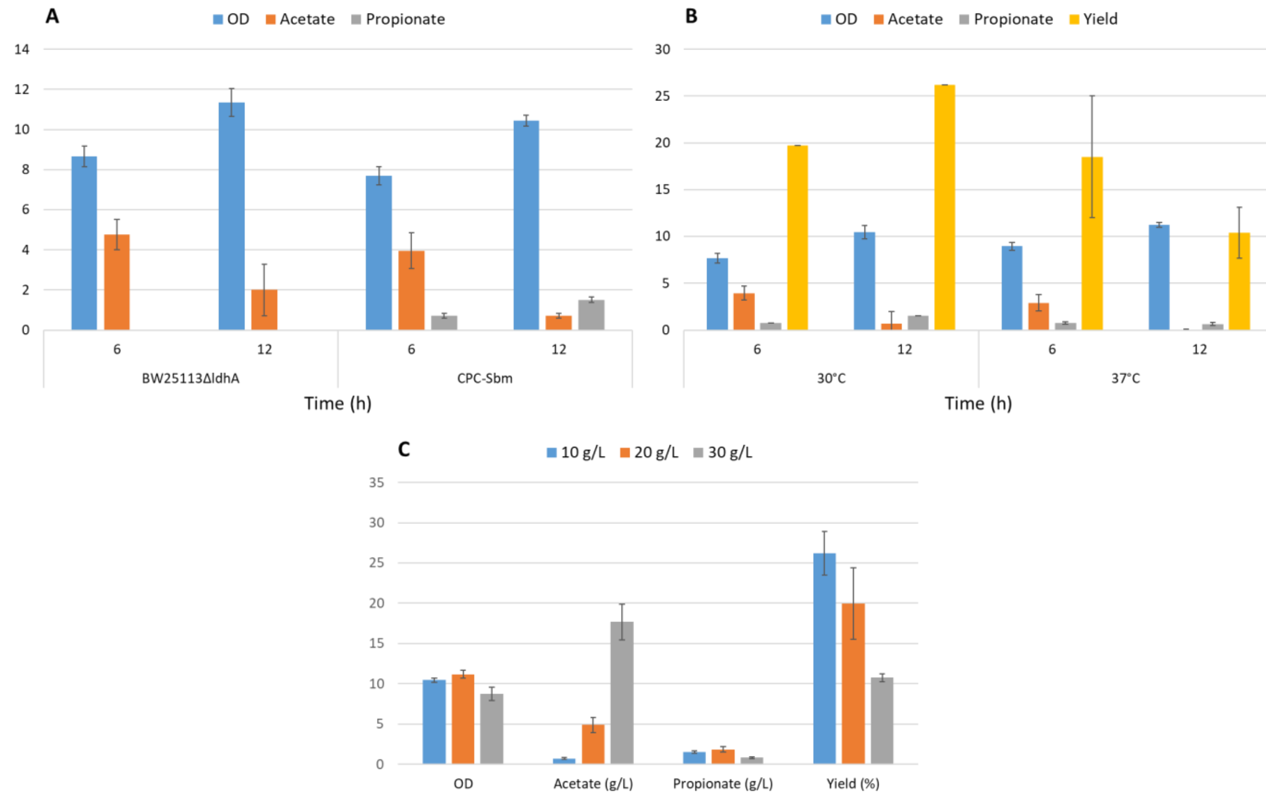

Figure 2. **a** Comparison between BW-Δ*ldhA* and CPC-Sbm for OD values and metabolites following growth on acetate as the sole carbon source at 30°C. **b** Effect of temperature on growth and propionate production in CPC-Sbm and **c** effect of initial acetate concentration on growth and propionate production in CPC-Sbm. OD is optical density measured at 600. Yield is percentage of the theoretical maximum calculated using a molar ratio of 2:1 for acetate to propionate. *Error bars* represent s.d. ($n = 3$).

3.2 – Strain engineering

A selection of *E. coli* genes were identified to be associated with acetate metabolism based on their expression levels when acetate, compared to glucose, was used as the sole carbon [1]. For metabolic engineering of CPC-Sbm, a selection of genes involved in the acetyl-CoA formation, TCA cycle, glyoxylate bypass, and phosphoenolpyruvate (PEP)-pyruvate interconversion pathways, respectively, were manipulated via genomic inactivation or episomal overexpression of them, as outlined in **Table 2** and **Figure 1**. The resulting engineered strains were used for evaluation of their cultivation performance, particularly in terms of cell growth, overall acetate utilization rate (both summarized in **Figure 3**) and propionate production (**Figures 5, 6, 8, and 9**).

Table 2. List of inactivated metabolic genes used in this study. Gene expression change is relative to growth on glucose as reported previously [1]. Product refers to the enzyme or enzyme complex corresponding to the mentioned gene(s). Having an A and/or B indicates involvement in either the pyruvate ('A') or OAA ('B') pathways in PEP-pyruvate interconversion (**Figure 8**). Involvement in carbon conservation or an energy generation is indicated by (+) and not involved is indicated by (-) (outlined in **Figure 1**).

Figure 3. Results for overall acetate utilization rate and maximum OD_{600} for CPC-Sbm and engineered strains containing **a** an inactivated gene involved in the TCA cycle and/or glyoxylate bypass, **b** an inactivated gene involved in gluconeogenesis or acetyl-CoA formation, or **c** overexpressed gene(s). CPC-Sbm and all genetically modified strains following cultivated using 20 g/L acetate at 30°C. Acetate utilization rates are averages calculated using cultivation times and associated acetate concentrations. Maximum OD_{600} was determined using the OD_{600} values observed during each strain's respective cultivation. OD_{600} is optical density measured at 600. *Error bars* represent s.d. (n = variable)

	Gene	Expression Change	Product	PEP Interconversion	Carbon Conservation	Energy Generating
Acetyl-CoA formation	*ackA*	0.51	Acetate kinase (AckA)	A and B	-	-
	pta	0.65	Phosphate acetyltransferase (Pta)	A and B	-	-
	acs	9.5	Acetyl-CoA synthase (Acs)	A and B	-	-
TCA cycle	*mdh*	3.9	Malate dehydrogenase (Mdh)	B	+	-
	gltA	4.9	Citrate synthase (GltA)	-	+	-
	icdA	1.8	Isocitrate dehydrogenase (IcdA)	-	-	+
	sucAB	1.6-2.2	α-ketoglutarate dehydrogenase (SucAB)	-	-	+
	sucCD	2.8-3.1	Succinyl-CoA synthetase (SucCD)	-	-	+
	sdhCDAB	1.0-2.4	Succinate dehydrogenase (SdhCDAB)	-	+	-
	frdABCD	1.1-1.5	Fumarate reductase (FrdABCD)	-	-	-
	fumA	3.5	Fumarase A (FumA)	-	+	-
	fumC	2.1	Fumarase C (FumC)	-	+	-
Glyoxylate bypass	*aceA*	15-39	Isocitrate lyase (AceA)	-	+	-
	aceB	N/A	Malate synthase A (AceB)	-	+	-
	glcB	17	Malate synthase G (GlcB)	-	+	-
PEP-pyruvate	*maeB*	5.1	Malate dehydrogenase (MaeB) NAD(P) requiring	A	-	+
	sfcA	1.7	Malate dehydrogenase (SfcA) NAD requiring	A	-	+
	pckA	8.3	Phosphoenolpyruvate carboxykinase (AckA)	B	-	+
	ppc	0.28	Phosphoenolpyruvate carboxylase (Ppc)	B	-	-
	ppsA	13	Phosphoenolpyruvate synthetase (PpsA)	A	-	-
	pykF	0.22	Pyruvate kinase I	A	-	+
	aceEF	0.29-0.44	Pyruvate dehydrogenase	-	-	+

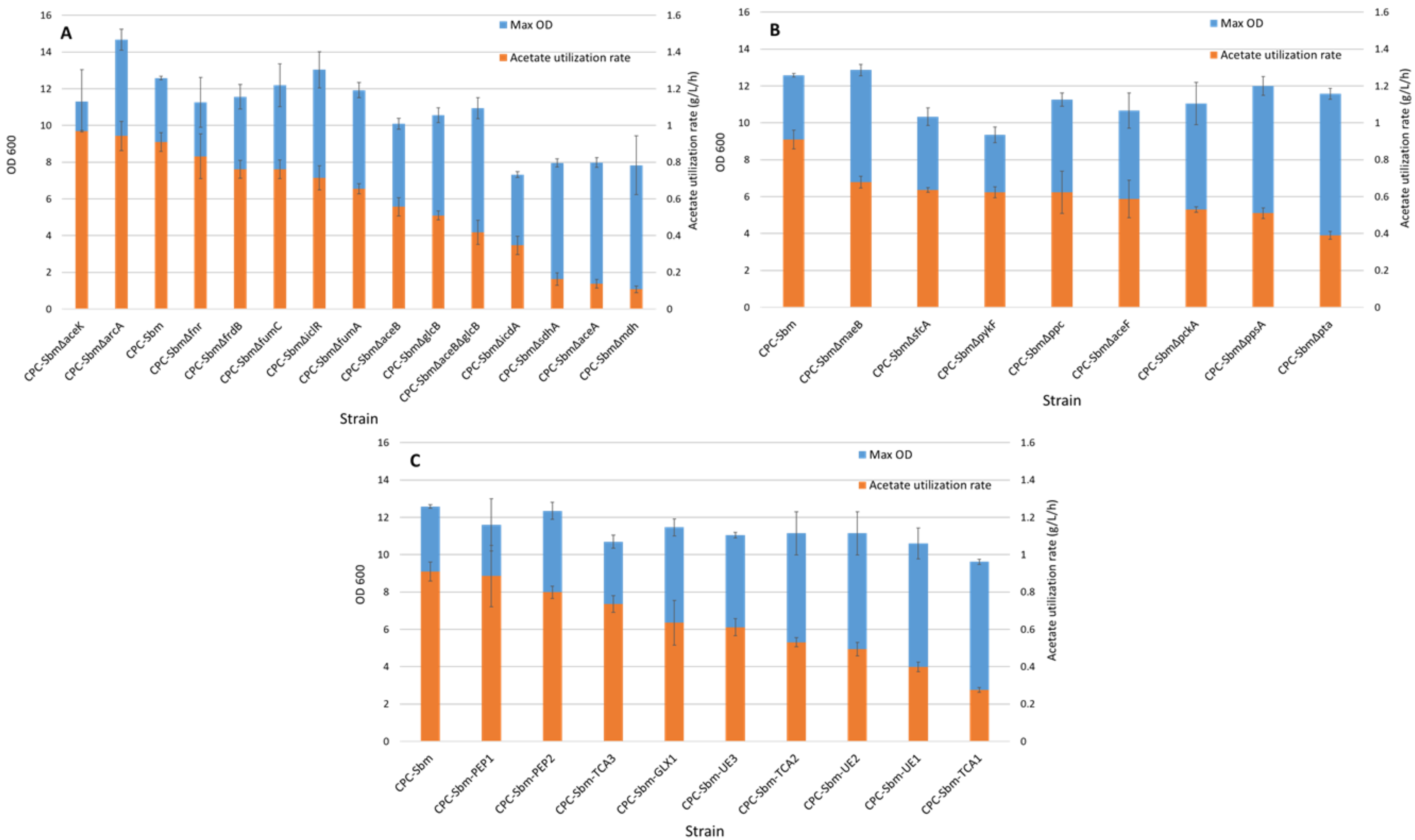
A
B
C
Max OD
Acetate utilization rate
OD 600
Acetate utilization rate (g/L/h)
Strain
0
2
4
6
8
10
12
14
16
0.2
0.4
0.6
0.8
1
1.2
1.4
1.6
CPC-SbmΔaceK
CPC-SbmΔarcA
CPC-Sbm
CPC-SbmΔfnr
CPC-SbmΔfrdB
CPC-SbmΔfumC
CPC-SbmΔiclR
CPC-SbmΔfumA
CPC-SbmΔaceB
CPC-SbmΔglcB
CPC-SbmΔaceBΔglcB
CPC-SbmΔicdA
CPC-SbmΔsdhA
CPC-SbmΔaceA
CPC-SbmΔmdh
CPC-SbmΔmaeB
CPC-SbmΔsfcA
CPC-SbmΔpykF
CPC-SbmΔppc
CPC-SbmΔaceF
CPC-SbmΔpckA
CPC-SbmΔppsA
CPC-SbmΔpta
CPC-Sbm-PEP1
CPC-Sbm-PEP2
CPC-Sbm-TCA3
CPC-Sbm-GLX1
CPC-Sbm-UE3
CPC-Sbm-TCA2
CPC-Sbm-UE2
CPC-Sbm-UE1
CPC-Sbm-TCA1

3.3 – Manipulation of acetyl-CoA formation genes

Although two pathways are present for acetate conversion to acetyl-CoA coupled with ATP consumption (**Figure 4**), only the Acs pathway is activated in conjunction with other acetate utilization pathways, such as the glyoxylate bypass, and is regulated both transcriptionally and post translationally [26]. On the other hand, the AckA-Pta pathway is primarily involved in acetate synthesis during growth on other carbon sources though the reaction is reversible [21]. We manipulated the genes associated with both acetyl-CoA formation pathways and the results are summarized in **Figure 5**. Compared to the control strain (i.e. CPC-Sbm), inactivation of *pta* significantly reduced the overall acetate utilization rate (0.91 vs 0.39 g/L/h) with no propionate being detected in CPC-SbmΔ*pta*, implying a critical role for the AckA-Pta pathway in propionate production. On the other hand, overexpression of the native *acs* gene in CPC-Sbm-UE1 slightly reduced the propionate yield but significantly reduced the overall acetate utilization rate (0.40 g/L/h). While overexpression of the native *ackA-pta* operon in CPC-Sbm-UE2 or the *acs* gene from *B. subtilis* in CPC-Sbm-UE3 increased the overall propionate yield by more than 20%, both strains had reduced overall acetate utilization rates.

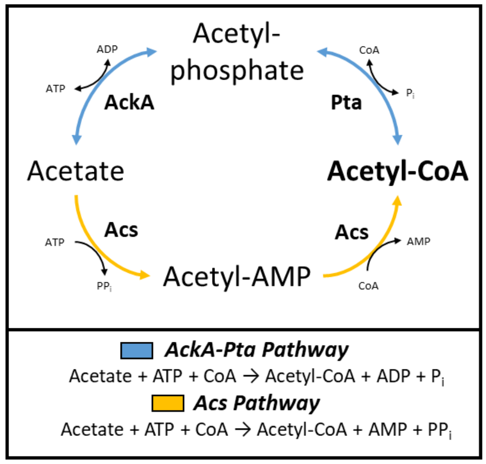

Figure 4. Acetate conversion to acetyl-CoA by AckA-Pta and Acs. Net reactions are shown below the pathways. Arrows color represents the AckA-Pta (blue) and Acs pathway (yellow).

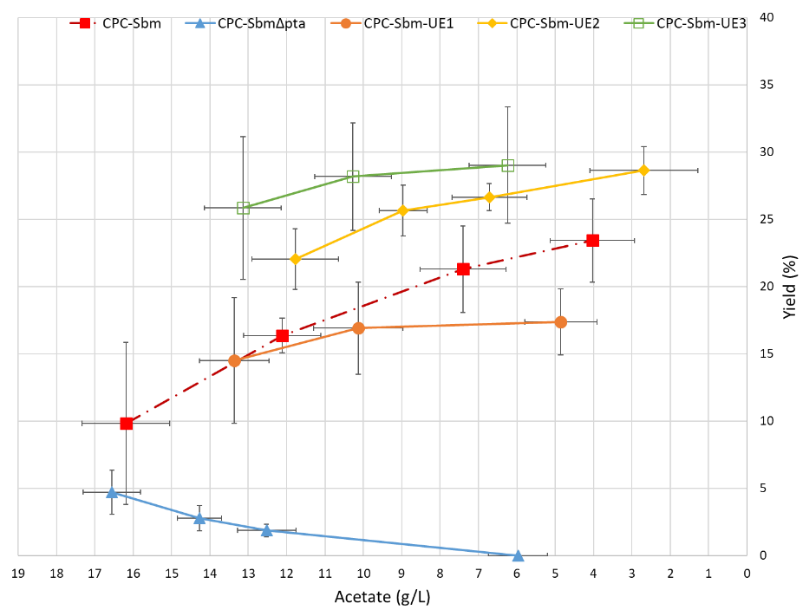

Figure 5. Time-independent propionate yield data for strains containing a manipulated acetyl-CoA formation pathway. Symbols represent averages of data points (i.e. acetate concentration and yield) contained within groupings based on similar acetate concentrations determined for each strain. *Vertical errors bars* represent s.d. in yield (*n* = variable). *Horizontal error bars* represent s.d. in acetate concentration (*n* = variable).

3.4 – Manipulation of TCA cycle and glyoxylate bypass genes

Depending on culture conditions, *E. coli* often utilizes the oxidative branch of the TCA cycle for energy generation or the reductive branch for mixed acid fermentation [43]. However, during acetate metabolism, the activation of the glyoxylate bypass adds complexity in carbon flow. We identified three potential routes, i.e. Route A, B, and C, within the TCA cycle to for the conversion of acetyl-CoA to succinyl-CoA, which enters the MM-CoA pathway for propionate production (**Figure 1**). Key genes within the TCA cycle and glyoxylate bypass were manipulated to determine the metabolic importance of each route to propionate production and the results are summarized in **Figures 6**. Among these genes, inactivation of *mdh*, *aceA*, *sdhA*, and *icdA* significantly reduced the overall acetate utilization rate and biomass generation compared to the control strain. In particular, CPC-SbmΔ*mdh*, CPC-SbmΔ*aceA*, and CPC-SbmΔ*sdhA* had the highest reductions with their overall acetate utilization rate and final cell density being less than 0.16 g/L/h and 8.0 OD_{600}, respectively, implying critical roles for these genes during growth on acetate. Such impacts appear to be less severe for CPC-SbmΔ*icdA*. Inactivation of glyoxylate bypass genes *aceB* and *glcB* also reduced the overall acetate utilization rate. Overexpression of oxidative TCA cycle genes *icdA*::*sucAB* in CPC-Sbm-TCA2 or glyoxylate bypass genes *aceABK* in CPC-SbmGLX1 also reduced the overall acetate utilization rate. Inactivation of reductive TCA cycle genes *frdB, fumA*, and *fumC* in CPC-SbmΔ*frdB*, CPC-SbmΔ*fumA*, and CPC-SbmΔ*fumC*, respectively, or overexpression of *sucCD* in CPC-Sbm-TCA3 minimally reduced the overall acetate utilization rate relative to the control strain, suggesting minor roles for these genes for acetate metabolism.

Manipulation of the TCA cycle and glyoxylate bypass also resulted in major changes in propionate production. Compared to the control strain, with an overall propionate yield up to 23.4%, propionate production was nearly abolished in CPC-SbmΔ*icdA*, CPC-SbmΔ*mdh*, and

CPC-SbmΔ*aceA* with the overall propionate yields being less than 4%. While the propionate yield was minimally affected by single knockout of *aceB* or *glcB*, the double mutant CPC-SbmΔ*aceB*Δ*glcB* had a noticeably hindered ability to produce propionate. Propionate production was also minimally altered in strains CPC-SbmΔ*frdB*, CPC-SbmΔ*fumA,* and CPC-SbmΔ*fumC*. While the propionate yields of CPC-Sbm-TCA3, CPC-Sbm-GLX1, and CPC-SbmΔ*sdhA* were initially significantly higher than the control strain, these high yields subsequently returned to the control strain levels by the end of the cultivation. Noticeably, CPC-Sbm-TCA-1 and CPC-Sbm-TCA2 maintained high-level propionate production throughout their cultivation, ending with respective propionate yields 20% and 34% higher than CPC-Sbm. These results imply overexpression of oxidative TCA cycle genes can drive additional carbon flux into the MM-CoA pathway for propionate production.

Figure 6. Time-independent propionate yield data for strains with **a** an inactivated TCA cycle gene, **b** overexpressed TCA cycle genes, or **c** a manipulated glyoxylate bypass. Symbols represent averages of data points (i.e. acetate concentration and yield) contained within groupings based on similar acetate concentrations determined for each strain. *Vertical errors bars* represent s.d. in yield (*n* = variable). *Horizontal error bars* represent s.d. in acetate concentration (*n* = variable).

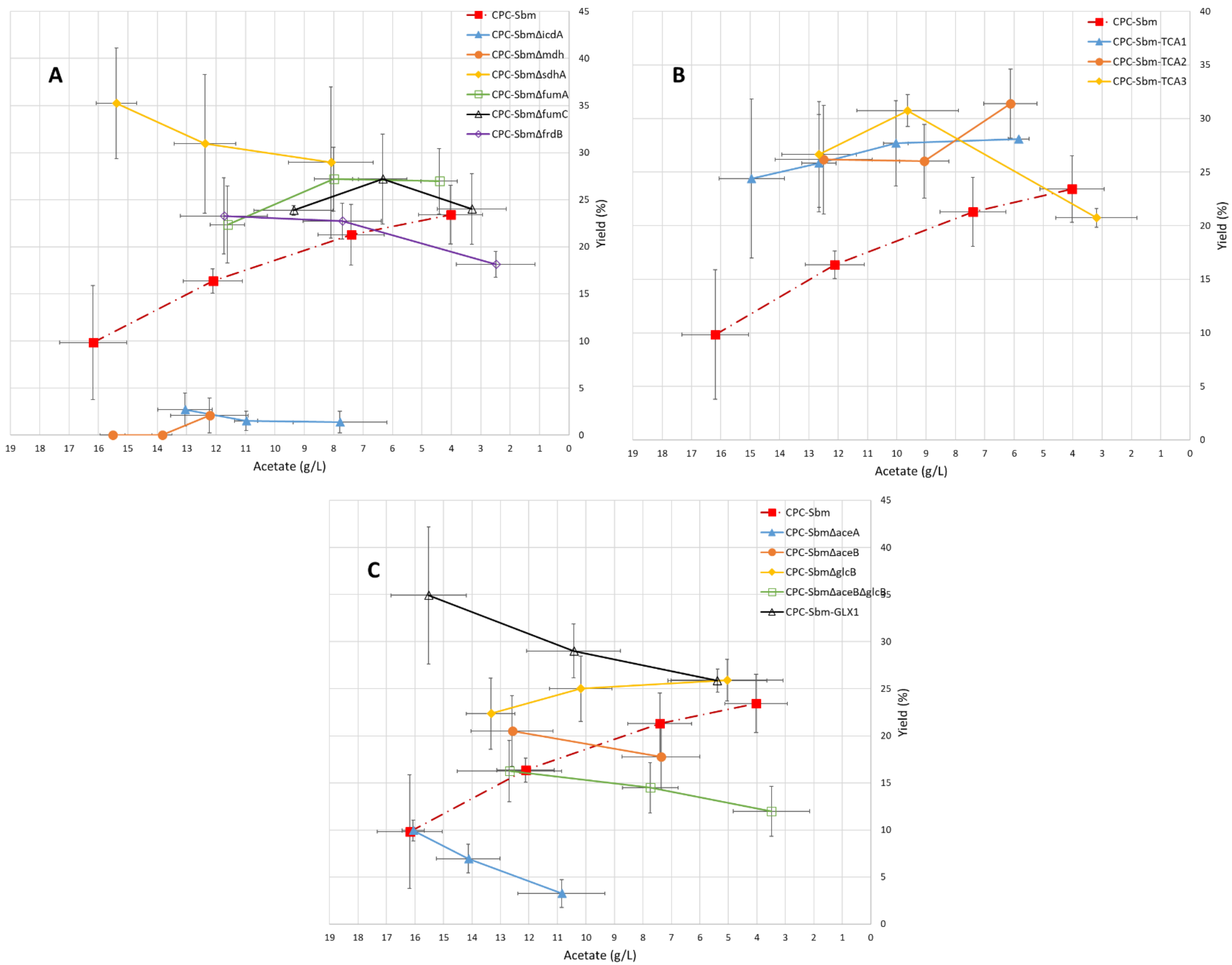

A
CPC-Sbm
CPC-SbmΔicdA
CPC-SbmΔmdh
CPC-SbmΔsdhA
CPC-SbmΔfumA
CPC-SbmΔfumC
CPC-SbmΔfrdB
Yield (%)
Acetate (g/L)
B
CPC-Sbm
CPC-Sbm-TCA1
CPC-Sbm-TCA2
CPC-Sbm-TCA3
Yield (%)
Acetate (g/L)
C
CPC-Sbm
CPC-SbmΔaceA
CPC-SbmΔaceB
CPC-SbmΔglcB
CPC-SbmΔaceBΔglcB
CPC-Sbm-GLX1
Yield (%)
Acetate (g/L)

3.5 – Manipulation of PEP-pyruvate pathway genes

In *E. coli*, the intermediates associated with central metabolic pathways are required for various cellular processes and these intermediates are made available via catabolic reactions for most carbon sources. In contrast, acetate metabolism requires gluconeogenesis for the anabolic synthesis of these essential intermediates. The TCA cycle and gluconeogenesis are connected via PEP-pyruvate interconversion. Two distinct pathways exist from the TCA cycle intermediate malate to PEP, proceeding through either OAA or pyruvate (**Figure 7A**) with different catabolic enzymes (**Figure 7B**). All genes involved in PEP-pyruvate interconversion, either anabolic and catabolic ones, were manipulated to determine their effects on growth and propionate production and the results are summarized in **Figure 8**. Compared to the control strain, inactivation of most genes involved in PEP-pyruvate interconversion, including *ppsA*, *pckA*, *aceF*, *ppc*, *pykF*, *maeB*, and *sfcA*, reduced the overall acetate utilization rate. On the other hand, overexpression of *ppc* and *pckA* did not alter the acetate utilization rate relative to CPC-Sbm. Manipulation of PEP-pyruvate interconversion genes also resulted in significant alterations to propionate production. The production was nearly eliminated in CPC-SbmΔ*ppsA*, implying that the conversion from pyruvate to PEP is critical for propionate production when acetate was used as the sole carbon source. Compared to the control strain, the propionate yield was significantly reduced in CPC-Sbm-PEP2 (23.4 vs 4.9%) in which the *ppc* gene was overexpressed. On the other hand, a mild reduction in the propionate yield was observed in CPC-SbmΔ*aceF*, while CPC-Sbm-PEP1, CPC-SbmΔ*pckA*, and CPC-SbmΔ*sfcA* had propionate yields similar to the control strain. Interestingly, the propionate yields of CPC-SbmΔ*pykF*, CPC-SbmΔ*ppc*, and CPC-SbmΔ*maeB* were 26%, 41%, and 45% higher than the control strain, suggesting that the carbon flux was directed into the MM-CoA pathway following inactivation of these genes.

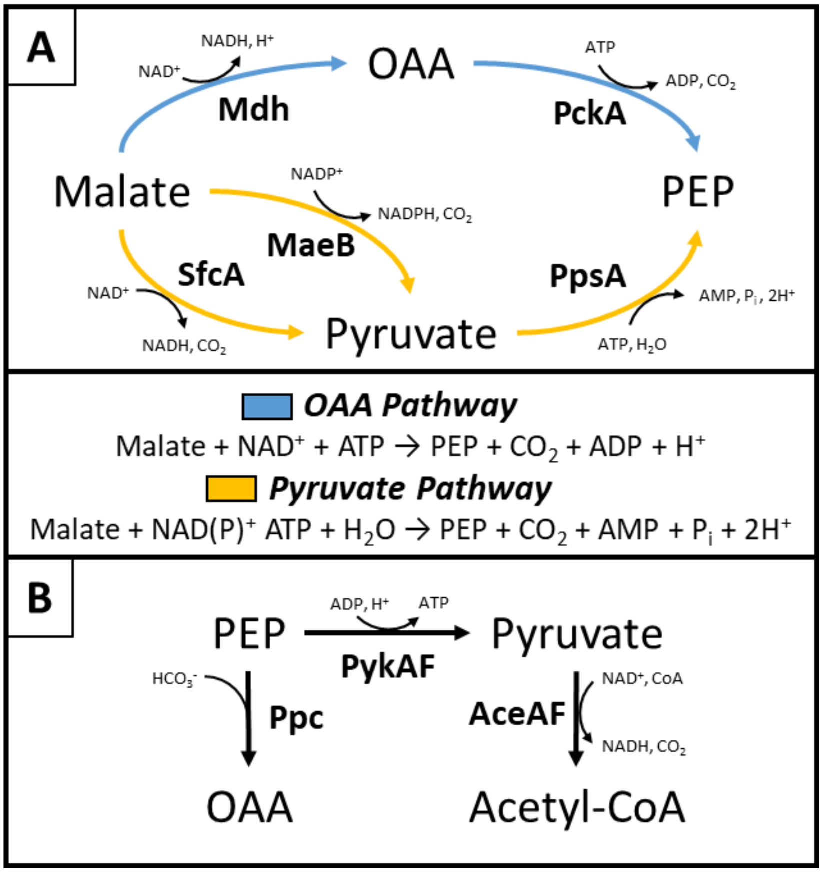

Figure 7. a PEP-pyruvate interconversion pathways connecting TCA cycle intermediate malate to PEP. Net reactions are shown below the pathways. Arrows color represents involving OAA (blue) and pyruvate (yellow). **b** Catabolic reactions opposing the PEP-pyruvate pathways.

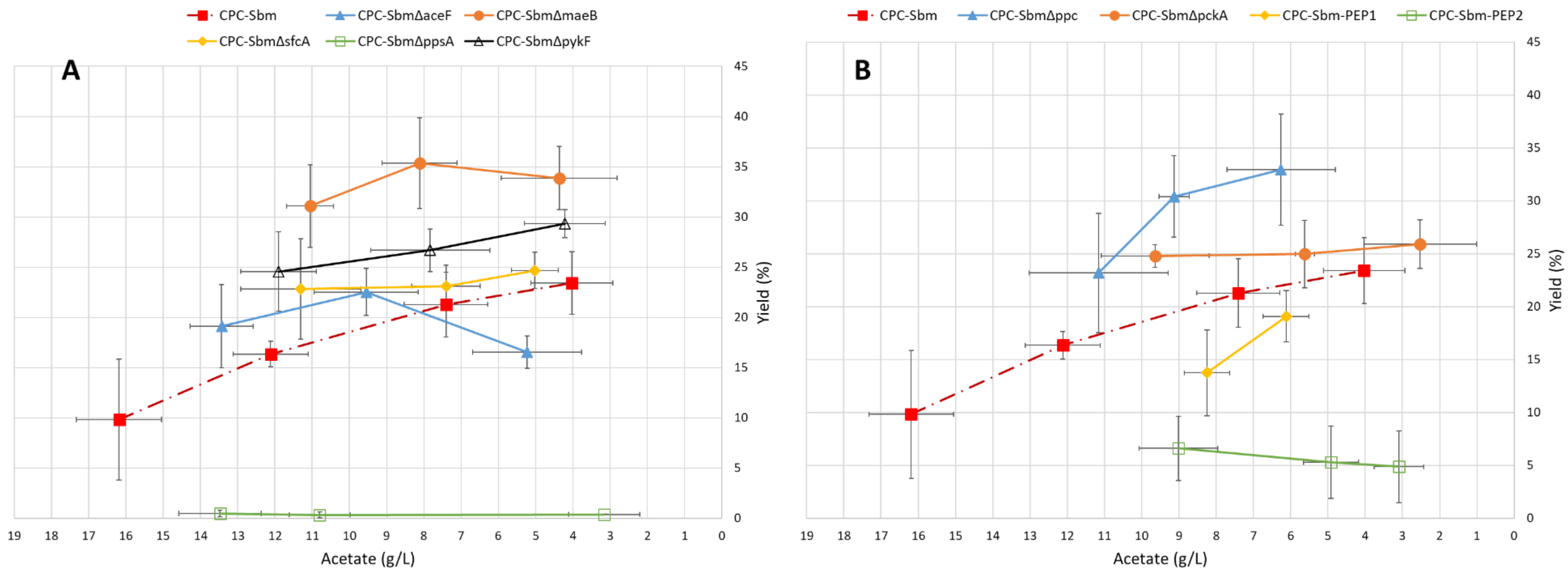

Figure 8. Time independent propionate yield data for strains containing **a** an inactivated gene associated with pyruvate or **b** a manipulated gene associated with OAA to PEP interconversion. Symbols represent averages of data points (i.e. acetate concentration and yield) contained within groupings based on similar acetate concentrations determined for each strain. *Vertical errors bars* represent s.d. in yield (*n* = variable). *Horizontal error bars* represent s.d. in acetate concentration (*n* = variable

3.6 – Inactivation of regulators

In the presence of multiple carbon sources, *E. coli* often has a preferential utilization of them through carbon catabolite repression, which is a regulatory process involving various global and carbon-specific regulatory proteins [44, 45]. Certain catabolic pathways, such as glycolysis, are conserved upon dissimilation of many carbon sources. However, this is not the case for acetate, which requires the transition from catabolic glycolysis to anabolic gluconeogenesis pathways. As such, there is an extended lag time for acetate metabolism activation [21], during which various regulatory proteins act to direct the drastic metabolic changes. We targeted four genes corresponding to the global and acetate-specific regulatory systems and the results are summarized in **Figure 9**. The global regulator system ArcAB (encoded by *arcAB*) and regulatory protein Fnr (encoded by *fnr*) mediate transcription of a selection of genes in the TCA cycle and glyoxylate bypass during acetate metabolism in accordance with oxygen availability [46, 47]. Mutant strains CPC-SbmΔ*arcA* and CPC-SbmΔ*fnr* were minimally altered in their ability to utilize acetate and biomass generation relative to the control strain. However, both mutant strains had significantly lower propionate yields, suggesting the regulatory roles that ArcAB and Fnr played are beneficial for propionate production. Specific to acetate metabolism, isocitrate dehydrogenase kinase (AceK encoded by *aceK*), is involved in reversible phosphorylation of IcdA to control the carbon flux splitting at the ICT node between the carbon-conserving glyoxylate bypass and energy-generating decarboxylating reactions of the TCA cycle [48, 49]. IclR (encoded by *iclR*) is the transcriptional repressor (with glyoxylate and pyruvate as effectors for decreasing and increasing IclR binding, respectively) of the *aceABK* operon which encodes enzymes for glyoxylate bypass and is induced during growth on acetate [45]. Inactivation of *aceK* in CPC-SbmΔ*aceK* minimally affected biomass generation and acetate utilization rate, but reduced propionate production compared to

CPC-Sbm. On the other hand, CPC-SbmΔ*iclR* had a significant increase in the propionate yield with a slight reduction in the overall acetate utilization rate.

rate.

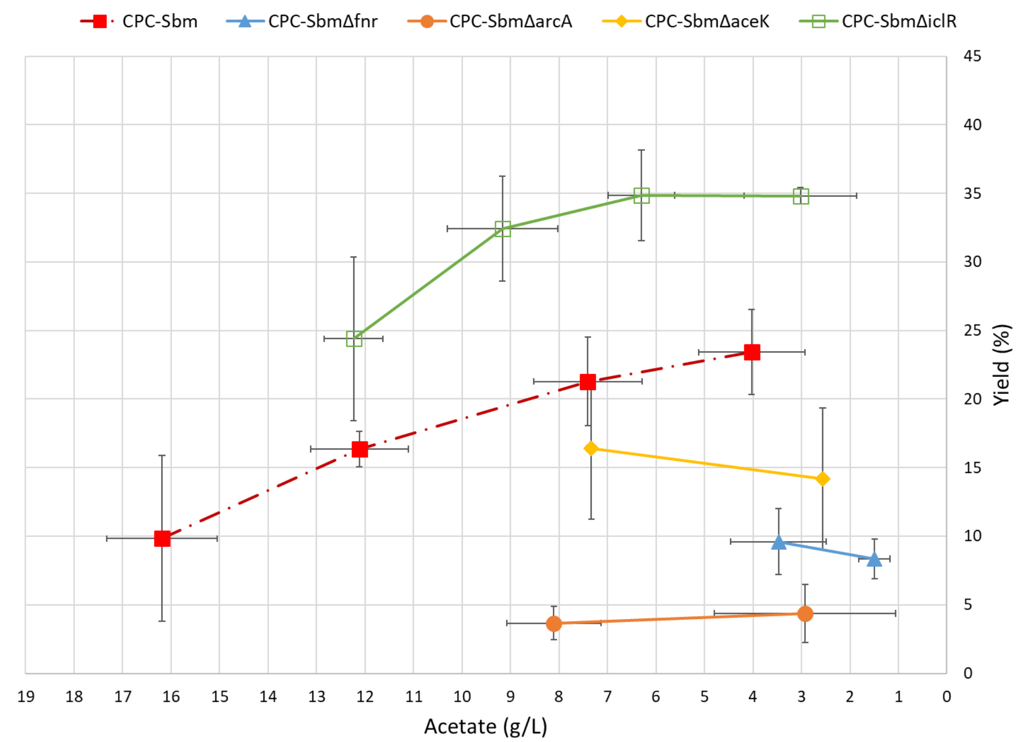

Figure 9. Time independent propionate yield data for strains with manipulated regulation of the TCA cycle and/or glyoxylate bypass. Symbols represent averages of data points (i.e. acetate concentration and yield) contained within groupings based on similar acetate concentrations determined for each strain. *Vertical errors bars* represent s.d. in yield (*n* = variable). *Horizontal error bars* represent s.d. in acetate concentration (*n* = variable).

Chapter 4 – Discussion and conclusions

Overexpression of the *acs* gene from *Acetobacter pasteurianus*, but not the native *acs* gene, was applied to enhance the production of β-caryophyllene from acetate in *E. coli* [50]. Consistent with their results [50], overexpression of the *acs* gene from *B. subtilis*, but not the native *acs* gene, increased the propionate yield. Note that overexpression of the native *acs* gene reduced the rates of acetate utilization and cell growth. This could be associated with the involvement of the AMP-Acs complex which acts as a regulator in restricting the carbon flux into the glyoxylate bypass, preventing the conservation of carbon [16, 21]. Compared to overexpression of the native Acs in CPC-Sbm-UE1, the introduction of an exogenous Acs in CPC-Sbm-UE3 could potentially bypass such endogenous regulation, improving acetyl-CoA formation. Under most of cultivation conditions with a decently high acetate concentration, the AckA-Pta system is more preferably used for acetyl-CoA formation due to its higher substrate affinity (K_m = 7-10 mM) than that of Acs (K_m = 200 μM) [25, 51]. Therefore, overexpression of high-affinity Acs from sources other than *E. coli* can potentially overcome this limitation in acetyl-CoA formation. The lack of propionate production for CPC-SbmΔ*pta* was potentially associated with the involvement of the AckA-Pta system in conversion of propionic-CoA to propionate. Consistent with this observation, overexpression of *ack-pta* in CPC-Sbm-UE2 resulted in more effective propionate synthesis.

While the control strain could steadily use acetate as the sole carbon source for cell growth with a final propionate yield of ~24%, mutant CPC-SbmΔ*icdA* hardly produced propionate, implying a critical metabolic role of Route A for propionate formation. Note that inactivation of *icdA* could reduce the pool of α-ketoglutarate, a key precursor for amino acid synthesis, hindering cell growth and acetate utilization. Although the flux through the oxidative TCA is regulated during acetate metabolism, sufficient energy must be generated to sustain cellular processes. IcdA exhibits

$NADP^+$-dependence, which is believed to compensate for the lost NADPH synthesis via the pentose phosphate pathway during acetate metabolism [52]. An additional energy generating route via MaeB/SfcA and AceEF is also available for reducing equivalent synthesis. Note that CPC-SbmΔ*icdA* retained viability, implying that MaeB-mediated synthesis of NADPH was sufficient to sustain *E. coli* growth on acetate. Compared to the control strain, obstructing energy generation through inactivation of *aceF* hindered growth and propionate production, suggesting the importance of energy generation. However, cell growth was more impacted in CPC-SbmΔ*icdA* than in CPC-SbmΔ*aceF*, suggesting that the oxidative TCA cycle was preferred for energy generation. The apparent scarcity of NADPH during growth on acetate reveals that manipulating $NADP^+$-dependent enzymes may be effective in altering the carbon flux. Hence, inactivation of *maeB* significantly increased the propionate yield as, under this genetic background, carbon flux would be diverted through the oxidative TCA cycle (i.e. Route A) to compensate for the reduction in NADPH synthesis by MaeB. The importance of Route A for propionate production was further confirmed by overexpression of *icdA* and *sucAB* with an elevated propionate yield by 34% in CPC-Sbm-TCA2, relative to the control strain. On the other hand, inactivation of *frdB* minimally impacted cell growth and propionate production, suggesting that Route C might not be a major contributive flux into the MM-CoA pathway. Inactivation of *mdh* blocked OAA synthesis in CPC-SbmΔ*mdh* and, therefore, eliminated the cyclic nature of both Route A and B, i.e. preventing the glyoxylate bypass and oxidative TCA cycle. Under this condition, flux contributions into the MM-CoA pathway had to stem from reduction of malate and follow Route C. The negligible propionate production in conjunction with restricted cell growth and eventual cell death for CPC-SbmΔ*mdh* suggest that the glyoxylate bypass and oxidative TCA cycle were critical for cell viability, as well as that both Route A and B were the major contributors to flux into the MM-CoA pathway for propionate production during cell growth on acetate. Mdh and GltA directly compete with enzymes for TCA-intermediates as the substrates (i.e. MaeB and SfcA for malate and PckA for OAA). Hence, overexpression of *mdh* and *gltA* in CPC-Sbm-TCA1 could potentially retain more carbon flux within the oxidative TCA cycle, resulting in a propionate yield 20% higher than the control strain. However, CPC-Sbm-TCA1 also had significantly reduced acetate utilization rate, likely due to the hindered carbon extraction from the TCA cycle for use in gluconeogenesis. Reinforcing this observation, overexpression of *pckA* did not affect acetate utilization, but significantly reduced propionate yield in CPC-Sbm-PEP2 relative to the control strain. Mutant CPC-SbmΔ*aceA* had significantly hindered cell growth and acetate utilization with a low propionate yield, compared to the control strain, suggesting that the glyoxylate bypass was also actively involved in propionate production. Note, replenishing carbon diverted from the TCA cycle requires the glyoxylate bypass and, in turn, a functional AceA. Overexpression of glyoxylate bypass genes *aceABK* or Route B specific genes *sucCD* were unsuccessful in altering the overall propionate yield, suggesting that Route B may not be critical for propionate production, but rather that a functional glyoxylate bypass facilitates flux into the MM-CoA pathway. Thus, the oxidative TCA cycle (i.e. Route A) appears to be the major contributor to the flux into the MM-CoA pathway for propionate production.

Compared to the control strain, mutant CPC-SbmΔ*sdhA* had a higher propionate yield though cell growth and acetate utilization appeared to be significantly retarded. Note that inactivation of *sdhA* maintains all three Routes to propionate while preventing progression through the oxidative TCA cycle, leaving only the reductive route towards succinyl-CoA available into the MM-CoA pathway. Attempts to restore cell growth for CPC-SbmΔ*sdhA* via supplementation of glucose, glycerol or fumarate were unsuccessful (data not shown). The results suggest that maintaining the oxidative TCA cycle can be critical for cell viability and acetate metabolism. As blocking the oxidative TCA cycle at SdhA did not affect the propionate yield (or even somehow increased the propionate yield during the initial cultivation stage), we targeted another conversion step from fumarate to malate. *E. coli* has three independent fumarases (i.e. FumA, FumB, FumC) associated with this step. Compared to the control strain, inactivation of *fumA* in CPC-SbmΔ*fumA* or *fumC* in CPC-SbmΔ*fumC* did not hamper cell growth with similar levels of propionate yield, suggesting overlapping function for these fumarases.

While the glyoxylate bypass plays a critical role for effective conversion of acetate to propionate, inactivation of *aceB* reduced the acetate utilization rate, but did not alter propionate production in CPC-SbmΔ*aceB*. Note that *E. coli* has a redundant malate synthase (i.e. malate synthase G (GlcB) encoded by *glcB*) that, in contrast to AceB, is primarily involved in glycolate metabolism [53]. However, the close association between glycolate and acetate metabolisms could mediate GlcB to complement inactivation of AceB in CPC-SbmΔ*aceB*. Accordingly, CPC-SbmΔ*aceB* and CPC-SbmΔ*glcB* had similar mutational effects, implicating that both AceB and GlcB are actively involved in the glyoxylate bypass. Further reduction in the acetate utilization rate with even lower propionate yields was observed upon inactivation of both genes in CPC-SbmΔ*aceB*Δ*glcB*, reiterating the critical function of the glyoxylate bypass for propionate production.

Gluconeogenesis is critical during acetate metabolism for the synthesis of sugar-phosphates required for the biosynthesis of various cellular components and key metabolites [21]. The importance of gluconeogenesis during acetate metabolism is also reflected by the significant alterations to the transcription levels of genes involved in PEP-pyruvate interconversion when compared to *E. coli* grown on glucose [1]. Hence, maintaining one of the two key routes for PEP synthesis, i.e. via OAA or pyruvate, is essential for growth on acetate [1]. Inactivation of either of these routes in CPC-SbmΔ*ppsA* or CPC-SbmΔ*pckA* resulted in similar reductions in the acetate utilization rate, but drastic differences in propionate production. While the propionate yield for CPC-SbmΔ*pckA* was similar to the control strain, inactivation of *ppsA* almost eliminated propionate production, suggesting the conversion step from pyruvate to PEP was critical for propionate production. While both the PpsA or PckA routes can generate PEP for growth on acetate [1], inactivation of *ppsA* is known to alter the expression level of many key regulators and genes for acetate metabolism [54]. Inactivation of *pykF* or *ppc* elevated the propionate yield in CPC-SbmΔ*pykF* and CPC-SbmΔ*ppc* by 26% and 41%, respectively, relative to CPC-Sbm. As PEP synthesis is preferred during acetate metabolism, overexpression of *ppc* in CPC-Sbm-PEP1 does not appear to significantly alter the propionate yield relative to CPC-Sbm. These results suggest that manipulation of the pathways associated with gluconeogenesis can affect the carbon flux into the MM-CoA pathway.

The pivotal role of regulatory proteins in facilitating acetate metabolism makes them a promising target for genetic manipulation to enhance propionate production potentially through altering carbon flux into the oxidative TCA cycle and glyoxylate bypass. The two-component anoxic respiratory control system ArcAB and global regulatory protein Fnr independently alter the transcription of numerous genes in response to oxygen availability [55]. Additionally, ArcAB regulation is known to alter the metabolic fluxes within the TCA cycle [43]. While, compared to the control strain, the rates of acetate utilization and cell growth were minimally affected by inactivation of *arcA* in CPC-SbmΔ*arcA* and *fnr* in CPC-SbmΔ*fnr*, the propionate yield was significantly reduced in both mutant strains. The results suggest the importance of these global regulators in directing carbon flux into the MM-CoA pathway. On the other hand, AceK inactivates

IcdA through phosphorylation of it, potentially directing more carbon flux into the glyoxylate bypass at the ICT node [48, 49]. Cell growth was minimally affected but propionate production was retarded by inactivation of *aceK* in CPC-SbmΔ*aceK*, compared to the control strain, suggesting that blocking phosphorylation of IcdA might not necessarily drive more carbon flux through the oxidative TCA pathway for enhancing propionate production. IclR represses transcription of the *aceABK* operon [45] and inactivation of *iclR* can eliminate such transcriptional repression, potentially enhancing the glyoxylate bypass. Interesting, compared to the control strain, inactivation of *iclR* in CPC-SbmΔ*iclR* led to a significant increase of ~50% in propionate yield with cell growth being minimally affected. However, overexpressing *aceABK* in CPC-Sbm-GLX1 did not alter the overall propionate yield relative to CPC-Sbm. The results suggest the complexity of these regulatory mechanisms indirectly affecting propionate production. For example, IclR has been shown to be indirectly involved in repression of *acs* [56], suggesting acetyl-CoA formation could be altered in CPC-SbmΔ*iclR*. Nonetheless, these results along with those described above reinforce the critical observation that glyoxylate bypass should be active for directing more carbon flux into the MM-CoA pathway for propionate production.

Chapter 5 – Applications of acetate as a feedstock

5.1 – Value-added product production

Biomass based biomanufacturing is a renewable alternative to petrochemical processes for the production of chemicals. However, substantial improvements to biological based processes are required to be competitive with their petrochemical counterparts [2]. The lower feedstock costs, easily scalability and consistent performance for petrochemical processes facilitate lower production costs and predictable outputs, represent two key advantages over bioprocesses [2, 10]. Accordingly, bioprocesses developed to produce chemicals readily supplied from petrochemical sources, such as propionate, must overcome large barriers to be commercialized. On the other hand, commercialization of a given bioprocess is facilitated by using waste feedstocks, such as acetate, to produce chemicals and by deriving products which are difficult to or cannot be synthesized synthetically.

Acetyl-CoA and propionyl-CoA are versatile intermediates which have been used for production of value-added products such as biopolymers, medium chain reduced and hydroxy acids, and ketones by engineered *E. coli* [36, 40, 57] (**Figure 10**). Given the success of generating propionate from acetate, deriving these and many other value-added products should be explored. The heavy involvement of the glyoxylate bypass during acetate metabolism allows for glyoxylate to be used as a potential building block within engineered pathways. For example, glyoxylate can be fused with acetyl-CoA or propionyl-CoA using malyl-CoA/methylmalonyl-CoA lysis (MMCL) from *Chloroflexus aurantiacus* or *Rhodobacter sphaeroides* to produce malyl-CoA or 2-methylmalyl-CoA respectively [58]. Malyl-CoA could be subsequently polymerized using polyhydroxyalkanoate polymerase/synthase (PhaC) from *Cupriavidus necator* to form a high-value biopolymer, i.e. poly(malate), used for drug delivery and in nanoparticles [40, 59].

Similarily, 2-methylmalyl-CoA could be polymerized by PhaC to generate a novel bio-co-polymer, i.e. poly(2-methylmalate-co-malate), or be converted to its monomer 2-methylmalate by a CoA removing enzyme such as acyl-CoA thioesterase II (TesB) from *E. coli*. The methods developed for directing flux during acetate metabolism detailed in the earlier chapters, can be implemented to genetically optimize the production of targeted value-added products, such as those mentioned above. Furthermore, engineered strains with increased flux into the MM-CoA pathway, such as CPC-SbmΔ*ppc* or CPC-SbmΔ*iclR*, could serve as a base strain to produce higher chain products derived using propionyl-CoA.

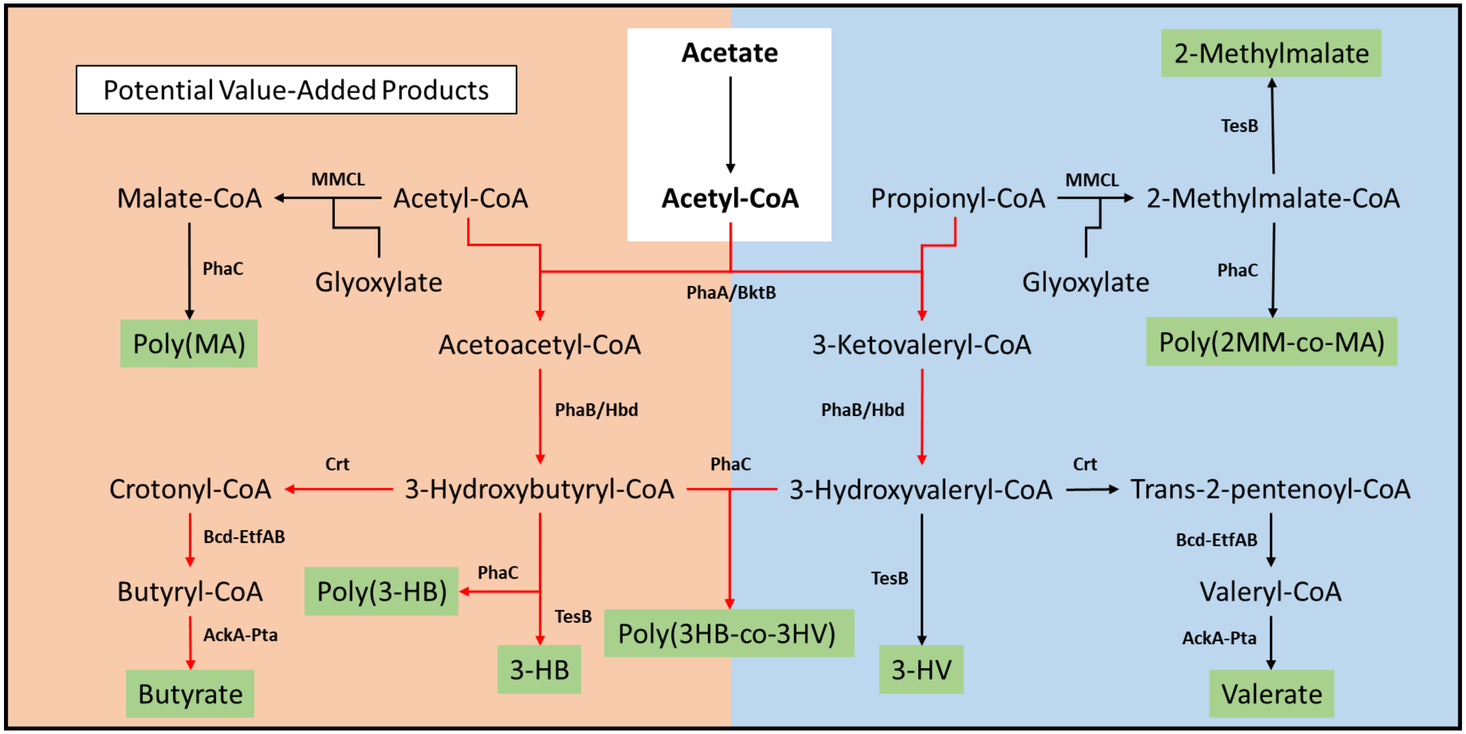

Figure 10. Proposed value-added products which can be derived from acetate. A green box indicates a valuable metabolite. Background color indicates pathways based on acetyl-CoA fusion (orange) or propionyl-CoA fusion (blue). Arrow color shows pathways which have been demonstrated in engineered E. coli (red) and proposed pathways (black). Enzymes: PhaA/BktB, β-ketothiolases; PhaB/HbD, 3-hydroxybutryl-CoA dehydrogenase; Crt, crotonase, Bcd-EtfAB, butyryl-CoA dehydrogenase and its electron-transfer flavoprotein complexes; AckA, acetate kinase; Pta, phosphotransacetylase; TesB, acyl-CoA thioesterase II; PhaC, polyhydroxyalkanoate polymerase/synthase; and MMCL, malyl-CoA/methylmalonyl-CoA lysis. Abbreviations: malate (MA), 2-methylmalate (2-MM), 3-hydroxybutyrate (3-HB), 3-hydroxyvalerate (3-HV).

5.2 – High yield conversion

The robust nature of *E. coli*'s metabolism allows it to utilize a wide verity of carbon sources. In the presence of multiple carbon sources, *E. coli* preferentially utilizes through carbon catabolite repression of the pathways associated with the less preferred carbon sources [44]. Carbon catabolite repression can be potentially manipulated via genetic modifications to facilitate the use and/or uptake of multiple carbon sources simultaneously. More importantly, segregating the use of each carbon source for different metabolic purposes within a strain capable of high efficiency co-feeding could enable high yield conversion of substrates to value-added products. Specifically, if one carbon source can be exclusively used to sustain grow and cellular functions, the other one could drive value-added product production, presumably leading to increased conversion efficiency.

Acetate is an ideal substrate for driving growth during co-feeding because; 1) it is cheap feedstock; 2) *E. coli*'s metabolism during growth on acetate is drastically different compared to growth on most carbon sources; and 3) it is a less preferred carbon source, therefore, its presence in the cultivation media is unlikely to favored over the other, potentially higher value, substrate. An example of this strategy is to produce value-added products derived directly from glycerol with growth sustained by acetate (**Figure 11**). Interestingly, during *E. coli* growth on glycerol the glyoxylate bypass is activated for acetate recycling [60], suggesting natural carbon catabolite repression may favor co-feeding of these substrates. However, to effectively segregate the use of acetate for growth and glycerol for product production, glycerol metabolism would need to be modified such that it cannot be used in endogenous pathways. Following uptake, intracellular glycerol enters either a respiratory or fermentative pathway, specific to glycerol utilization, to produce glycolysis intermediate dihydroxyacetone-phosphate [61]. An effective strategy to prevent glycerol utilization would be eliminating the first conversion step of the respiratory and fermentative pathways via inactivating genes *glpK* and *gldA* which encode glycerol kinase (GlpK) and glycerol dehydrogenase (GldA) respectively [62, 63].

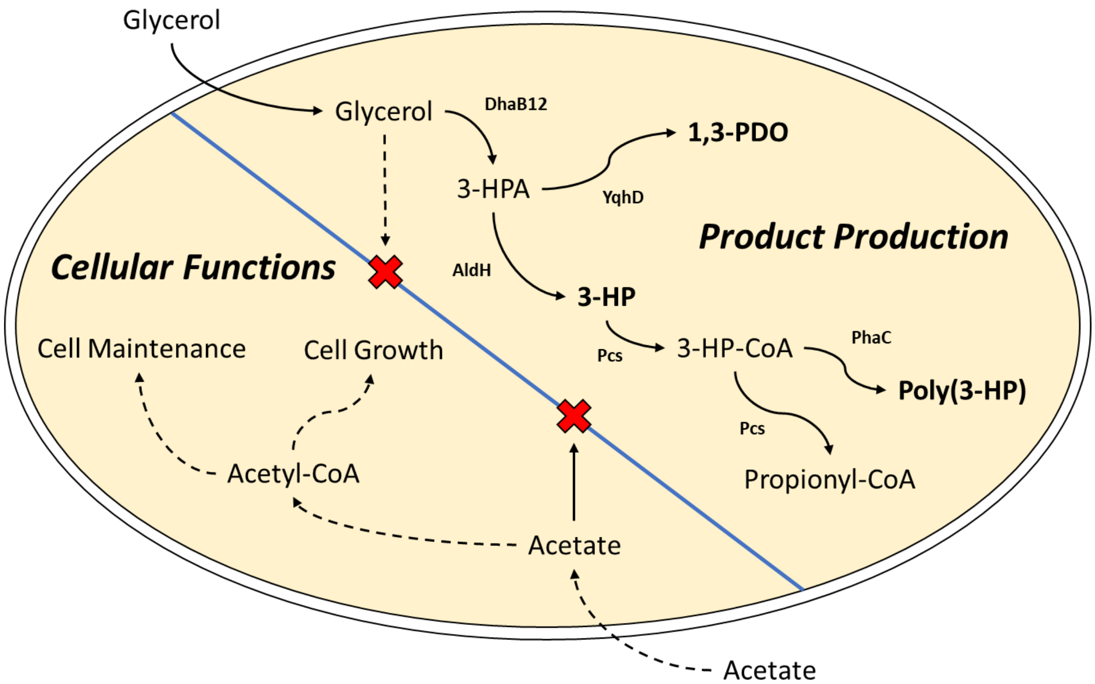

Figure 11. Proposed substrate co-feeding with segregated substrate utilization. The blue line represents the theoretical separation of functions. Arrow type represents use for cellular functions (dashed) or product production (solid). Enzymes: DhaB12, glycerol dehydratase and its activating enzyme; AldH, aldehyde dehydrogenase; YqhD, 1,3-PDO oxidoreductase; Pcs, propionyl-CoA synthase complex; PhaC, polyhydroxyalkanoate polymerase/synthase. Abbreviations: 3-hydroxypropionaldehyde (3-HPA), hydroxypropionate (3-HP) and 1,3-Propandiol (1,3-PDO).

Additionally, glycerol is an ideal carbon source for product productions because it is also a waste feedstock and can be directly converted to value-added products. For example, 3-hydroxypropionate (3-HP) and 1,3-Propandiol (1,3-PDO) can be synthesized from glycerol in two-steps. First, glycerol dehydratase and an accessory enzyme, such as DhaB12 from *Clostridium butyricum* [64], converts glycerol to 3-hydroxypropionaldehyde (3-HPA). 3-HPA can be subsequently converted to 1,3-PDO by a 1,3-PDO oxidoreductase, such as YqhD from *E. coli* [64], or to 3-HP by an aldehyde dehydrogenase, such as AldH from *E. coli* [65]. 3-HP can be further processed into 3-HP-CoA using various enzymes such as the 3-hydroxypropionate:CoA ligase domain of the propionyl-CoA synthase complex (Pcs) from *C. aurantiacus* [66] or propionyl-CoA synthetase (PrpE) from *E. coli* [67], and polymerized using PhaC to produce poly(3-HP) [68]. Note, the complete Ppc complex from *C. aurantiacus* can be used for extended 3-HP dissimilation to propionyl-CoA for deriving products such as propionate, propanol and C5 products.

5.3 – Co-culture

The considerable issues associated with acetate biosynthesis and accumulation have hindered not only *E. coli* bioprocesses performance [15] but other industrially important strains, such as various species of yeast [69]. Accordingly, major research efforts have been made towards minimizing acetate biosynthesis [17, 70-72].

Co-culture involving genetically similar strains represents a novel solution to addressing the issues associated with acetate accumulation (**Figure 12**). Using *E. coli* biosynthesis of propionate as an example, it was previously demonstrated that a CPC-Sbm variant (i.e. containing a modified fermentative branch for glycerol dissimilation) was capable of high-level propionate production from glycerol [28]. Although propionate was the major fermentative product, significant acetate was also produced during the cultivation. As we have now shown that acetate can also be efficiently converted to propionate by CPC-Sbm and various engineered strains, the propionate titer would likely continue to increase following glycerol exhaustion. However, extending the cultivation time does not alleviate acetate biosynthesis issues throughout the cultivation. To accomplish this and maintain the elevated titer, a co-culture strategy involving a second variant of CPC-Sbm which cannot utilize glycerol as a carbon source (i.e. containing inactivated *glpK* and *gldA* genes) could be used. As the second CPC-Sbm variant cannot utilize the primary carbon source (i.e. glycerol), it would be dependent on by-products of the first CPC-Sbm variant for its supply of carbon, in this case acetate. As both strains can produce propionate, the forced symbiotic relationship would alleviate any issues with acetate accumulation and increase the propionate titer, yield, and rate of production.

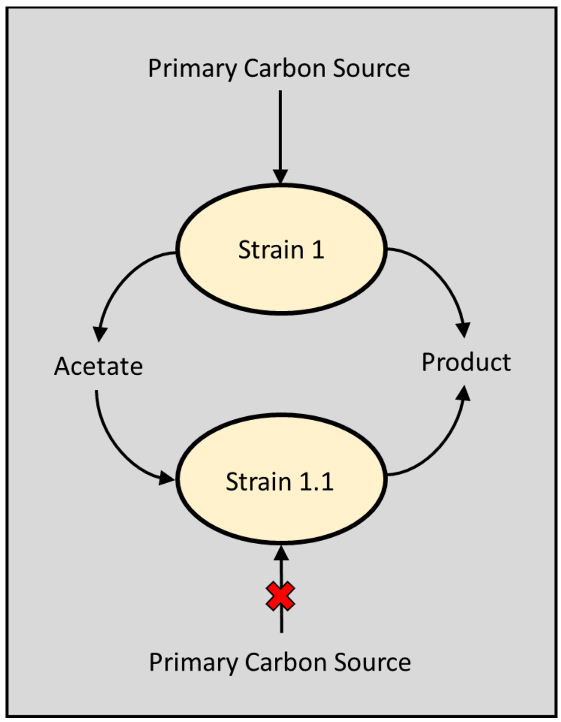

Figure 12. Proposed co-culture strategy for mitigation of acetate accumulation/inhibition. Strain 1 and Strain 1.1 are the same species and genetically similar (i.e. both contain the necessary genes for target product production), expect that strain 1.1 is unable to utilize the primary carbon source due to appropriate gene inactivation(s). Acetate is produced by Strain 1 as a byproduct of primary carbon source utilization and subsequently serves as the carbon source for Strain 1.1. The net result of this co-culture strategy is limited acetate accumulation and increased target product production.

References

1. Oh, M.-K., et al., *Global expression profiling of acetate-grown Escherichia coli.* Journal of Biological Chemistry, 2002. **277**(15): p. 13175-13183.
2. Srirangan, K., et al., *Towards sustainable production of clean energy carriers from biomass resources.* Applied energy, 2012. **100**: p. 172-186.
3. Lucia, L.A., et al., *Chemicals, Materials, and Energy from Biomass: A Review*, in *Materials, Chemicals, and Energy from Forest Biomass*. 2007, American Chemical Society. p. 2-30.
4. Werpy, T., et al., *Top value added chemicals from biomass. Volume 1-Results of screening for potential candidates from sugars and synthesis gas*. 2004, DTIC Document.
5. Klass, D.L., *Biomass for renewable energy, fuels, and chemicals*. 1998: Academic press.
6. Cherubini, F., *The biorefinery concept: using biomass instead of oil for producing energy and chemicals.* Energy conversion and management, 2010. **51**(7): p. 1412-1421.
7. Carere, C.R., et al., *Third generation biofuels via direct cellulose fermentation.* International journal of molecular sciences, 2008. **9**(7): p. 1342-1360.
8. Kamm, B. and M. Kamm, *Principles of biorefineries.* Applied Microbiology and Biotechnology, 2004. **64**(2): p. 137-145.
9. Metsoviti, M., et al., *Enhanced 1, 3-propanediol production by a newly isolated Citrobacter freundii strain cultivated on biodiesel-derived waste glycerol through sterile and non-sterile bioprocesses.* Journal of biotechnology, 2013. **163**(4): p. 408-418.
10. Pandey, A., *Biofuels: alternative feedstocks and conversion processes*. 2011: Academic Press.
11. Munasinghe, P.C. and S.K. Khanal, *Biomass-derived syngas fermentation into biofuels: opportunities and challenges.* Bioresource technology, 2010. **101**(13): p. 5013-5022.
12. Zhang, Y.-H.P., *Reviving the carbohydrate economy via multi-product lignocellulose biorefineries.* Journal of industrial microbiology & biotechnology, 2008. **35**(5): p. 367-375.
13. Fleisch, T., R. Sills, and M. Briscoe, *A review of global GTL developments.* journal of natural gas chemistry, 2002. **11**: p. 1-14.
14. Periana, R.A., et al., *Catalytic, oxidative condensation of CH4 to CH3COOH in one step via CH activation.* Science, 2003. **301**(5634): p. 814-818.
15. Bernal, V., S. Castaño-Cerezo, and M. Cánovas, *Acetate metabolism regulation in Escherichia coli: carbon overflow, pathogenicity, and beyond.* Applied microbiology and biotechnology, 2016. **100**(21): p. 8985-9001.
16. Contiero, J., et al., *Effects of mutations in acetate metabolism on high-cell-density growth of Escherichia coli.* Journal of industrial microbiology & biotechnology, 2000. **24**(6): p. 421-430.
17. Luli, G.W. and W.R. Strohl, *Comparison of growth, acetate production, and acetate inhibition of Escherichia coli strains in batch and fed-batch fermentations.* Applied and environmental microbiology, 1990. **56**(4): p. 1004-1011.
18. Eiteman, M.A. and E. Altman, *Overcoming acetate in Escherichia coli recombinant protein fermentations.* Trends in biotechnology, 2006. **24**(11): p. 530-536.
19. Jantama, K., et al., *Eliminating side products and increasing succinate yields in engineered strains of Escherichia coli C.* Biotechnology and bioengineering, 2008. **101**(5): p. 881-893.
20. Enjalbert, B., et al., *Acetate exposure determines the diauxic behavior of Escherichia coli during the glucose-acetate transition.* Journal of bacteriology, 2015. **197**(19): p. 3173-

3181.
21. Wolfe, A.J., *The Acetate Switch.* Microbiology and Molecular Biology Reviews, 2005. **69**(1): p. 12-50.
22. Treitz, C., et al., *Differential quantitative proteome analysis of Escherichia coli grown on acetate versus glucose.* Proteomics, 2016. **16**(21): p. 2742-2746.
23. Gimenez, R., et al., *The gene yjcG, cotranscribed with the gene acs, encodes an acetate permease in Escherichia coli.* Journal of bacteriology, 2003. **185**(21): p. 6448-6455.
24. Sá-Pessoa, J., et al., *SATP (YaaH), a succinate–acetate transporter protein in Escherichia coli.* Biochemical journal, 2013. **454**(3): p. 585-595.
25. Kumari, S., et al., *Cloning, characterization, and functional expression of acs, the gene which encodes acetyl coenzyme A synthetase in Escherichia coli.* Journal of bacteriology, 1995. **177**(10): p. 2878-2886.
26. Starai, V. and J. Escalante-Semerena, *Acetyl-coenzyme A synthetase (AMP forming).* Cellular and molecular life sciences, 2004. **61**(16): p. 2020.
27. Liu, L., et al., *Microbial production of propionic acid from propionibacteria: current state, challenges and perspectives.* Critical reviews in biotechnology, 2012. **32**(4): p. 374-381.
28. Akawi, L., et al., *Engineering Escherichia coli for high-level production of propionate.* Journal of industrial microbiology & biotechnology, 2015. **42**(7): p. 1057-1072.
29. Miller, J.H., *A short course in bacterial genetics: a laboratory manual and handbook for Escherichia coli and related bacteria*. 1992, NY: Cold Spring Harbor Laboratory Press.
30. Srirangan, K., et al., *Biochemical, genetic, and metabolic engineering strategies to enhance coproduction of 1-propanol and ethanol in engineered Escherichia coli.* Applied Microbiology and Biotechnology, 2014. **98**(22): p. 9499-9515.
31. Baba, T., et al., *Construction of Escherichia coli K-12 in-frame, single-gene knockout mutants: the Keio collection.* Molecular systems biology, 2006. **2**(1).
32. Cherepanov, P.P. and W. Wackernagel, *Gene disruption in Escherichia coli: Tc^R and Km^R cassettes with the option of Flp-catalyzed excision of the antibiotic-resistance determinant.* Gene, 1995. **158**(1): p. 9-14.
33. Casadaban, M.J., *Transposition and fusion of the lac genes to selected promoters in Escherichia coli using bacteriophage lambda and Mu.* Journal of Molecular Biology, 1976. **104**(3): p. 541-555.
34. Datsenko, K.A. and B.L. Wanner, *One-step inactivation of chromosomal genes in Escherichia coli K-12 using PCR products.* Proceedings of the National Academy of Sciences of the United States of America, 2000. **97**(12): p. 6640-6645.
35. Srirangan, K., et al., *Manipulating the sleeping beauty mutase operon for the production of 1-propanol in engineered Escherichia coli.* Biotechnol Biofuels, 2013. **6**(139).
36. Srirangan, K., et al., *Engineering Escherichia coli for microbial production of butanone.* Applied and environmental microbiology, 2016. **82**(9): p. 2574-2584.
37. Sukhija, K., et al., *Developing an extended genomic engineering approach based on recombineering to knock-in heterologous genes to Escherichia coli genome.* Molecular biotechnology, 2012. **51**(2): p. 109-118.
38. Jobling, M.G. and R.K. Holmes, *Construction of vectors with the pl5A replicon, kanamycin resistance, inducible lacZα and pUC18 or pUC19 multiple cloning sites.* Nucleic Acids Research, 1990. **18**(17): p. 5315-5316.
39. Kovach, M.E., et al., *Four new derivatives of the broad-host-range cloning vector pBBR1MCS, carrying different antibiotic-resistance cassettes.* Gene, 1995. **166**(1): p. 175-

176.
40. Srirangan, K., et al., *Engineering of Escherichia coli for direct and modulated biosynthesis of poly (3-hydroxybutyrate-co-3-hydroxyvalerate) copolymer using unrelated carbon sources.* Scientific reports, 2016. **6**.
41. Gibson, D.G., et al., *Enzymatic assembly of DNA molecules up to several hundred kilobases.* Nature methods, 2009. **6**(5): p. 343-345.
42. Srirangan, K., et al., *Manipulating the sleeping beauty mutase operon for the production of 1-propanol in engineered Escherichia coli.* Biotechnology for biofuels, 2013. **6**(1): p. 139.
43. Cronan Jr, J. and D. Laporte, *Tricarboxylic acid cycle and glyoxylate bypass.* EcoSal Plus, 2005. **1**(2).
44. Görke, B. and J. Stülke, *Carbon catabolite repression in bacteria: many ways to make the most out of nutrients.* Nature Reviews Microbiology, 2008. **6**(8): p. 613-624.
45. Lorca, G.L., et al., *Glyoxylate and pyruvate are antagonistic effectors of the Escherichia coli IclR transcriptional regulator.* Journal of Biological Chemistry, 2007. **282**(22): p. 16476-16491.
46. Salmon, K., et al., *Global gene expression profiling in Escherichia coli K12 the effects of oxygen availability and FNR.* Journal of Biological Chemistry, 2003. **278**(32): p. 29837-29855.
47. Gunsalus, R. and S.-J. Park, *Aerobic-anaerobic gene regulation in Escherichia coli: control by the ArcAB and Fnr regulons.* Research in microbiology, 1994. **145**(5-6): p. 437-450.
48. Walsh, K. and D.E. Koshland, *Determination of flux through the branch point of two metabolic cycles. The tricarboxylic acid cycle and the glyoxylate shunt.* Journal of Biological Chemistry, 1984. **259**(15): p. 9646-9654.
49. Borthwick, A.C., W.H. Holms, and H.G. Nimmo, *The phosphorylation of Escherichia coli isocitrate dehydrogenase in intact cells.* Biochemical Journal, 1984. **222**(3): p. 797-804.
50. Yang, J. and Q. Nie, *Engineering Escherichia coli to convert acetic acid to β-caryophyllene.* Microbial cell factories, 2016. **15**(1): p. 74.
51. Brown, T., M. Jones-Mortimer, and H. Kornberg, *The enzymic interconversion of acetate and acetyl-coenzyme A in Escherichia coli.* Microbiology, 1977. **102**(2): p. 327-336.
52. Zhu, G., G.B. Golding, and A.M. Dean, *The selective cause of an ancient adaptation.* Science, 2005. **307**(5713): p. 1279-1282.
53. Vanderwinkel, E. and M. De Vlieghere, *Physiology and genetics of isocitritase and the malate synthases of Escherichia coli.* European journal of biochemistry, 1968. **5**(1): p. 81.
54. Kao, K.C., L.M. Tran, and J.C. Liao, *A global regulatory role of gluconeogenic genes in Escherichia coli revealed by transcriptome network analysis.* Journal of Biological Chemistry, 2005. **280**(43): p. 36079-36087.
55. Lin, E. and S. Iuchi, *Regulation of gene expression in fermentative and respiratory systems in Escherichia coli and related bacteria.* Annual review of genetics, 1991. **25**(1): p. 361-387.
56. Shin, S., et al., *Involvement of iclR and rpoS in the induction of acs, the gene for acetyl coenzyme A synthetase of Escherichia coli K-12.* FEMS microbiology letters, 1997. **146**(1): p. 103-108.
57. Srirangan, K., et al., *Recent advances in engineering propionyl-CoA metabolism for microbial production of value-added chemicals and biofuels.* Critical Reviews in Biotechnology, 2016: p. 1-22.

58. Zarzycki, J. and C.A. Kerfeld, *The crystal structures of the tri-functional Chloroflexus aurantiacus and bi-functional Rhodobacter sphaeroides malyl-CoA lyases and comparison with CitE-like superfamily enzymes and malate synthases.* BMC structural biology, 2013. **13**(1): p. 28.
59. Loyer, P. and S. Cammas-Marion, *Natural and synthetic poly (malic acid)-based derivates: a family of versatile biopolymers for the design of drug nanocarriers.* Journal of drug targeting, 2014. **22**(7): p. 556-575.
60. Martínez-Gómez, K., et al., *New insights into Escherichia coli metabolism: carbon scavenging, acetate metabolism and carbon recycling responses during growth on glycerol.* Microbial cell factories, 2012. **11**(1): p. 46.
61. Gonzalez, R., et al., *A new model for the anaerobic fermentation of glycerol in enteric bacteria: trunk and auxiliary pathways in Escherichia coli.* Metabolic Engineering, 2008. **10**(5): p. 234-245.
62. Hayashi, S.-I. and E. Lin, *Purification and properties of glycerol kinase from Escherichia coli.* Journal of Biological Chemistry, 1967. **242**(5): p. 1030-1035.
63. Tang, C., F. Ruch, and C. Lin, *Purification and properties of a nicotinamide adenine dinucleotide-linked dehydrogenase that serves an Escherichia coli mutant for glycerol catabolism.* Journal of bacteriology, 1979. **140**(1): p. 182-187.
64. Tang, X., et al., *Microbial conversion of glycerol to 1, 3-propanediol by an engineered strain of Escherichia coli.* Applied and environmental microbiology, 2009. **75**(6): p. 1628-1634.
65. Raj, S.M., et al., *Production of 3-hydroxypropionic acid from glycerol by a novel recombinant Escherichia coli BL21 strain.* Process Biochemistry, 2008. **43**(12): p. 1440-1446.
66. STRAUSS, G. and G. FUCHS, *Enzymes of a novel autotrophic CO2 fixation pathway in the phototrophic bacterium Chloroflexus aurantiacus, the 3-hydroxypropionate cycle.* The FEBS Journal, 1993. **215**(3): p. 633-643.
67. Feng, X., et al., *Biosynthesis of poly (3-hydroxypropionate) from glycerol using engineered Klebsiella pneumoniae strain without vitamin B12.* Bioengineered, 2015. **6**(2): p. 77-81.
68. Wang, Q., et al., *Biosynthesis of poly (3-hydroxypropionate) from glycerol by recombinant Escherichia coli.* Bioresource technology, 2013. **131**: p. 548-551.
69. Moon, N.J., *Inhibition of the growth of acid tolerant yeasts by acetate, lactate and propionate and their synergistic mixtures.* Journal of Applied Microbiology, 1983. **55**(3): p. 453-460.
70. De Mey, M., et al., *Minimizing acetate formation in E. coli fermentations.* Journal of industrial microbiology & biotechnology, 2007. **34**(11): p. 689-700.
71. Farmer, W.R. and J.C. Liao, *Reduction of aerobic acetate production by Escherichia coli.* Applied and environmental microbiology, 1997. **63**(8): p. 3205-3210.
72. De Mey, M., et al., *Comparison of different strategies to reduce acetate formation in Escherichia coli.* Biotechnology progress, 2007. **23**(5): p. 1053-1063.

Appendix 1 – Time-dependent data

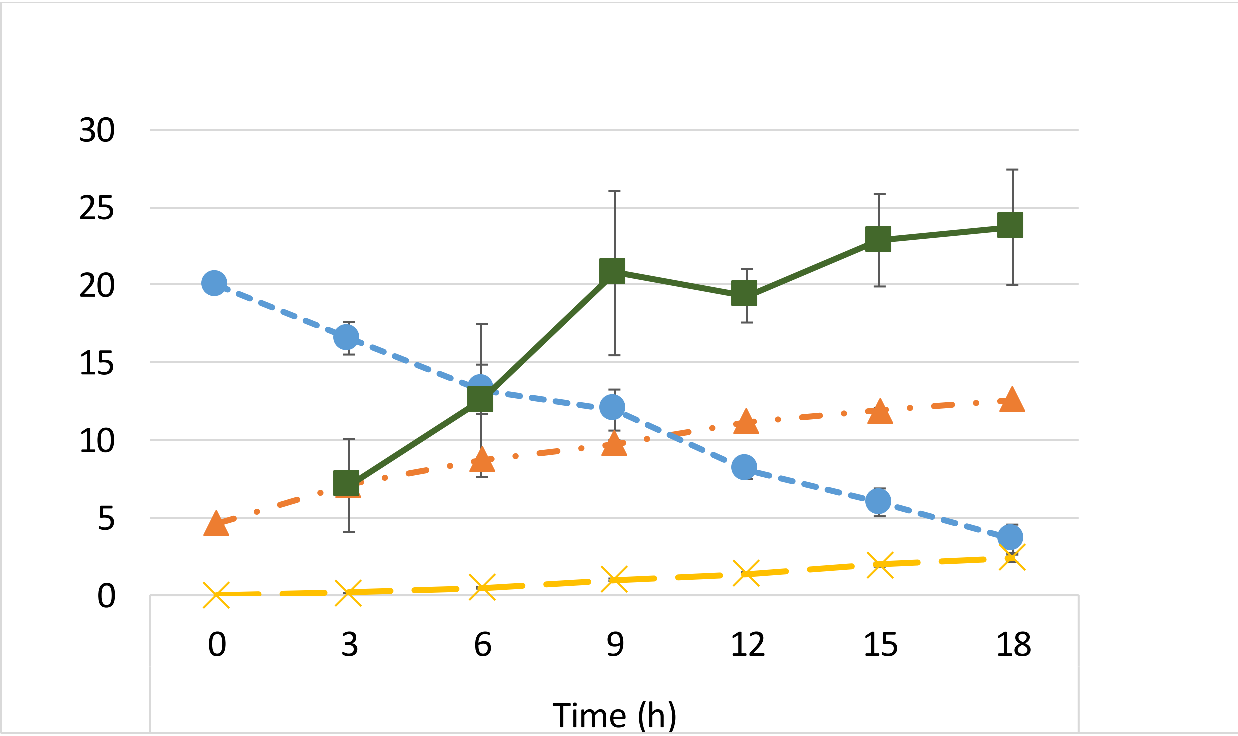

Figure S1. Time-dependent data for CPC-Sbm. Symbols and line color and type represent the average values for OD_{600} (orange, dash-dot, ▲), acetate concentration (blue, dash, ●), propionate concentration (yellow, long dash, **X**), and yield (green, solid, ■). *Vertical errors bars* represent s.d. (n = 3).

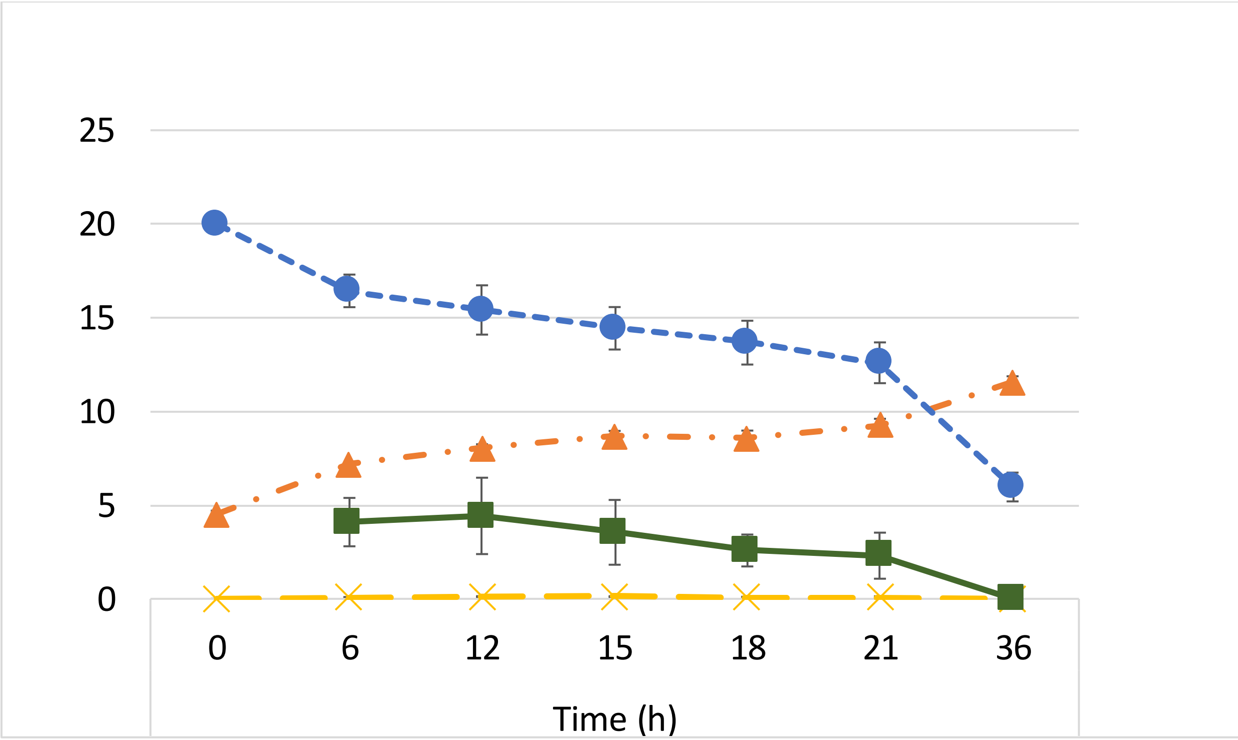

Figure S2. Time-dependent data for CPC-SbmΔ*pta*. Symbols and line color and type represent the average values for OD_{600} (orange, dash-dot, ▲), acetate concentration (blue, dash, ●), propionate concentration (yellow, long dash, **X**), and yield (green, solid, ■). *Vertical errors bars* represent s.d. (n = 3).

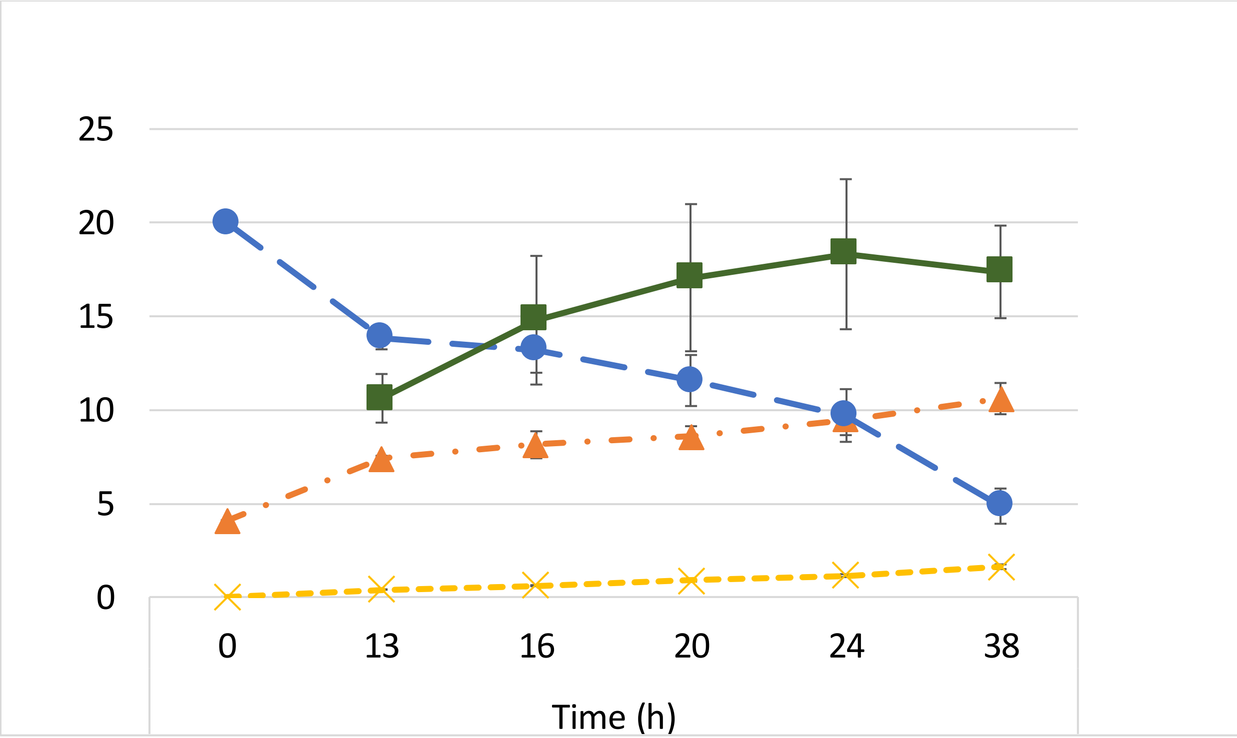

Figure S3. Time-dependent data for CPC-Sbm-UE1. Symbols and line color and type represent the average values for OD_{600} (orange, dash-dot, ▲), acetate concentration (blue, dash, ●), propionate concentration (yellow, long dash, **X**), and yield (green, solid, ■). *Vertical errors bars* represent s.d. (n = 3).

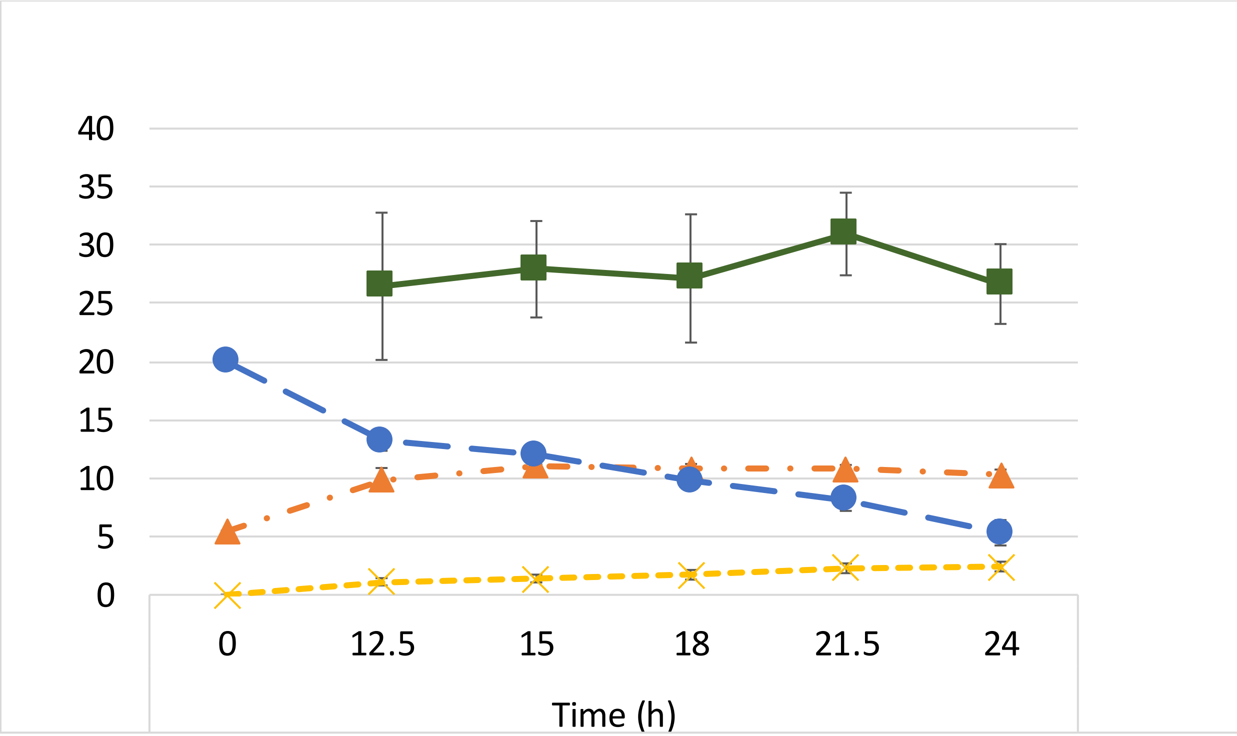

Figure S4. Time-dependent data for CPC-Sbm-UE2. Symbols and line color and type represent the average values for OD_{600} (orange, dash-dot, ▲), acetate concentration (blue, dash, ●), propionate concentration (yellow, long dash, **X**), and yield (green, solid, ■). *Vertical errors bars* represent s.d. (n = 3).

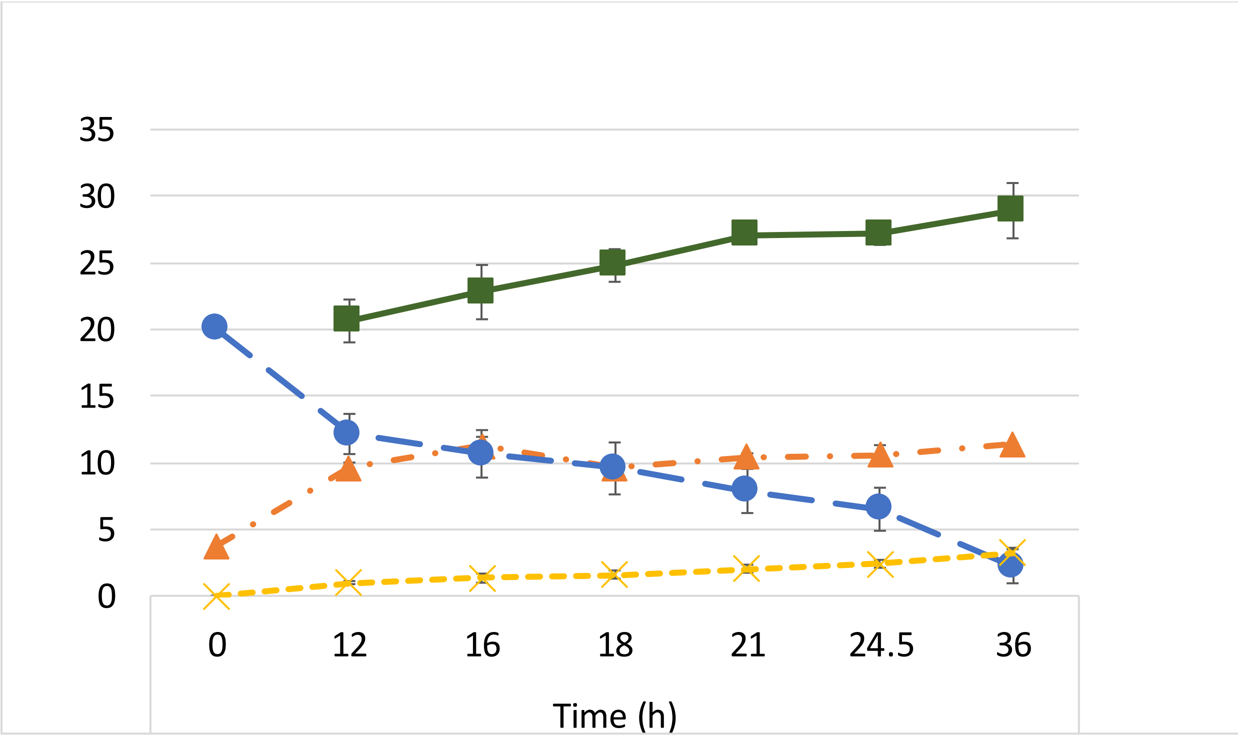

Figure S5. Time-dependent data for CPC-Sbm-UE3. Symbols and line color and type represent the average values for OD_{600} (orange, dash-dot, ▲), acetate concentration (blue, dash, ●), propionate concentration (yellow, long dash, **X**), and yield (green, solid, ■). *Vertical errors bars* represent s.d. (n = 3).

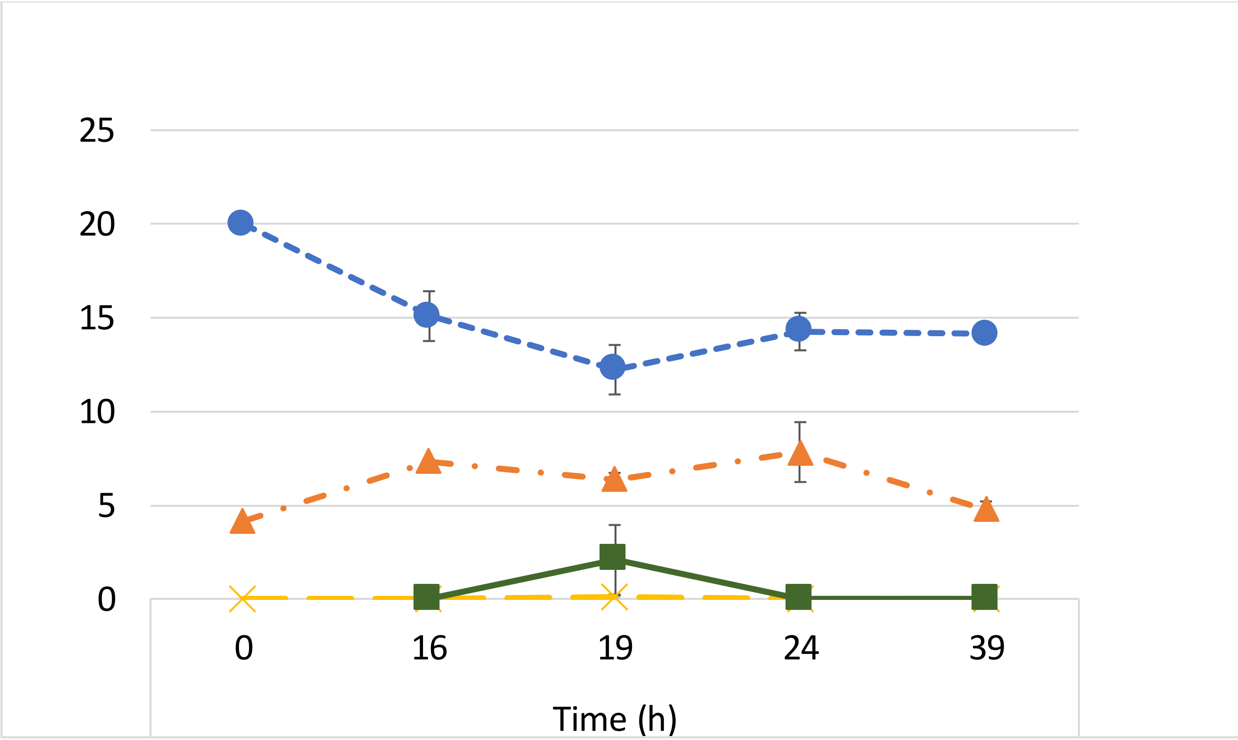

Figure S6. Time-dependent data for CPC-SbmΔ*mdh*. Symbols and line color and type represent the average values for OD_{600} (orange, dash-dot, ▲), acetate concentration (blue, dash, ●), propionate concentration (yellow, long dash, **X**), and yield (green, solid, ■). *Vertical errors bars* represent s.d. (n = 3).

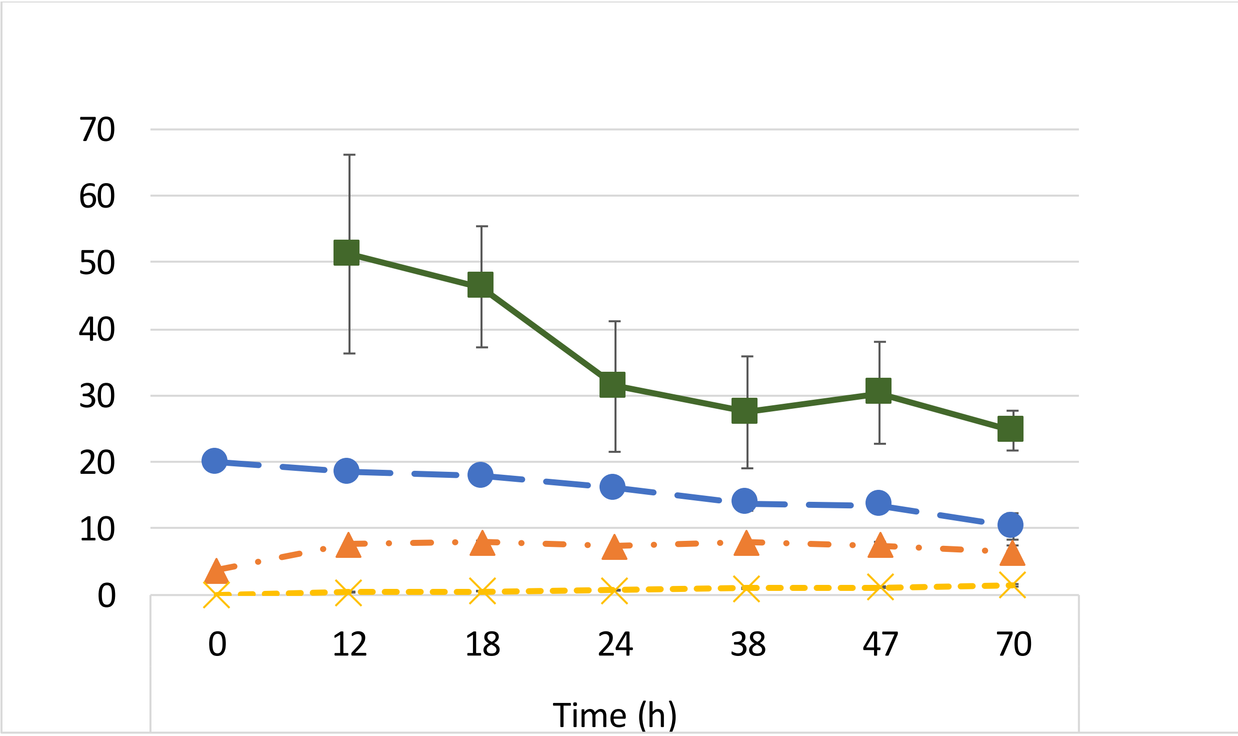

Figure S7. Time-dependent data for CPC-SbmΔ*sdhA*. Symbols and line color and type represent the average values for OD_{600} (orange, dash-dot, ▲), acetate concentration (blue, dash, ●), propionate concentration (yellow, long dash, **X**), and yield (green, solid, ■). *Vertical errors bars* represent s.d. (n = 3).

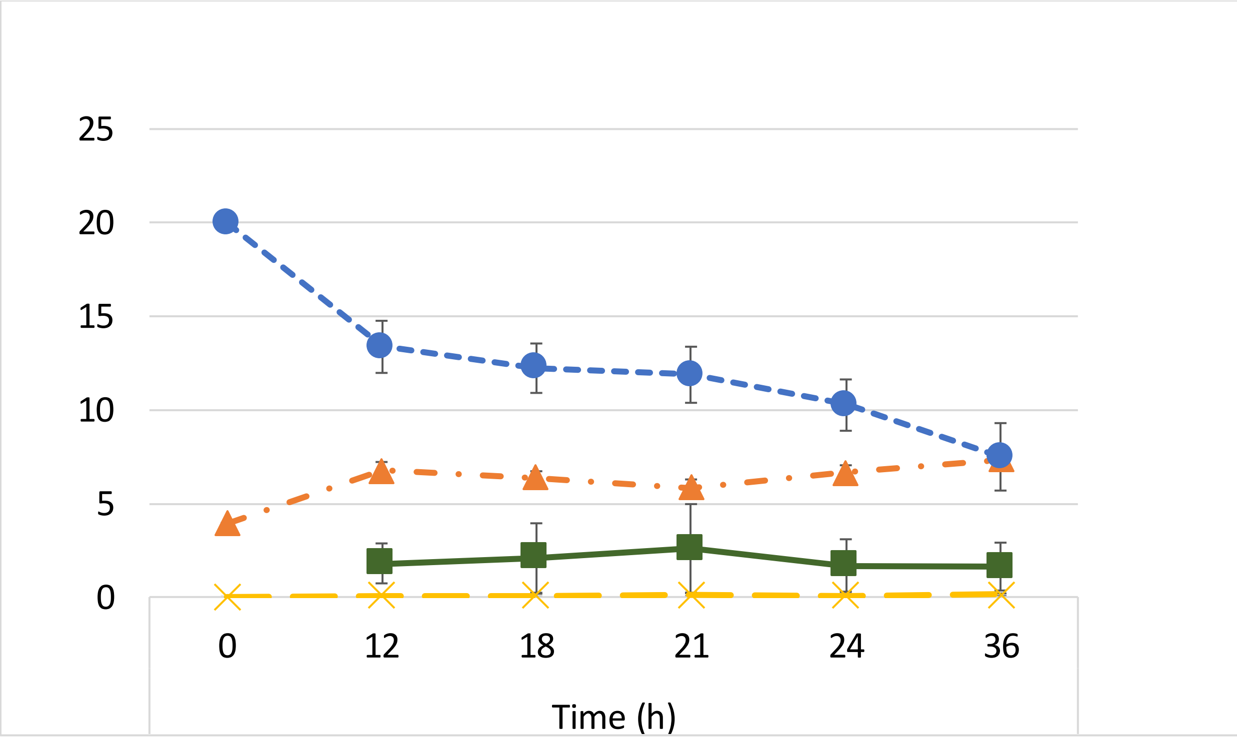

Figure S8. Time-dependent data for CPC-SbmΔ*icdA*. Symbols and line color and type represent the average values for OD_{600} (orange, dash-dot, ▲), acetate concentration (blue, dash, ●), propionate concentration (yellow, long dash, **X**), and yield (green, solid, ■). *Vertical errors bars* represent s.d. (n = 3).

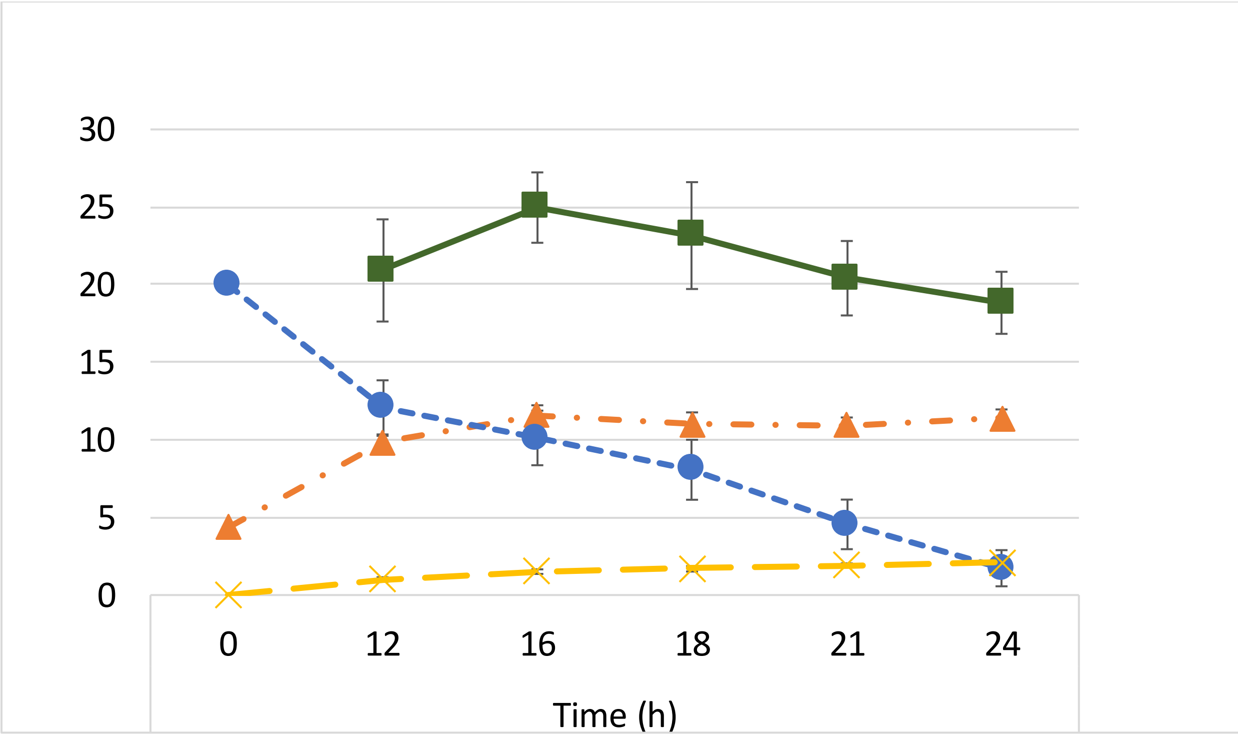

Figure S9. Time-dependent data for CPC-SbmΔ*frdB*. Symbols and line color and type represent the average values for OD_{600} (orange, dash-dot, ▲), acetate concentration (blue, dash, ●), propionate concentration (yellow, long dash, **X**), and yield (green, solid, ■). *Vertical errors bars* represent s.d. (n = 3).

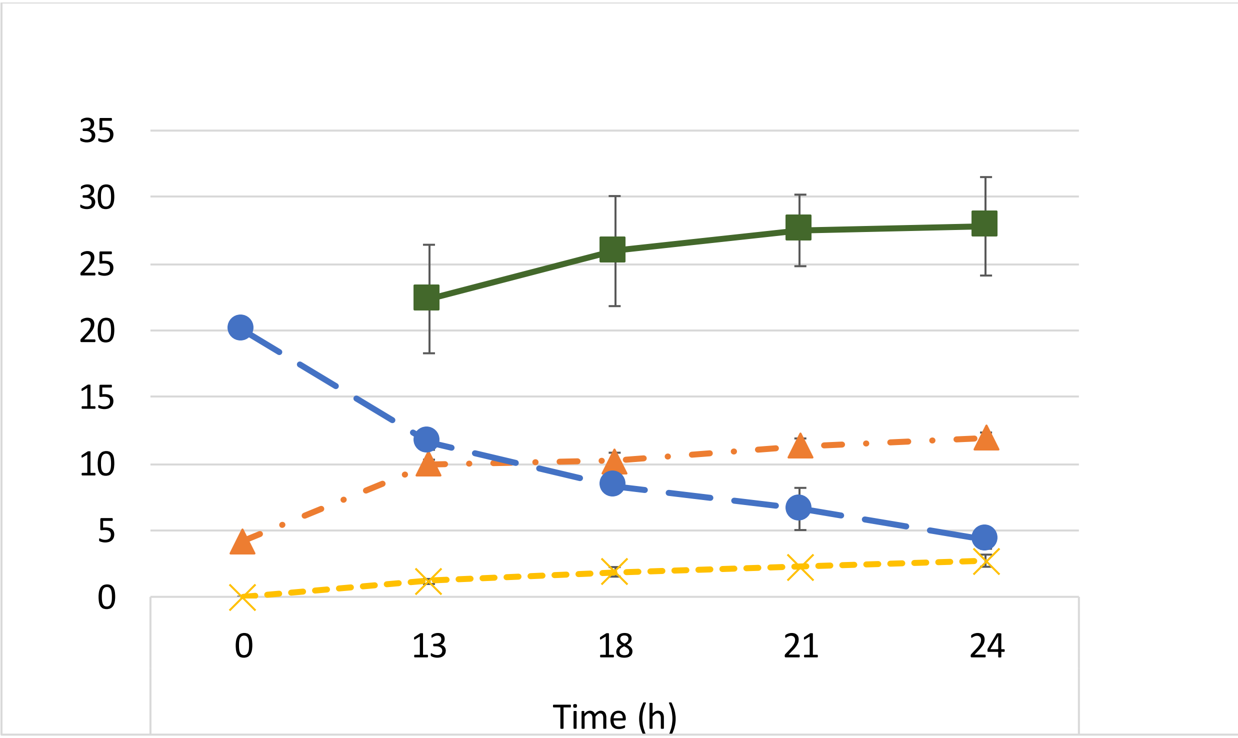

Figure S10. Time-dependent data for CPC-SbmΔ*fumA*. Symbols and line color and type represent the average values for OD_{600} (orange, dash-dot, ▲), acetate concentration (blue, dash, ●), propionate concentration (yellow, long dash, **X**), and yield (green, solid, ■). *Vertical errors bars* represent s.d. (n = 3).

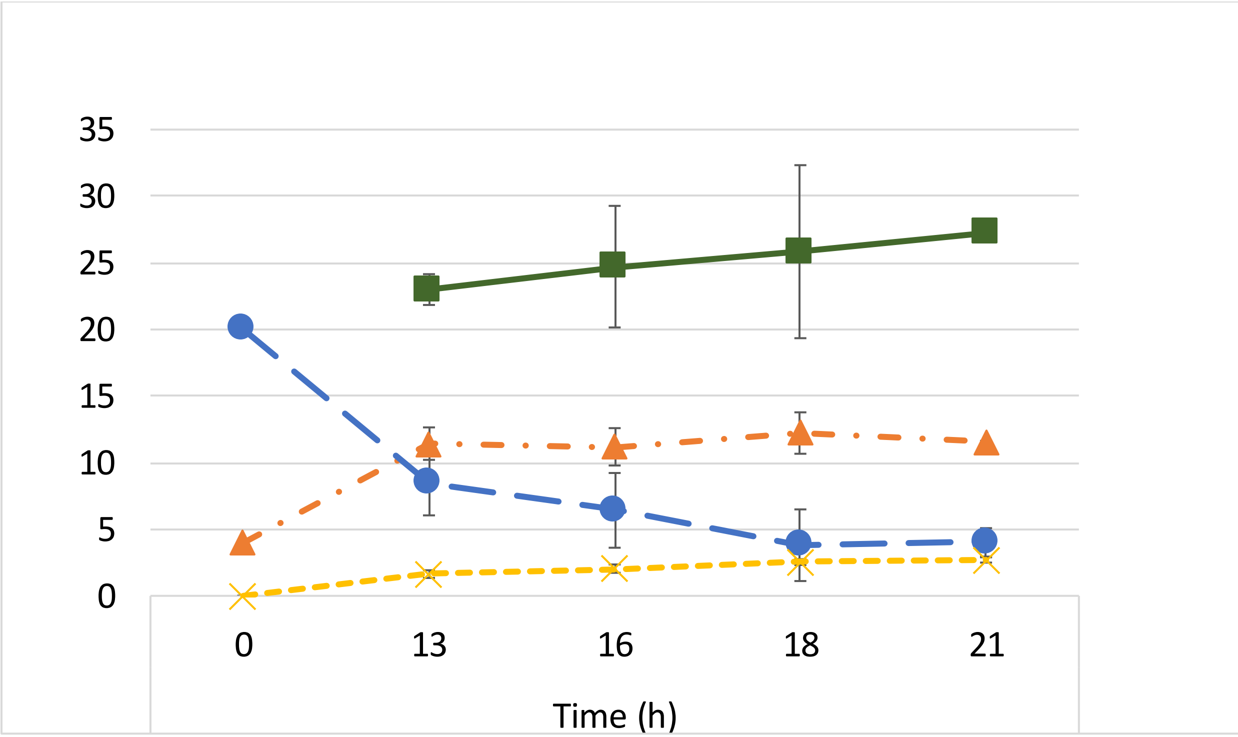

Figure S11. Time-dependent data for CPC-SbmΔ*fumC*. Symbols and line color and type represent the average values for OD_{600} (orange, dash-dot, ▲), acetate concentration (blue, dash, ●), propionate concentration (yellow, long dash, **X**), and yield (green, solid, ■). *Vertical errors bars* represent s.d. (n = 3).

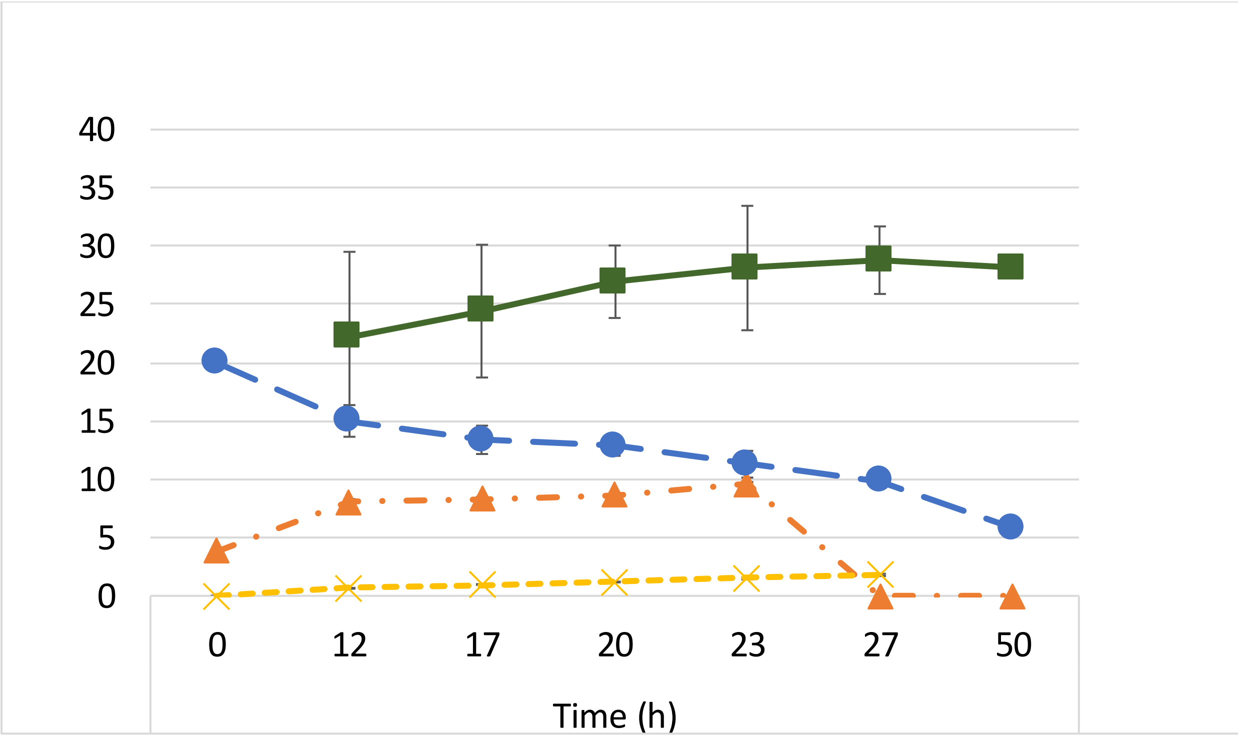

Figure S12. Time-dependent data for CPC-Sbm-TCA1. Symbols and line color and type represent the average values for OD_{600} (orange, dash-dot, ▲), acetate concentration (blue, dash, ●), propionate concentration (yellow, long dash, **X**), and yield (green, solid, ■). *Vertical errors bars* represent s.d. (n = 3).

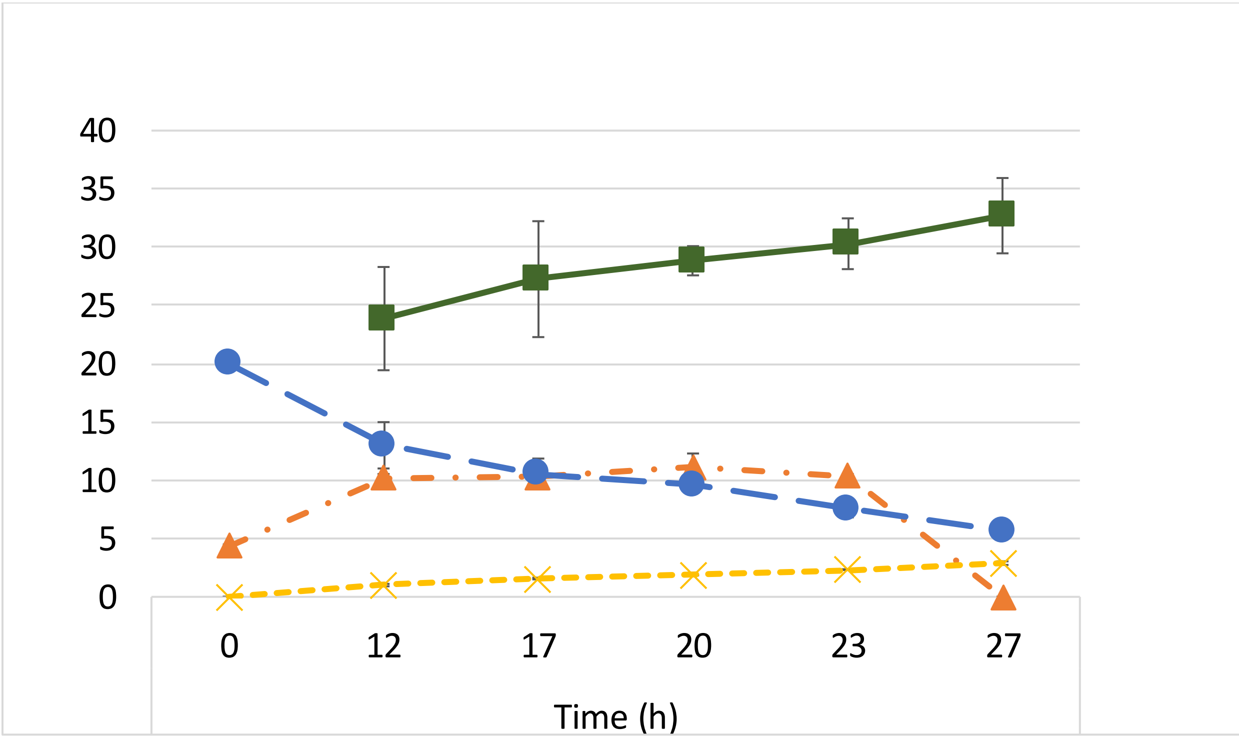

Figure S13. Time-dependent data for CPC-Sbm-TCA2. Symbols and line color and type represent the average values for OD_{600} (orange, dash-dot, ▲), acetate concentration (blue, dash, ●), propionate concentration (yellow, long dash, **X**), and yield (green, solid, ■). *Vertical errors bars* represent s.d. (*n* = 2).

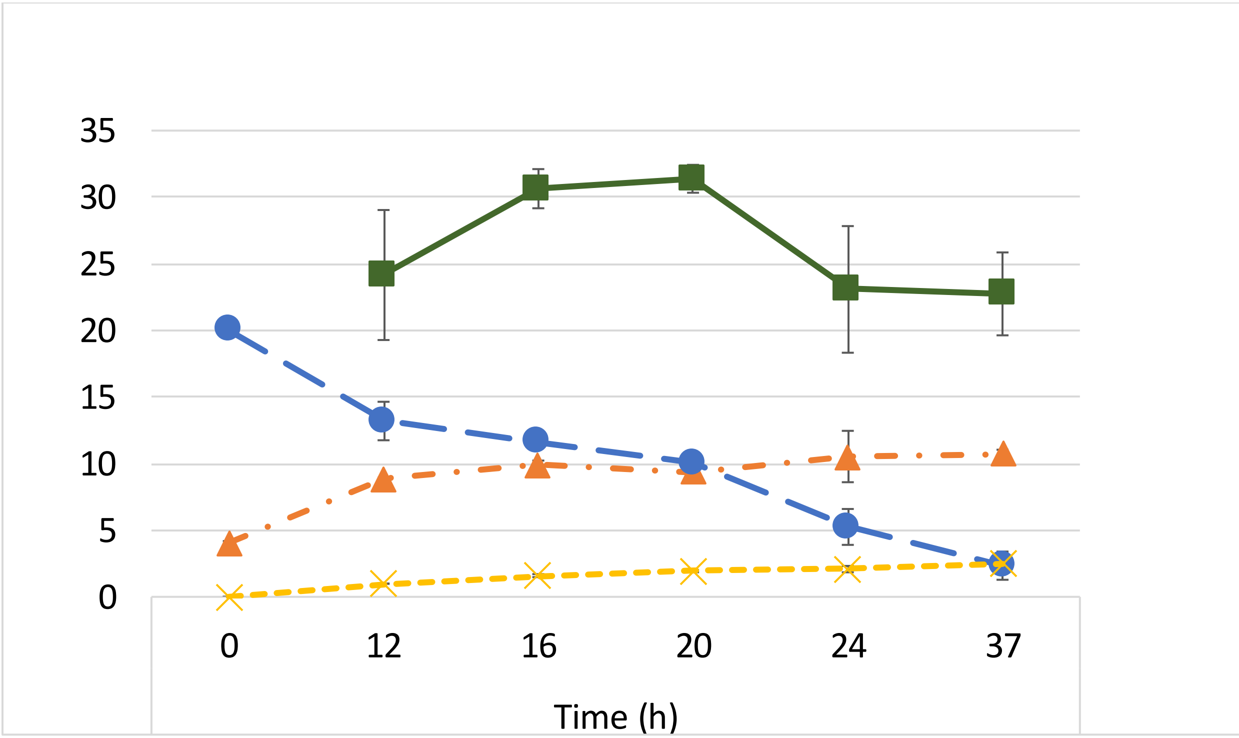

Figure S14. Time-dependent data for CPC-Sbm-TCA3. Symbols and line color and type represent the average values for OD_{600} (orange, dash-dot, ▲), acetate concentration (blue, dash, ●), propionate concentration (yellow, long dash, **X**), and yield (green, solid, ■). *Vertical errors bars* represent s.d. ($n = 3$).

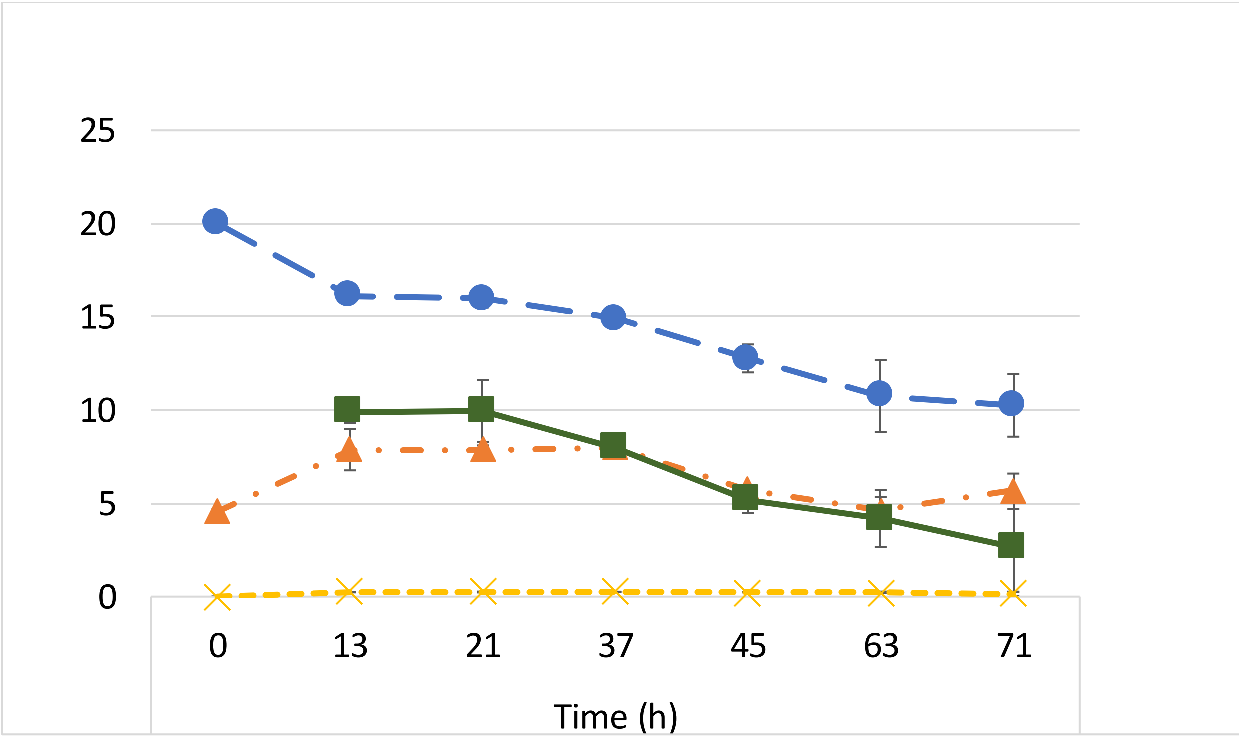

Figure S15. Time-dependent data for CPC-SbmΔ*aceA*. Symbols and line color and type represent the average values for OD_{600} (orange, dash-dot, ▲), acetate concentration (blue, dash, ●), propionate concentration (yellow, long dash, **X**), and yield (green, solid, ■). *Vertical errors bars* represent s.d. (n = 3).

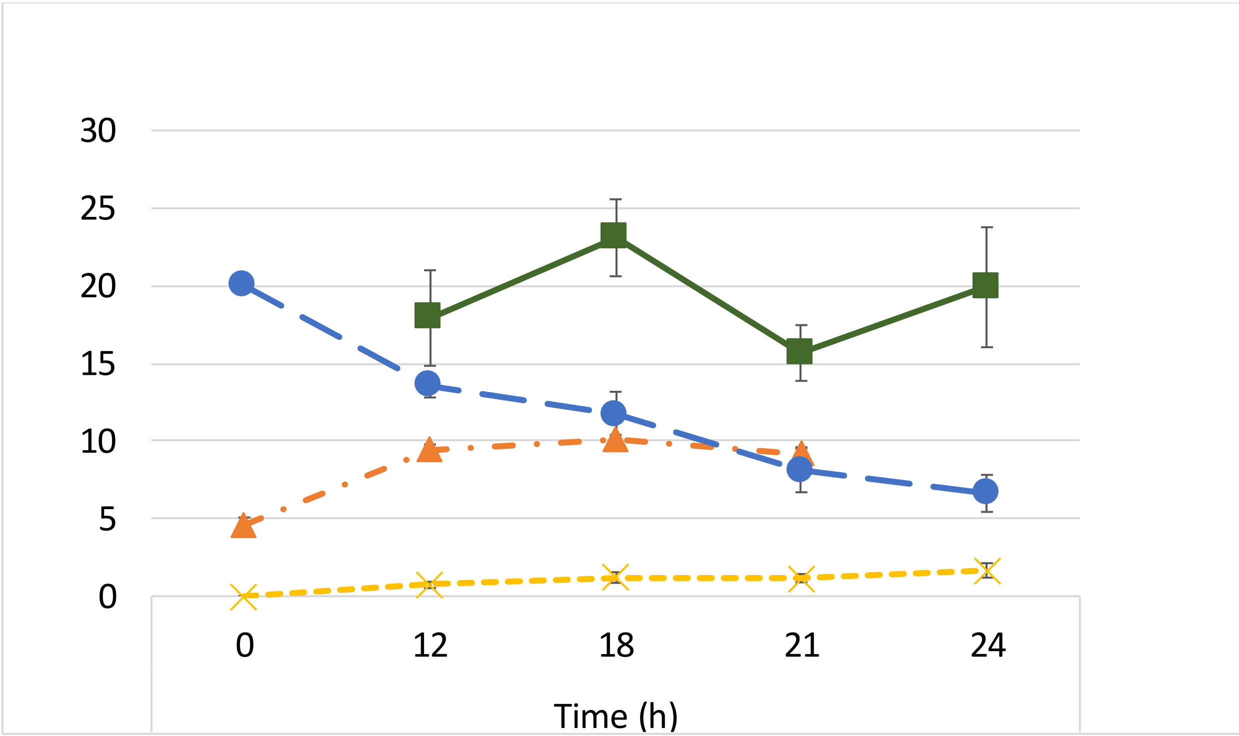

Figure S16. Time-dependent data for CPC-SbmΔ*aceB*. Symbols and line color and type represent the average values for OD_{600} (orange, dash-dot, ▲), acetate concentration (blue, dash, ●), propionate concentration (yellow, long dash, **X**), and yield (green, solid, ■). *Vertical errors bars* represent s.d. (n = 2).

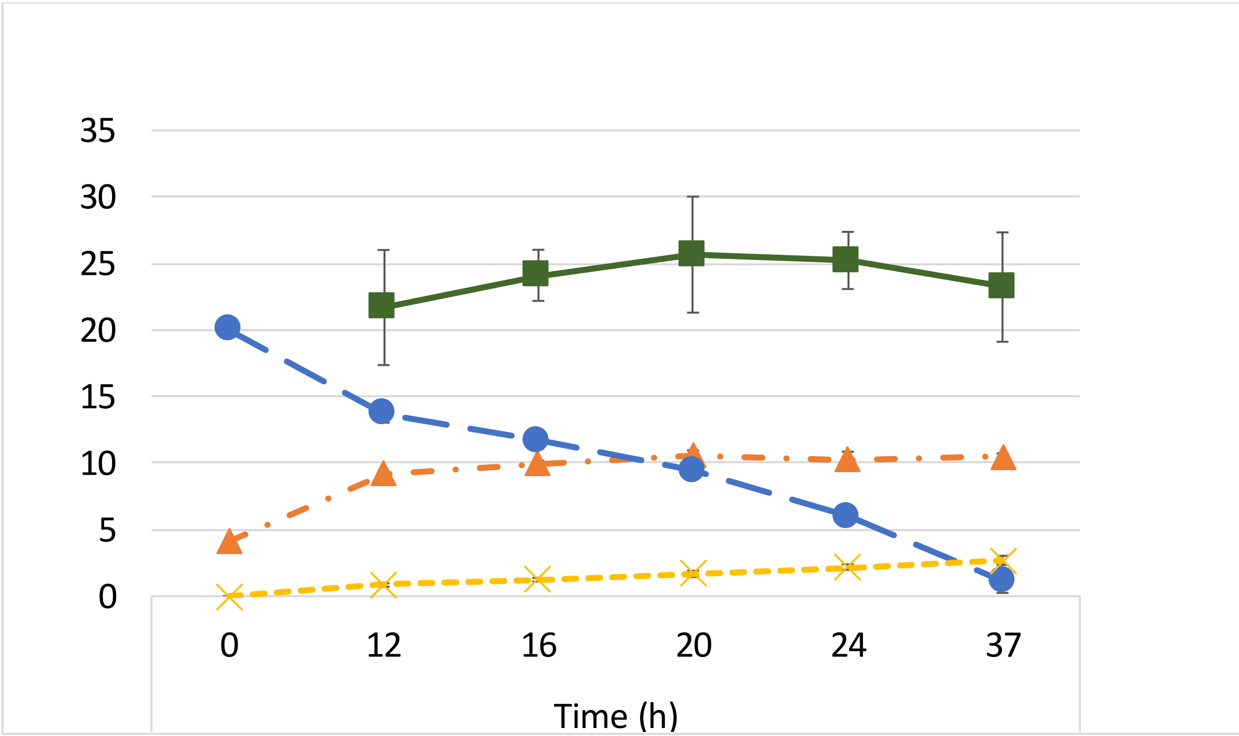

Figure S17. Time-dependent data for CPC-SbmΔ*glcB*. Symbols and line color and type represent the average values for OD_{600} (orange, dash-dot, ▲), acetate concentration (blue, dash, ●), propionate concentration (yellow, long dash, **X**), and yield (green, solid, ■). *Vertical errors bars* represent s.d. ($n = 3$).

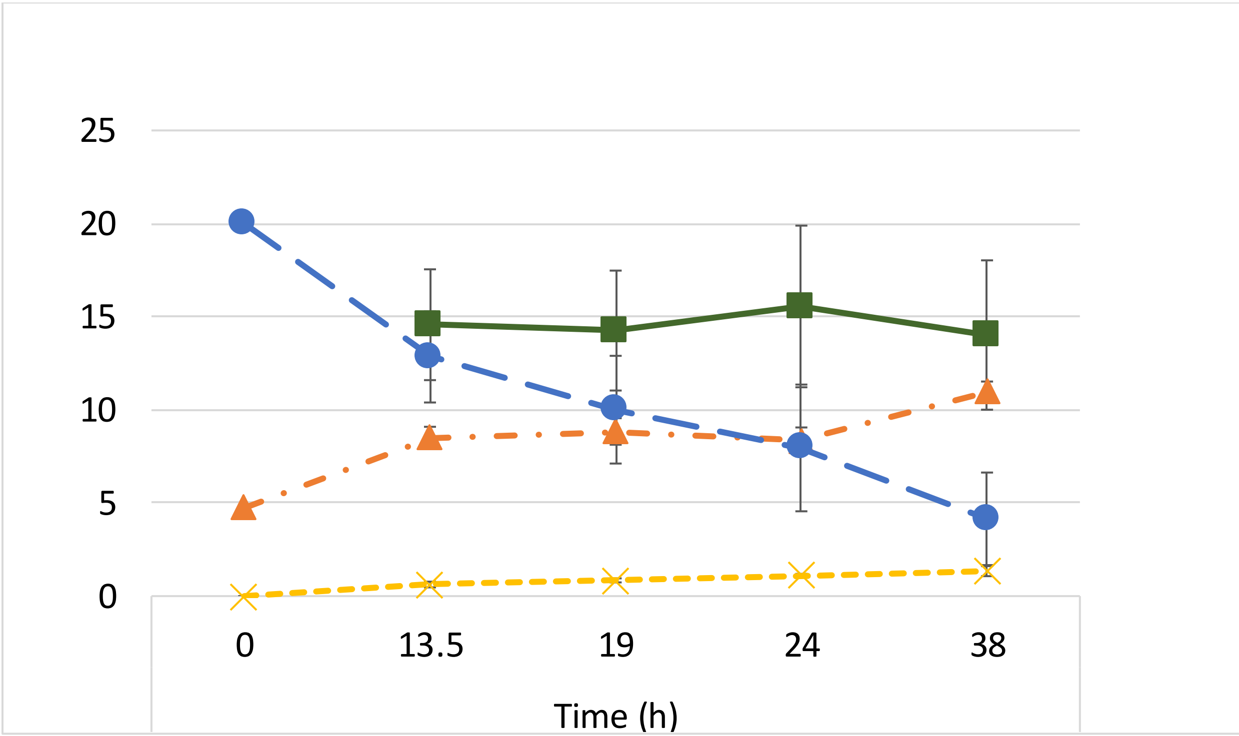

Figure S18. Time-dependent data for CPC-SbmΔ*aceB*Δ*glcB*. Symbols and line color and type represent the average values for OD_{600} (orange, dash-dot, ▲), acetate concentration (blue, dash, ●), propionate concentration (yellow, long dash, **X**), and yield (green, solid, ■). *Vertical errors bars* represent s.d. (n = 3).

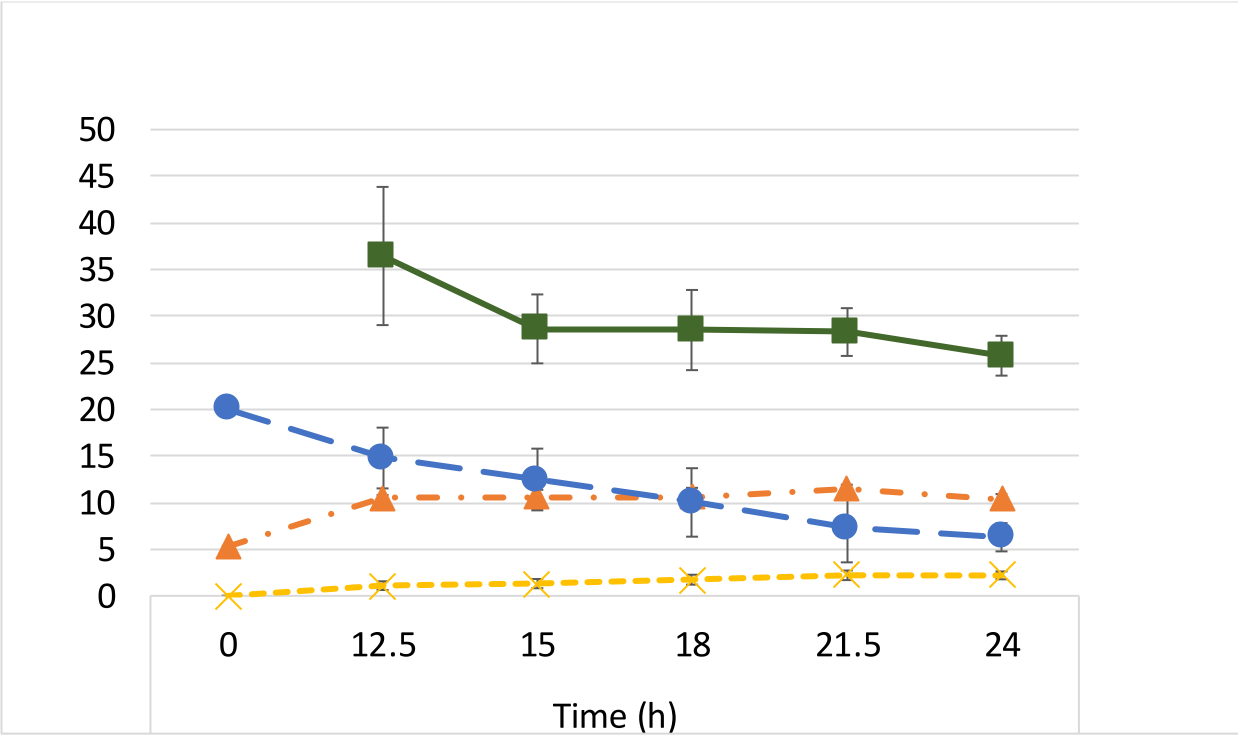

Figure S19. Time-dependent data for CPC-Sbm-GLX1. Symbols and line color and type represent the average values for OD_{600} (orange, dash-dot, ▲), acetate concentration (blue, dash, ●), propionate concentration (yellow, long dash, **X**), and yield (green, solid, ■). *Vertical errors bars* represent s.d. (n = 3).

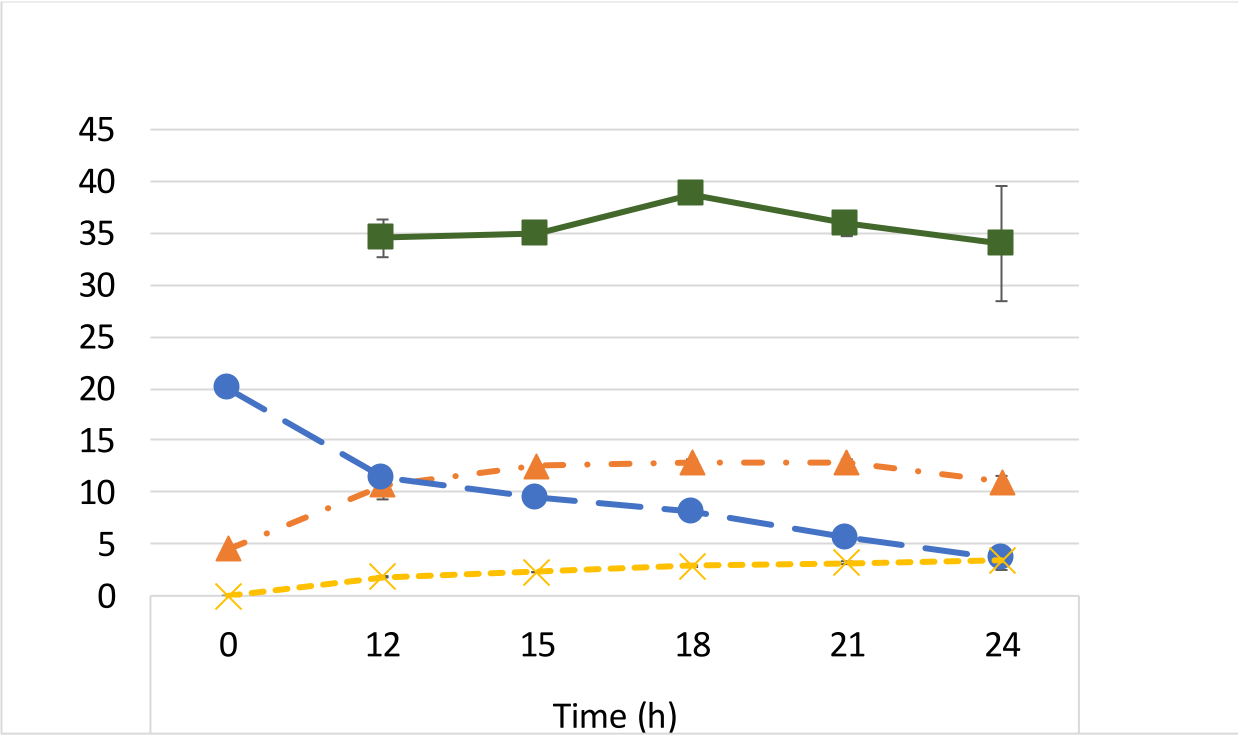

Figure S20. Time-dependent data for CPC-SbmΔ*maeB*. Symbols and line color and type represent the average values for OD_{600} (orange, dash-dot, ▲), acetate concentration (blue, dash, ●), propionate concentration (yellow, long dash, **X**), and yield (green, solid, ■). *Vertical errors bars* represent s.d. ($n = 2$).

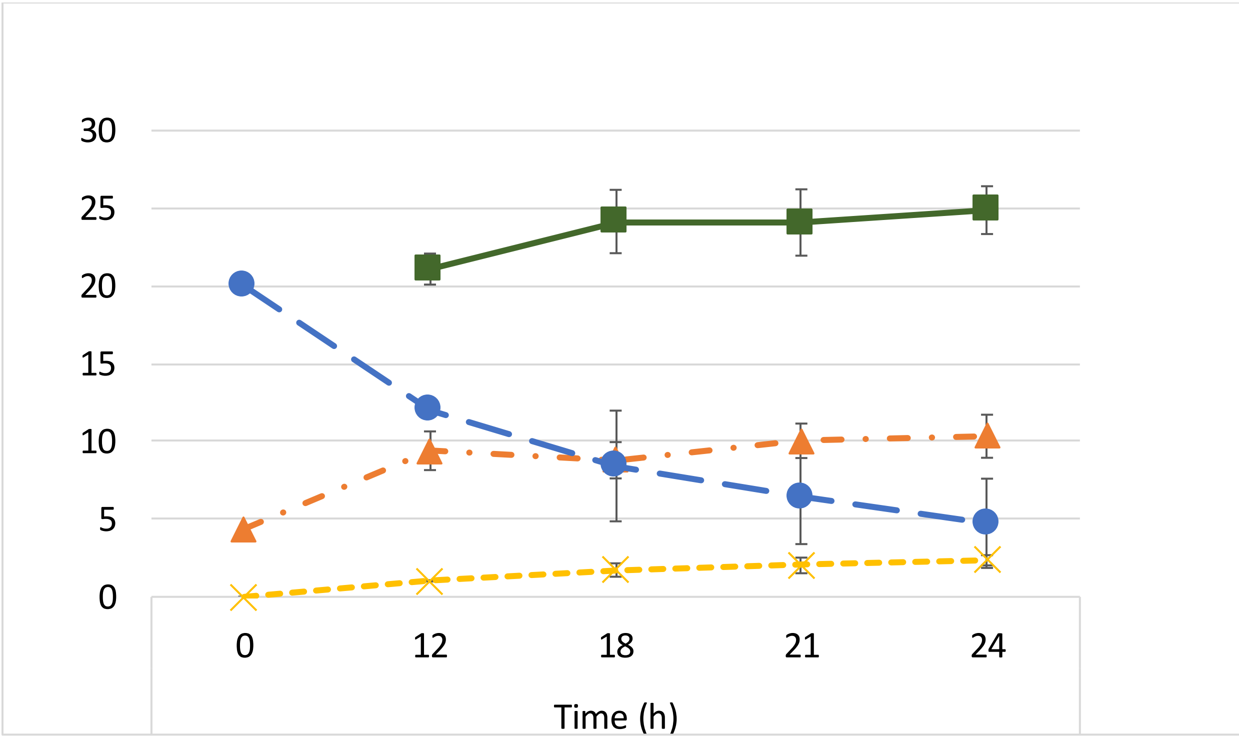

Figure S21. Time-dependent data for CPC-SbmΔ*sfcA*. Symbols and line color and type represent the average values for OD_{600} (orange, dash-dot, ▲), acetate concentration (blue, dash, ●), propionate concentration (yellow, long dash, **X**), and yield (green, solid, ■). *Vertical errors bars* represent s.d. (n = 3).

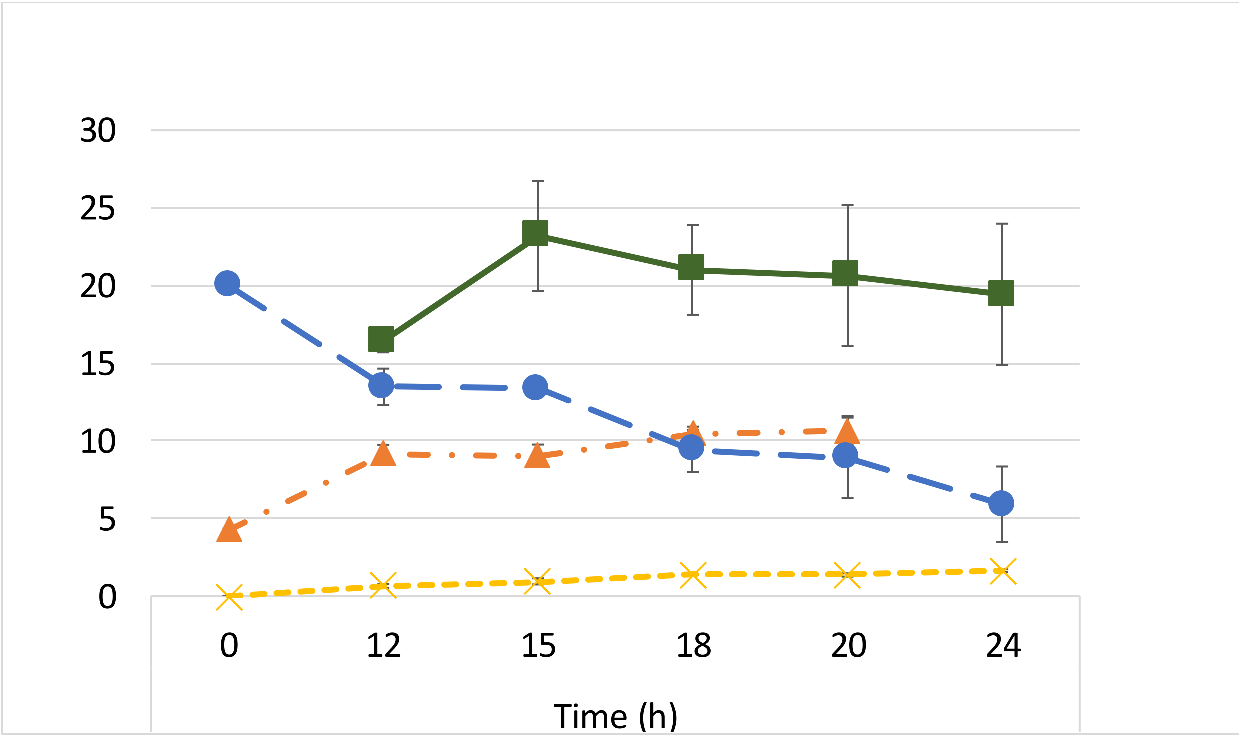

Figure S22. Time-dependent data for CPC-SbmΔ*aceF*. Symbols and line color and type represent the average values for OD_{600} (orange, dash-dot, ▲), acetate concentration (blue, dash, ●), propionate concentration (yellow, long dash, **X**), and yield (green, solid, ■). *Vertical errors bars* represent s.d. (n = 3).

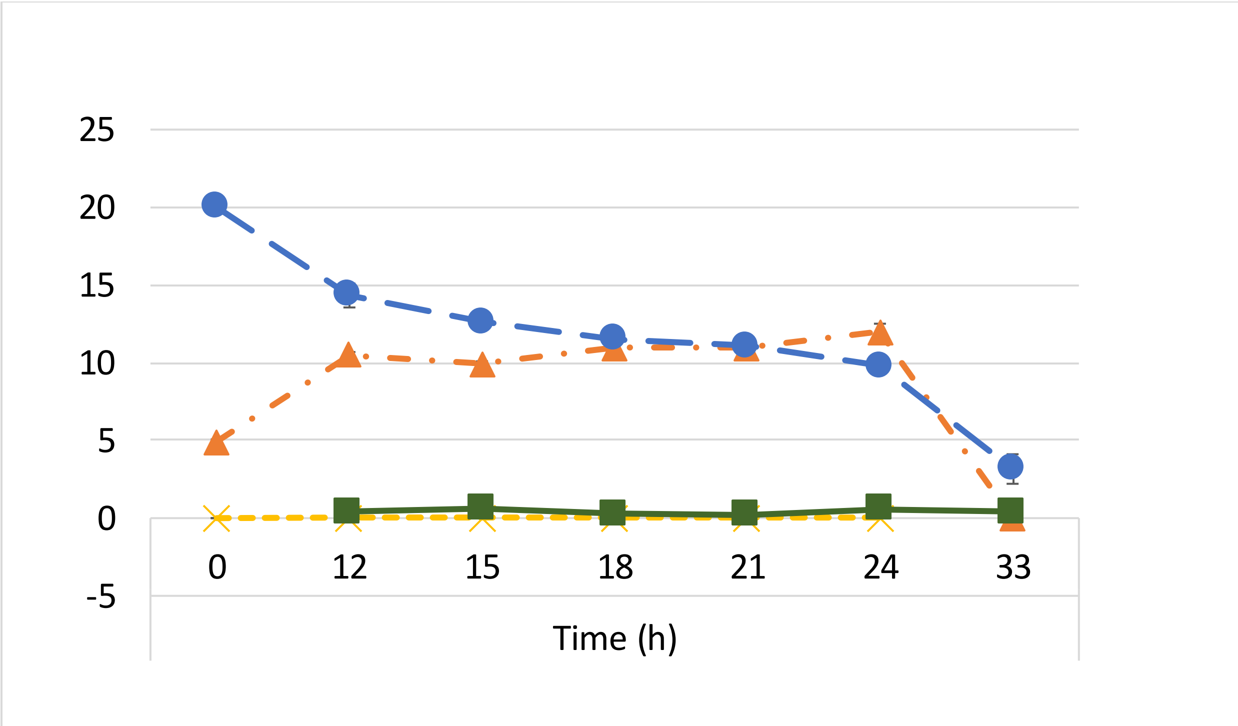

Figure S23. Time-dependent data for CPC-SbmΔ*ppsA*. Symbols and line color and type represent the average values for OD_{600} (orange, dash-dot, ▲), acetate concentration (blue, dash, ●), propionate concentration (yellow, long dash, **X**), and yield (green, solid, ■). *Vertical errors bars* represent s.d. (n = 2).

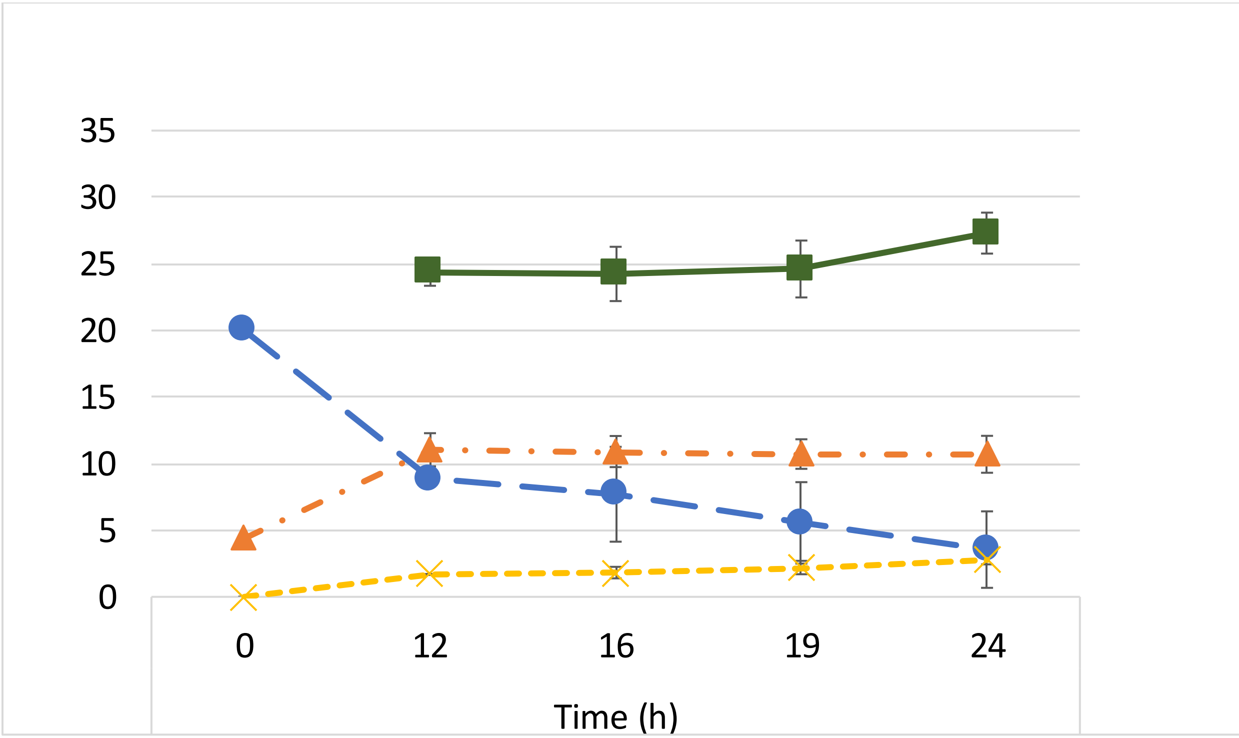

Figure S24. Time-dependent data for CPC-SbmΔ*pckA*. Symbols and line color and type represent the average values for OD_{600} (orange, dash-dot, ▲), acetate concentration (blue, dash, ●), propionate concentration (yellow, long dash, **X**), and yield (green, solid, ■). *Vertical errors bars* represent s.d. (n = 3).

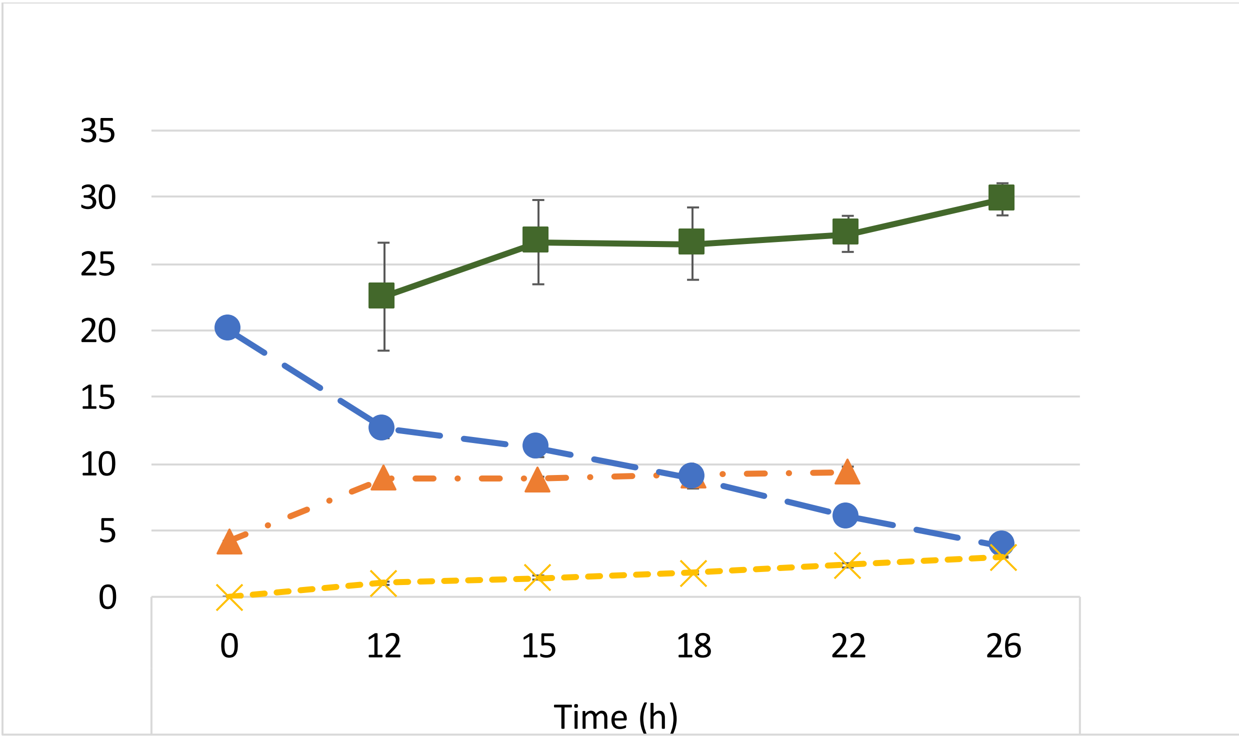

Figure S25. Time-dependent data for CPC-SbmΔ*pykF*. Symbols and line color and type represent the average values for OD_{600} (orange, dash-dot, ▲), acetate concentration (blue, dash, ●), propionate concentration (yellow, long dash, **X**), and yield (green, solid, ■). *Vertical errors bars* represent s.d. ($n = 3$).

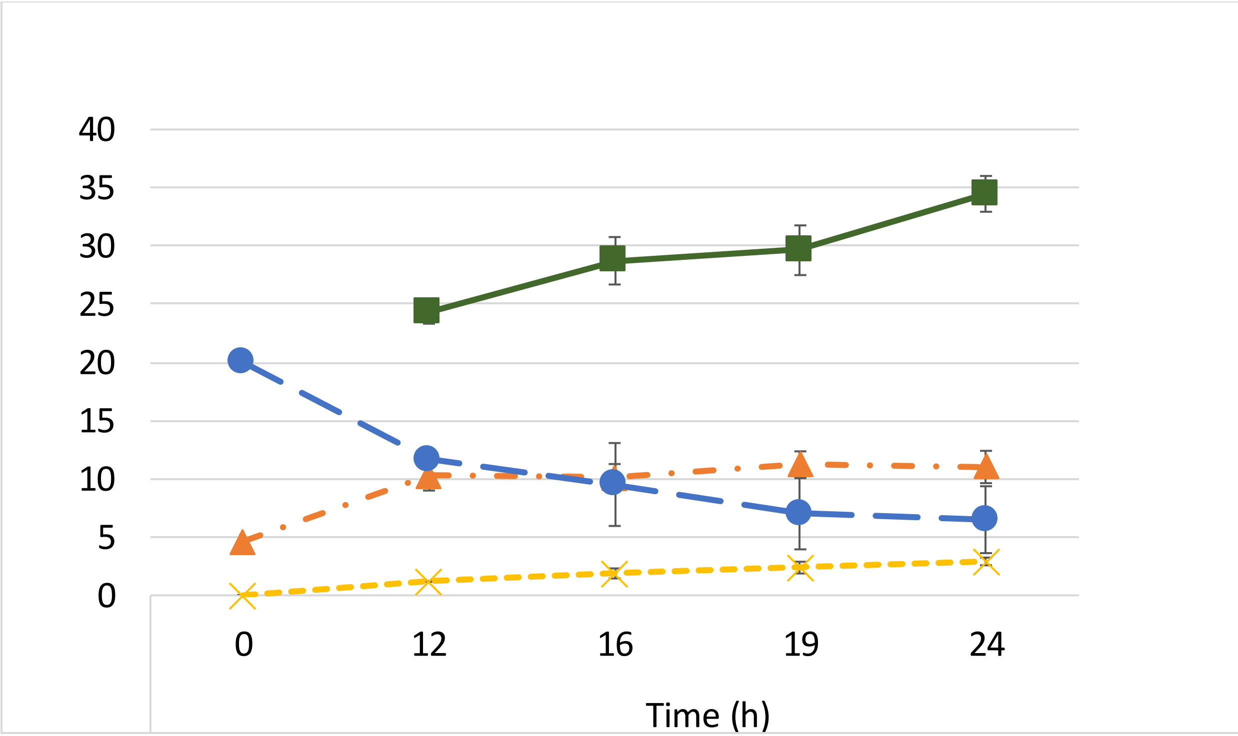

Figure S26. Time-dependent data for CPC-Sbm∆*ppc*. Symbols and line color and type represent the average values for OD_{600} (orange, dash-dot, ▲), acetate concentration (blue, dash, ●), propionate concentration (yellow, long dash, **X**), and yield (green, solid, ■). *Vertical errors bars* represent s.d. (n = 3).

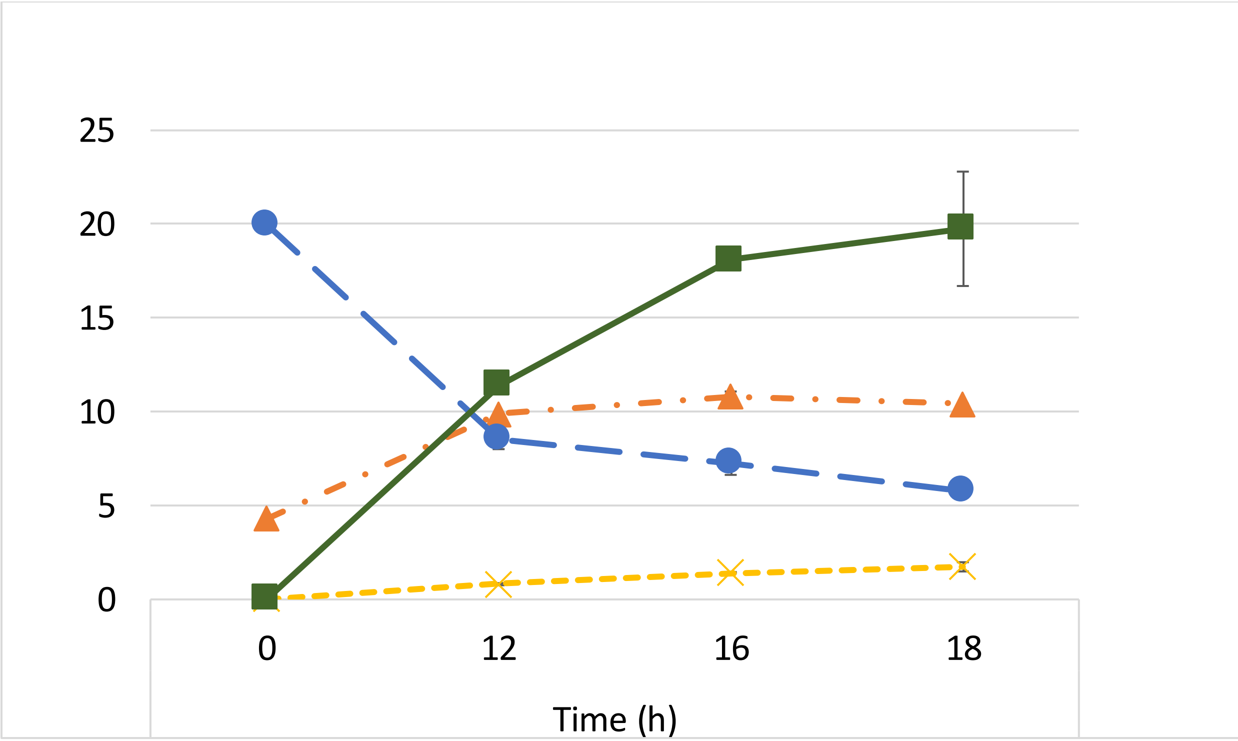

Figure S27. Time-dependent data for CPC-Sbm-PEP1. Symbols and line color and type represent the average values for OD_{600} (orange, dash-dot, ▲), acetate concentration (blue, dash, ●), propionate concentration (yellow, long dash, **X**), and yield (green, solid, ■). *Vertical errors bars* represent s.d. (n = 2).

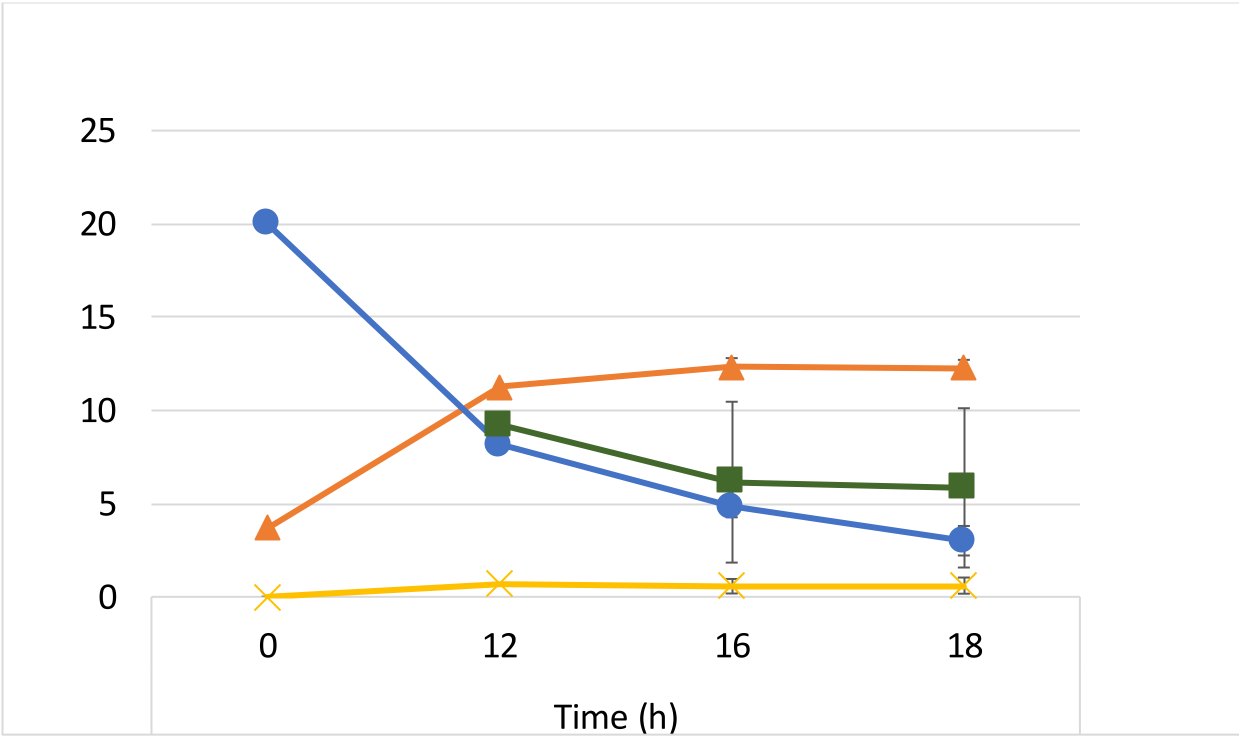

Figure S28. Time-dependent data for CPC-Sbm-PEP2. Symbols and line color and type represent the average values for OD_{600} (orange, dash-dot, ▲), acetate concentration (blue, dash, ●), propionate concentration (yellow, long dash, **X**), and yield (green, solid, ■). *Vertical errors bars* represent s.d. (n = 3).

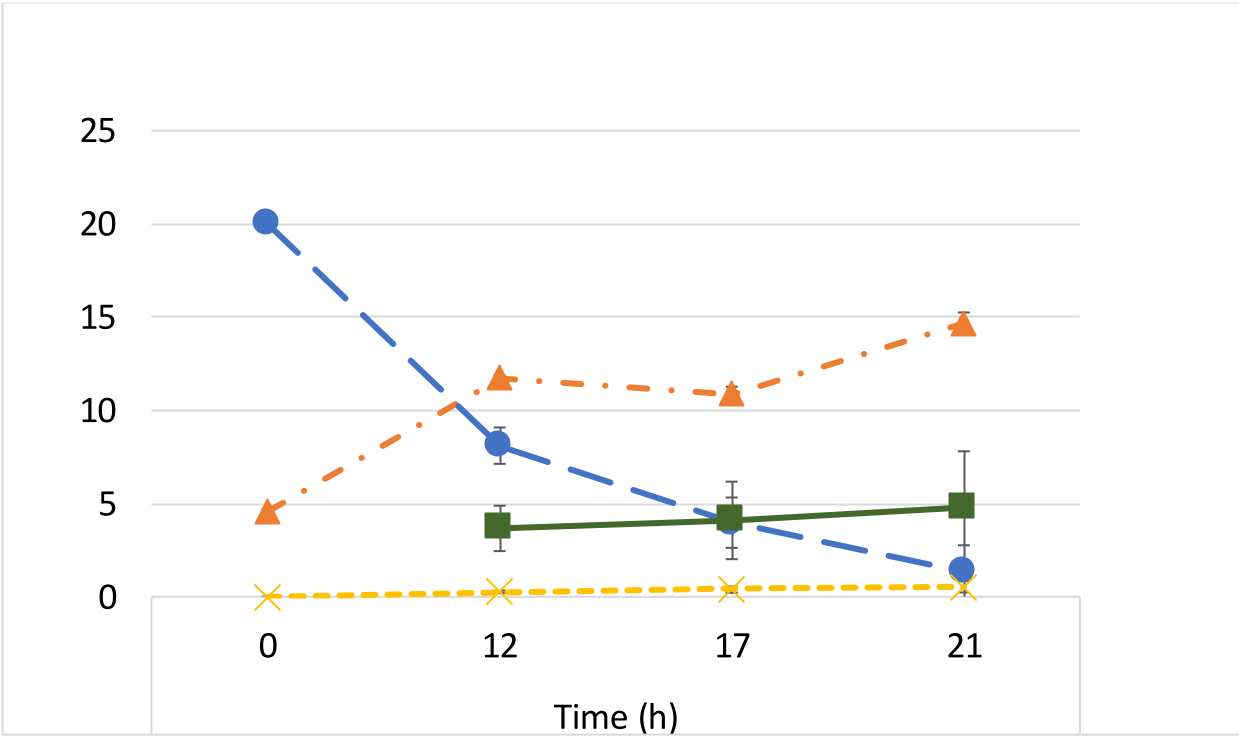

Figure S29. Time-dependent data for CPC-SbmΔ*arcA*. Symbols and line color and type represent the average values for OD_{600} (orange, dash-dot, ▲), acetate concentration (blue, dash, ●), propionate concentration (yellow, long dash, **X**), and yield (green, solid, ■). *Vertical errors bars* represent s.d. ($n = 3$).

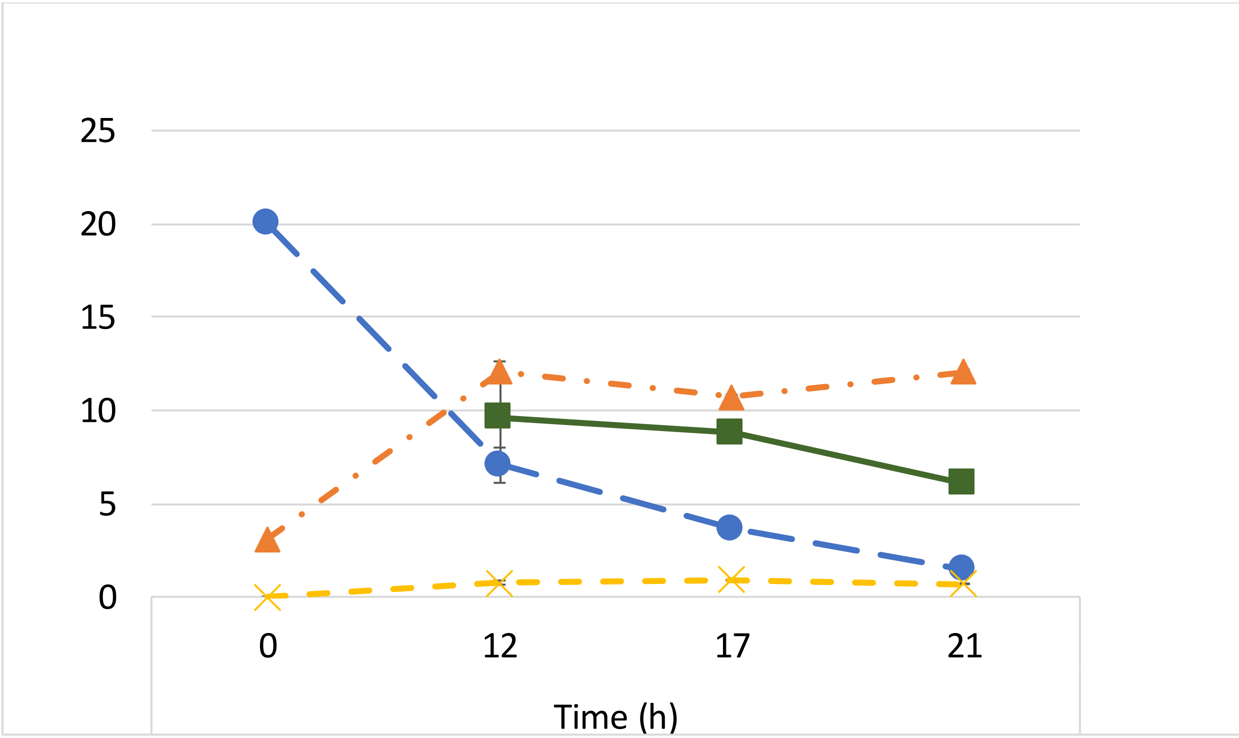

Figure S30. Time-dependent data for CPC-SbmΔ*fnr*. Symbols and line color and type represent the average values for OD_{600} (orange, dash-dot, ▲), acetate concentration (blue, dash, ●), propionate concentration (yellow, long dash, **X**), and yield (green, solid, ■). *Vertical errors bars* represent s.d. ($n = 2$).

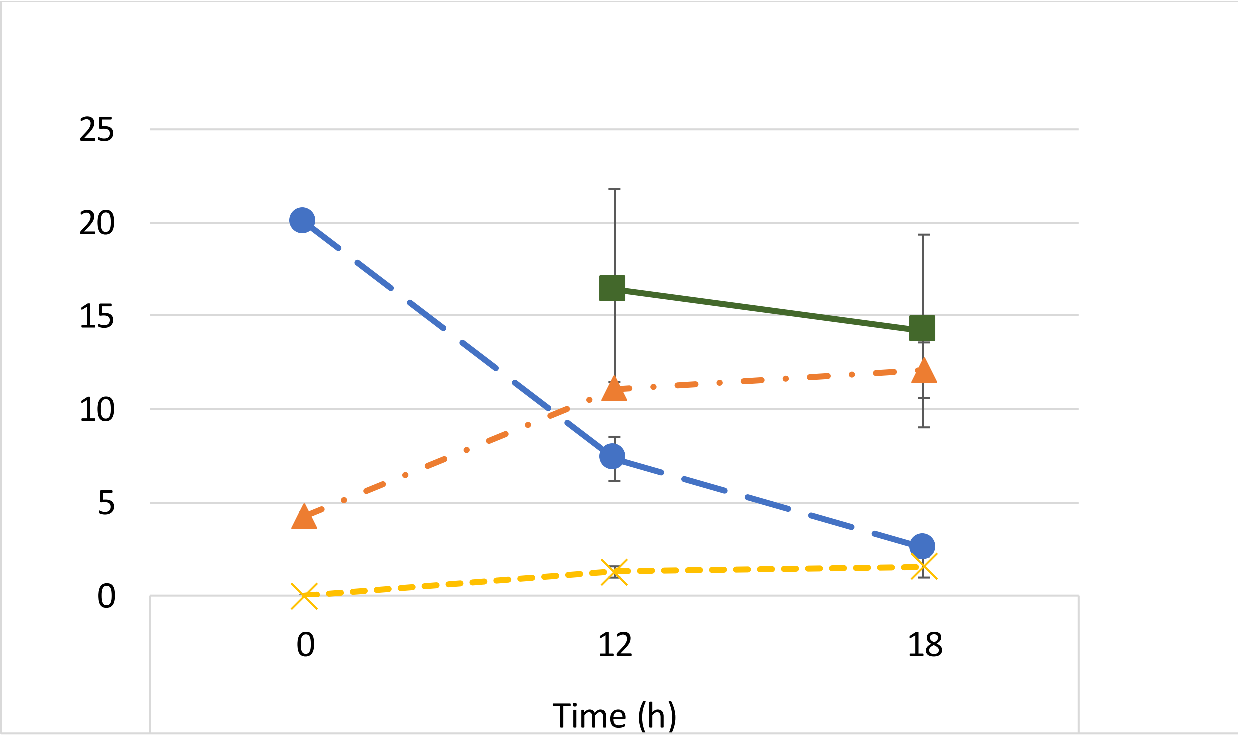

Figure S31. Time-dependent data for CPC-SbmΔ*aceK*. Symbols and line color and type represent the average values for OD_{600} (orange, dash-dot, ▲), acetate concentration (blue, dash, ●), propionate concentration (yellow, long dash, **X**), and yield (green, solid, ■). *Vertical errors bars* represent s.d. ($n = 2$).

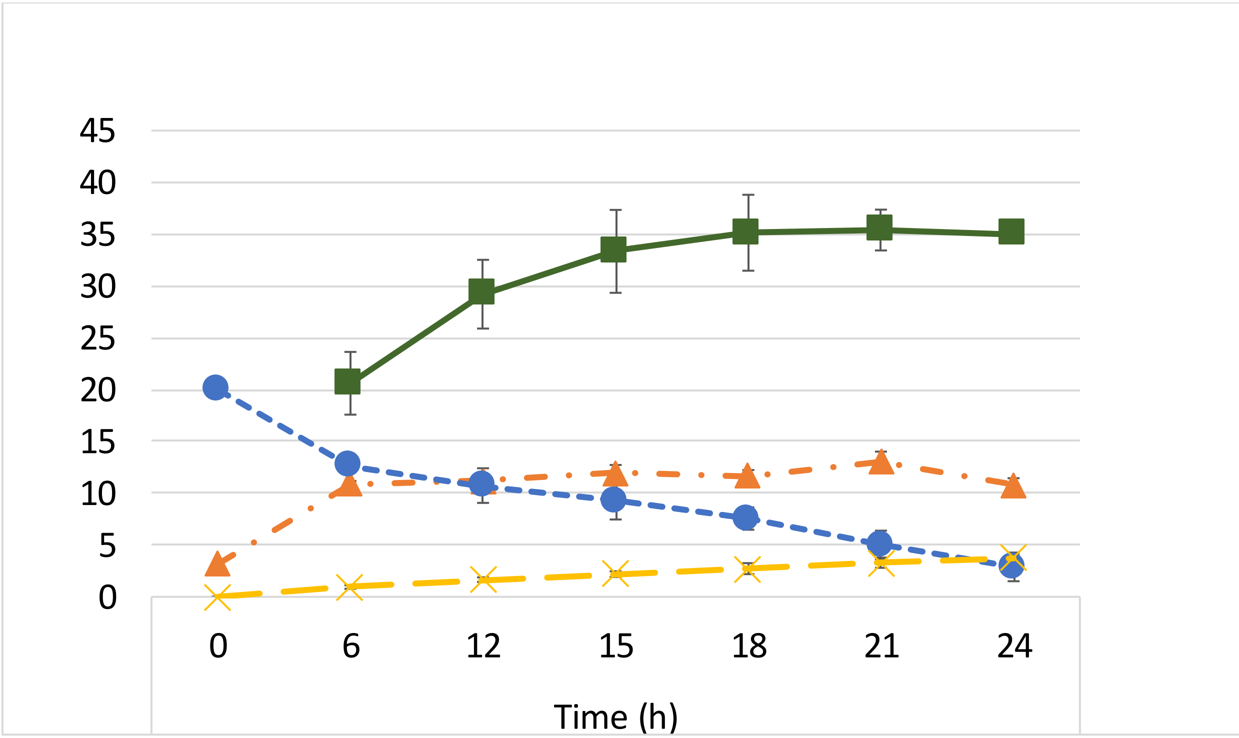

Figure S32. Time-dependent data for CPC-SbmΔ*iclR*. Symbols and line color and type represent the average values for OD_{600} (orange, dash-dot, ▲), acetate concentration (blue, dash, ●), propionate concentration (yellow, long dash, **X**), and yield (green, solid, ■). *Vertical errors bars* represent s.d. (n = 3).